



M.Sc. Bastian Daniel

The Family of Berberine Bridge Enzyme-like
Proteins from *Arabidopsis thaliana*

Dissertation

Zur Erlangung des akademischen Grades

Doktor der technischen Wissenschaften (Dr. *techn.*)

Erreicht an der

Technischen Universität Graz

Betreuer: Prof. Dr. Peter Macheroux

Institut für Biochemie

Technische Universität Graz

Graz, 2015

Acknowledgments

I heartily want to thank everyone who helped me in this project during the last four years. I want to express gratitude to my supervisor Prof. Peter Macheroux for giving me the opportunity to catch a tiny glimpse of the fascinating world of flavoproteins. I would like to thank him for his constant support and encouragement during the whole project.

I want to thank all my colleagues who contributed to the nice working atmosphere and the fruitful discussions. My special thanks go to Dr. Silvia Wallner for introducing me to the diverse aspects of the BBE-like protein family and for her sheer endless patience with me during my adaption from chemical engineering to biochemistry. I would like to thank M.Sc. Barbara Steiner and Dr. Domen Zafred for joining the team BBE. It was a pleasure to unravel the mysteries of BBE-like protein family with you in joined forces.

Furthermore I would like to thank my thesis committee members Prof. Karl Gruber and Prof. Wolfgang Kroutil. Karl kindly gave me an insight into structural biology which is a very valuable gift for an enzymologist. Wolfgang deserves special thanks for guiding me in respect to the biocatalytic aspects of my work.

This project would not have been realized without the help of various collaboration partners. Therefore I thank Prof. Christoph W. Sensen and B.Sc. Andreea M. Grecu for their support in the elaboration of the phylogenetics of the BBE-like protein family. The support of Prof. Bernd Nidetzky and Dr. Alexander Gutmann who provided me with various monolignol glycosides is friendly appreciated. Dr. Jörg Schrittwieser was a tremendous help supporting me with his expertise in biocatalysis and analytic chemistry. I spent so much time in the department of structural biology that I was sometimes mistaken for a regular employee there. Therefore I would like to thank all members of this institute for the pleasant working atmosphere and fruitful discussions. Special thanks go to Dr. Tea Pavkov-Keller and Dr. Andela Dordic for their support in the elucidation of the structure of *At*BBE-like 15 and much more. Dr. Prashant Kumar I want to thank for his help during the elucidation of the structure of *At*BBE-like 28. I want to thank Prof. Thomas Roitsch and Dr. Eric van der Graaff for their work on the *At*BBE-like knock out plants. Prof. Rolf Breinbauer and Dipl.-Ing. Marko Kljajic I want to thank for their work concerning the development of activity based probes for monolignol oxidoreductases.

During the last years I had the pleasure to guide several young and talented researches during their very early steps of their scientific career. I would like to thank M.Sc. Daniel Prinz, M.Sc. Altijana Hromic, B.Sc. Sabine M. Pils, M.Sc. Barbara Steiner and Markus M. Swoboda.

Last but not least I want to express my gratitude towards my family. I want to thank my parents for their love and support. I would like to thank my dear wife for being on my side during the past wonderful years. Theodor and Konrad, I thank you for brightening up my days with their laughter and thus I dedicate my thesis to my children.

Abstract

Flavoproteins are a diverse protein class employing the isoalloxazine ring for catalysis in form of the flavin mononucleotide (FMN) or flavin adenine dinucleotide (FAD). Among them is the berberine bridge enzyme-like (BBE-like) protein family (pfam 08031) that was named after the berberine bridge enzyme (*EcBBE*) from California poppy (*Eschscholzia californica*). BBE-like proteins occur in fungi, archaea, bacteria and plants, in the latter they form a multigene family and the number of members varies from one in the moss *Physcomitrella patens* to sixty four in the western poplar (*Populus trichocarpa*). Despite of the frequent occurrence of these proteins their function is largely unknown. Therefore we chose to address the BBE-likes occurring in *Arabidopsis thaliana* to broaden our understanding of this protein family. The genome of *A. thaliana* harbours 28 genes for BBE-like proteins that can be divided into 7 phylogenetic groups. The aim of this thesis was the characterization of *AtBBE*-like protein 15 and *AtBBE*-like protein 28.

AtBBE-like protein 15 was identified as a monolignol oxidoreductase. Subsequently *AtBBE*-like protein 13 was characterized by my dear colleague Barbara Steiner and was shown to possess the same function. *AtBBE*-like protein 15 is localized in the plant cell wall and catalyses the oxidation of one of the major cell wall components, the monolignols, to the corresponding aldehydes. This activity suggests a role of BBE-like proteins in monolignol metabolism and lignin formation that was prior not recognized for this protein family. The structure of *AtBBE*-like protein 15 was elucidated by protein crystallography, in respect to the active site composition a site directed mutagenesis study was conducted to probe the catalytic mechanism of the enzyme. Sequence alignments reveal that four different active site compositions are present in the 28 different *AtBBE*-like proteins. 14 out of 28 *AtBBE*-like proteins share the *AtBBE*-like protein 15 active site composition and therefore a similar mechanism is anticipated for these enzymes.

AtBBE-like protein 15 is a monolignol dehydrogenase, *i.e.* the enzyme inhibits the reaction between the reduced flavin and oxygen. The enzyme was engineered towards higher oxygen reactivity and the potential of the enzyme as biocatalyst for oxidative reactions was tested. The pH- and temperature optimum (pH 7, 50 °C) was determined. The enzyme shows enhanced activity in the presence of various organic solvents and accepts various allylic and

benzylic alcohols as substrates. Secondary allylic alcohols were converted with good to excellent enantioselectivity ($E>34$ to $E>200$).

*At*BBE-like protein 28 was expressed heterologously in *Komagataella pastoris*, the structure was elucidated employing X-ray crystallography. A BBE-like featuring the active site composition of *At*BBE-like protein 28 has not been characterized before. The most salient and distinguishing features of the active site found in *At*BBE-like protein 28 are a mono-covalent instead of a bi-covalent cofactor tethering. In addition, the structure reveals the interaction of a glutamic acid (Glu426) with an aspartic acid (Asp369). This arrangement leads to the delocalization of a negative charge in the active site that may be exploited for catalysis. The structure also indicates a shift of the position of the isoalloxazine ring in comparison to other members of the BBE-like protein family. The dioxygen surrogate chloride was found near the C(4a) position of the isoalloxazine ring in the oxygen pocket rationalizing a rapid reoxidation of reduced enzyme by dioxygen. Multiple sequence analysis showed that this particular active site composition in BBE-like enzymes is confined to the *Brassicaceae* suggesting that they play a specific role in the metabolism of this plant family.

Kurzfassung

Flavoproteine sind eine mannigfaltige Proteinklasse, in welcher der Isoalloxazinring in Form des Flavinmononukleotides (FMN) oder des Flavin-Adenin-Dinukleotid (FAD) als Katalysator eingesetzt wird. Zu dieser Proteinklasse gehört die Familie (pfam08031) der *berberine bridge enzyme-like* Proteine (BBE-like). Benannt wurde diese Proteinfamilie nach dem *berberine Bridge enzyme* aus dem kalifornischen Goldmohn (*Eschscholzia californica*) (*EcBBE*), welches die Umsetzung von (*S*)-Reticulin zu (*S*)-Scoulerin katalysiert. BBE-like Proteine kommen in Pilzen, Bakterien, Archaeen und Pflanzen vor. In Letzteren stellen sie eine Multigenfamilie dar, mit einer sehr variablen Anzahl an Genen, die von einem im Moos *Physcomitrella patens* bis zu 64 in der Pappel (*Populus trichocarpa*) reicht. Obwohl Mitglieder dieser Proteinfamilie ubiquitär vorkommen, ist über ihre Funktion nur wenig bekannt. Daher haben wir beschlossen, unser Verständnis dieser Proteinfamilie anhand des Beispiels der BBE-like Proteine aus der gemeinen Acker-Schmalwand (*Arabidopsis thaliana*) zu erweitern. Im Genom der Acker-Schmalwand sind Gene für 28 verschiedene BBE-like Proteine zu finden, die sieben phylogenetischen Gruppen zugeordnet werden können. Ziel dieser Arbeit war es zwei BBE-like Proteine (*AtBBE-like* Protein 15 und *AtBBE-like* Protein 28) heterolog zu exprimieren und zu charakterisieren.

AtBBE-like Protein 15 konnte als Monolignoloxidoreduktase identifiziert werden. Nachfolgend wurde auch *AtBBE-like* Protein 13 von meiner Kollegin Barbara Steiner charakterisiert und ebenfalls als Monolignoloxidoreduktase klassifiziert. *AtBBE-like* Protein 15 ist in der pflanzlichen Zellwand lokalisiert und oxidiert eine der Hauptkomponenten der Zellwand, die Monolignole, zu den korrespondierenden Aldehyden. Diese Aktivität legt nahe, dass die BBE-like Proteine eine Rolle im Monolignolmetabolismus und in der Ligninbildung spielen, die für diese Proteinfamilie zuvor noch nicht bekannt war. Die Struktur von *AtBBE-like* Protein 15 wurde mit Hilfe von Proteinkristallographie gelöst, unter Berücksichtigung der Zusammensetzung des aktiven Zentrums wurden gezielt Aminosäuren im aktiven Zentrum ausgetauscht, um den enzymatischen Mechanismus von *AtBBE-like* Protein 15 aufzuklären. Sequenzvergleiche legen nahe, dass es in den 28 *AtBBE-like* Proteinen der Acker-Schmalwand vier verschiedenen Arten von aktiven Zentren gibt. In vierzehn der achtundzwanzig *AtBBE-like*s ist das aktive Zentrum identisch zu *AtBBE-like* Protein 15, weshalb für diese *AtBBE-like* Proteine ein ähnlicher enzymatischer Mechanismus angenommen werden kann.

Bei *AtBBE*-like Protein 15 handelt es sich um eine Monolignoldehydrogenase, das heißt, das Enzym inhibiert die Reaktion zwischen dem reduzierten Flavin und Sauerstoff. Das Enzym wurde modifiziert, um eine höhere Reaktivität gegenüber Sauerstoff zu erzielen und sein Potential als Biokatalysator für Oxidationen getestet. Es wurde das pH- und Temperaturoptimum (pH 7, 50 °C) bestimmt. Das Enzym zeigt erhöhte Aktivität in der Anwesenheit von verschiedenen organischen Lösungsmitteln, als Substrate werden verschiedene allylische und benzyllische Alkohole akzeptiert. Sekundäre allylische Alkohole werden mit guter bis exzellenter Enantioselektivität ($E > 34$ bis $E > 200$) umgesetzt.

AtBBE-like Protein 28 wurde heterolog in *Komagataella pastoris* exprimiert. Die Struktur wurde mit Hilfe der Röntgenkristallographie aufgeklärt. Die Struktur eines Enzyms mit ähnlicher Zusammensetzung des aktiven Zentrums war bis zu diesem Zeitpunkt noch nicht dokumentiert. Bemerkenswert an dem aktiven Zentrum von *AtBBE*-like Protein 28 ist die monokovalente Verknüpfung des Flavins an Stelle einer wie für *BBE*-like Proteine üblichen bikovalenten Verknüpfung. Auffällig sind weiterhin Asp369 und Glu426 deren Säuregruppen in sehr kurzer Distanz zueinander stehen. Diese Konformation legt nahe, dass diese beiden Reste sich ein Proton teilen und dass auf diese Weise eine negative Ladung im aktiven Zentrum delokalisiert und damit stabilisiert wird, um sie für den katalytischen Mechanismus bereitzustellen. Während die Position des Isoalloxazinrings innerhalb der *BBE*-like Proteinfamilie hoch konserviert ist, weicht sie in *AtBBE*-like Protein 28 bemerkenswert ab. Ein Chloridion wurde als Sauerstoffsurogat in der Sauerstoffbindetasche gefunden. Kinetische Messungen bestätigten die Funktionalität der Sauerstoffbindetasche, das Enzym wurde als Oxidase klassifiziert. Durch Sequenzvergleiche konnte ermittelt werden, dass die Zusammensetzung des aktiven Zentrums, wie sie bei *AtBBE*-like Protein 28 vorliegt, nur in *Brassicaceae* (Kreuzblütengewächsen) vorkommt.

Eidesstattliche Erklärung

Ich erkläre an Eides statt, dass ich die vorliegende Arbeit selbständig verfasst, andere als die angegebenen Quellen/Hilfsmittel nicht benutzt, und die die den benutzten Quellen wörtlich und Inhaltlich entnommenen Stellen als solche kenntlich gemacht habe.

Statutory Declaration

I declare that I have authored this thesis independently, that I have not used other than the declared sources / resources, and that I have explicitly marked all material which has been quoted either literally or by contend from the used sources.

Graz,.....

.....

Table of contents

Acknowledgments	2
Abstract	4
Kurzfassung	6
Statutory Declaration	8
Chapter 1: Berberine bridge enzyme and the family of bicovalent flavoenzymes	12
Abstract	13
Introduction	14
The paradigm of bicovalent flavoenzymes: Berberine bridge enzyme (BBE) from <i>Eschscholzia californica</i>	18
The family of BBE-like enzymes in the plant kingdom: how many and what for?	25
The occurrence of BBE-like enzymes in fungi	35
BBE-like enzymes in bacteria: oxidative power for the biosynthesis of antibiotics	38
Conclusions	41
Chapter 2: Oxidation of monolignols by members of the berberine bridge enzyme family suggests a role in plant cell wall metabolism	51
Abstract	52
Experimental Procedures.....	56
Chemicals	56
Molecular cloning.....	56
Protein expression and purification	56
Site-directed mutagenesis: Generation of the L182V variant	57
Crystallization	57
Data collection and processing.....	58
Rapid reaction kinetics using stopped flow spectrophotometry	59
Product identification	60
Synthesis of monolignol glycosides	60
Phylogenetic tree construction	61
Docking	61
Results	61
Enzymatic properties and identification of substrates of <i>At</i> BBE-like 13 and <i>At</i> BBE-like 15.....	61
Crystal structure of <i>At</i> BBE-like 15.....	64
Docking of substrates to the active site	67

Functional and structural characterisation of the BBE-like family in <i>A. thaliana</i>	68
Discussion	73
Catalytic mechanism of monolignol oxidation.....	73
Structural comparison with other members of the VAO family	73
Proposed role of <i>At</i> BBE-like15/monolignol oxidoreductases in plants	76
Chapter 3: Form follows function: structure based reaction mechanism of monolignol oxidoreductases.....	89
Abstract	90
Introduction	90
Experimental and Procedures	94
Mutagenesis, Protein Expression and Purification	94
Determination of the extinction coefficient.....	94
Rapid Reaction Kinetics Using Stopped Flow	94
Results	94
Expression and Purification.....	94
Determination of the extinction coefficient.....	95
Rapid Reaction Kinetics Using Stopped Flow	96
Discussion	98
Expression and purification.....	98
Determination of the extinction coefficient.....	98
Stopped flow kinetics and crystal structure: Structure function relationships in the <i>At</i> BBE-like 15 active site.....	99
Conclusion.....	103
Chapter 4: Characterization of a monolignol oxidoreductase from <i>Arabidopsis thaliana</i> for biocatalytic applications.....	106
Abstract	107
Introduction	107
Experimental	111
pH optimum.....	111
Temperature optimum	111
Activity in the presence of 10% (v/v) of organic co-solvents	111
Activity in the presence of 10–50% (v/v) of organic co-solvents	112
Long-term stability in the presence of 30% (v/v) of organic co-solvents	112
Substrate Screening	112

Product identification	113
Kinetic resolutions.....	115
Results and discussion.....	117
pH optimum.....	117
Temperature optimum	117
Activity in presence of 10% (v/v) of organic co-solvents	118
Activity in the presence of 10–50% (v/v) of organic co-solvents	119
Long-term stability in the presence of 30% (v/v) of organic co-solvents	120
Substrate Screening	121
Kinetic resolutions.....	123
Conclusions	125
Chapter 5: Structure of a berberine bridge enzyme-like enzyme with an active site specific to the plant family of <i>Brassicaceae</i>	127
Abstract	128
Introduction	129
Results	131
Structural characterization of <i>AtBBE</i> -like 28.....	131
Biochemical characterization	134
Sequence comparison and phylogenetic inference.....	136
Conclusions	145
Experimental Procedures.....	145
Cloning and transformation.....	145
Expression and purification.....	146
Crystallization and data collection	147
Redox potential determination	149
Photoreduction.....	149
Determination of the oxidative rate.....	149
Phylogenetic analysis	150
<i>Curriculum vitae</i>.....	161

Chapter 1: Berberine bridge enzyme and the family of bicovalent flavoenzymes

Silvia Wallner, Corinna Dully, Bastian Daniel and Peter Macheroux*

*From the Graz University of Technology, Institute of Biochemistry, Petersgasse 12, A-8010
Graz, Austria; Tel.: +43-316-873 6450, Fax: +43-316-873 6952,
Email: peter.macheroux@tugraz.at

This chapter was published as: Wallner S. *et al.*: Berberine Bridge Enzyme and the Family of Bicovalent Flavoenzymes, Handbook of Flavoproteins. Volume 2 Complex Flavoproteins, Dehydrogenase and Physical Methods 2013, Boston: De Gruyter. ISBN: 978-3-11-029834-5.

Author contributions:

S.W., B.D. and P.M. wrote the manuscript. S.W. performed BLAST searches, C.D. analysed the homology models.

Abstract

Flavoproteins are a large and diverse group of proteins that employ either FMN or FAD for catalysis. In the majority of flavoproteins (~90%) the flavin coenzyme is tightly but non-covalently bound in the active site of the enzyme. In the 1950s the first example of a covalently attached flavocoenzyme was discovered in succinate dehydrogenase followed by several more cases where either the 8 α - or 6-position of the isoalloxazine forms a covalent bond to the amino acid side chain of a cysteine, histidine or tyrosine. Very recently, in 2005, the first representative of a bicovalently linked flavocoenzyme was discovered in glucooligosaccharide oxidase. Since then, the number of bicovalently linked flavoproteins has risen rapidly and appears to be more common than any of the monocovalent attachment modes. These enzymes have extraordinary properties, such as unusually high redox potentials that enable catalysis of challenging chemical reactions in plants, fungi and bacteria. Moreover, bicovalent linkage appears to be crucial for structural integrity of the protein and correct positioning of the flavin in the active site. As a starting point, we review the wealth of information available for berberine bridge enzyme from *Eschscholzia californica* which can be considered a paradigm for the family of bicovalent flavoproteins. Moreover, we discuss the scope of reactions catalyzed by these enzymes in plants, fungi and bacteria. Finally, genomic information is explored to predict the number of bicovalent flavoenzymes present in nature. This analysis suggests that some genera are rich in bicovalent flavoproteins while others appear to have only a few members of this family of enzymes.

Introduction

The majority of flavoproteins (approximately 90%) contain non-covalently bound (dissociable) FMN or FAD as cofactor [1]. The first example of a covalently bound flavin was discovered in the 1950ies by Singer and coworkers. Singer's group demonstrated that succinate dehydrogenase, a central enzyme of the tricarboxylic acid cycle and entry point of electrons into the mitochondrial electron transport chain („complex II“), contains a covalently attached FAD [2]. Further studies demonstrated a linkage of the 8 α -methyl group of the isoalloxazine ring to N-3 of a histidine residue of the protein [3]. In the following years several other covalent linkages in flavoenzymes emerged such as tyrosinylation and cysteinylation at the 8 α -methyl group and cysteinylation of C-6 [4, 5]. At the end of the last century, Mewies *et al.* listed 24 flavoenzymes with a known linkage to either the 8 α - or 6-position of the flavin [4, 6]. A few years later, in 2005, the elucidation of the crystal structure of glucooligosaccharide oxidase (GOOX) provided the first example of a bicovalently linked FAD cofactor [7]. In this fungal enzyme the FAD is linked to a histidine and cysteine residue at the 8 α -methyl and C-6 position of the flavin, respectively. In other words, in this flavoenzyme the already known monocovalent attachments are combined to give a bicovalently linked flavin. At the time, this finding may have been regarded as a peculiarity of an enzyme that catalyzes the oxidation of a variety of mono- and oligosaccharides in a pathogenic fungus (for structures, see later). However, in the meantime it appears that bicovalent attachment occurs in many bacterial, fungal and plant enzymes and may eventually outnumber monocovalent attachment. From the current list of 43 flavoproteins bearing a covalent flavin cofactor, eleven are reported or predicted to feature bicovalent flavin attachment (Tab.1). Interestingly, bicovalent flavin attachment is confined to bacteria, fungi and plants and is absent from archaea and the animal kingdom as is evident from BlastP searches. It is also notable that all bicovalently attached flavins are found in proteins adopting a fold first observed in *p*-cresolmethylhydroxylase (PCMH) in the clan FAD_binding_4 of the PCMH protein family. With only a few exceptions this structural environment appears to prefer covalent binding of the flavin cofactor either mono- (as in PCMH) or in a bicovalent fashion [1]. On the other hand, monocovalent attachment occurs in at least three different protein topologies: NADP_Rossmann and GMC_oxred_C for FAD-containing and TIM_barrel for FMN-containing enzymes (Tab.1). Recent research offers several explanations for the role of bicovalent flavin tethering in flavoenzymes [8]. It increases the midpoint potential of the flavin cofactor to unprecedented high

values and thus enables challenging substrate oxidations [9-11]. Furthermore, it appears that these enzymes have very bulky substrates and hence the binding cavity near the flavin cofactor is very large potentially leading to high mobility of the isoalloxazine ring. This mobility is severely restricted by bicovalent linkage and freezes out translational modes that could compromise catalytic efficiency [8]. Indeed, these two factors play a role in chito oligosaccharide oxidase (ChitO) from *Fusarium graminearum* where bicovalent flavinylation modulates the redox potential and is required for correct positioning of cofactor and substrate in the active site and hence is a prerequisite for the formation of a catalytically competent Michaelis-Menten-complex [10]. Moreover, bicovalent linkage appears to be crucial for structural integrity as is evident from the low yields of protein variants, which lack one or both flavinylated sites [12]. Thus it appears that several factors must be considered to rationalize bicovalent linkage of the flavin and their relative contribution may also vary depending on the enzyme.

Tab.1: Covalent attachment of FMN and FAD to flavoenzymes. Bicovalent attachment is marked by an asterisk.

No.	E.C.	Enzyme	Cofactor	Structure Clan (Family)	Genus
1*	1.1.3.5	hexose oxidase	8 α -(His, 6-Cys)-FAD	-----	<i>Chondrus</i>
2	1.1.3.6	cholesterol oxidase	8 α -(N1-His)-FAD	FAD_PCMH (FAD_binding_4)	<i>Brevibacterium</i>
3	1.1.3.8	L-gulonolactone oxidase	8 α -(N1-His)-FAD	-----	ubiquitous
4	1.1.3.10	pyranose 2-oxidase	8 α -(N3-His)-FAD	GMC_oxred_C	<i>Trametes</i> , <i>Peniophora</i>
5	1.1.3.17	choline oxidase	8 α -(N3-His)-FAD	NADP_Rossmann (GMC_oxred_N)	<i>Arthrobacter</i>
6	1.1.3.23	thiamine oxidase	8 α -(N1-His)-FAD	-----	soil bacteria
7	1.1.3.37	D-arabino-1,4-lactone oxidase	8 α -(N1-His)-FAD	-----	<i>Candida</i> , <i>Saccharomyces</i>
8	1.1.3.38	vanillyl-alcohol oxidase	8 α -(N3-His)-FAD	FAD_PCMH (FAD_binding_4)	<i>Penicillium</i>
9	1.1.3.39	nucleoside oxidase (H ₂ O ₂ -forming)	FAD (covalent)	-----	<i>Elizabethkingia</i>
10	1.1.3.41	alditol oxidase	8 α -(N1-His)-FAD	FAD_PCMH (FAD_binding_4)	<i>Streptomyces</i>
11*	1.1.3.-	acilominocin oxidoreductase	8 α -(N1-His, 6-Cys)-FAD	FAD_PCMH (FAD_binding_4)	<i>Streptomyces</i>
12*	1.1.3.-	chitoooligosaccharide oxidase	8 α -(N1-His, 6-Cys)-FAD	predicted ^a	<i>Fusarium</i>
13	1.1.3.-	eugenol oxidase	8 α -(N3-His)-FAD	predicted ^a	<i>Rhodococcus</i>
14	1.1.3.-	D-gluconolactone oxidase	8 α -(N3-His)-FAD	predicted ^a	<i>Penicillium</i>
15*	1.1.3.-	glucooligosaccharide oxidase	8 α -(N1-His, 6-Cys)-FAD	FAD_PCMH (FAD_binding_4)	<i>Acetomonium</i>
16*	1.1.3.-	glycopeptide hexose oxidase (Dbv29)	8 α -(N1-His, 6-Cys)-FAD	FAD_PCMH (FAD_binding_4)	<i>Actinomadura</i>
17*	1.1.3.-	10-hydroxy-dehydrogenase in tirandamycin biosynthesis (TrdL, TamL)	8 α -(N1-His, 6-Cys)-FAD	FAD_PCMH (FAD_binding_4)	<i>Streptomyces</i>
18	1.1.3.-	nectarin V (putative sugar oxidase)	FAD (covalent)?	-----	<i>Nicotiana</i>
19*	1.1.3.-	pregilvocarcin V dehydrogenase, GilR	8 α -(N1-His, 6-Cys)-FAD	FAD_PCMH (FAD_binding_4)	<i>Streptomyces</i>
20	1.1.99.3	gluconate 2-dehydrogenase (acceptor)	8 α -(N3-His)-FAD	-----	bacteria
21	1.1.99.4	dehydrogluconate dehydrogenase	8 α -(N3-His)-FAD	-----	bacteria
22*	1.3.3.8	(S)-tetrahydropteroberbine oxidase	8 α -(N1-His, 6-Cys)-FAD	predicted from homology modelling ^b	<i>Argemone</i>
23	1.3.5.1	succinate dehydrogenase (ubiquinone)	8 α -(N3-His)-FAD	NAPH_Rossmann (FAD_binding_2)	ubiquitous

24	1.3.99.1	succinate dehydrogenase / fumarate reductase	8 α -(N3-His)-FAD	NADP_Rossmann (FAD_binding_2)	<i>Shewanella</i> , <i>Wolmetella</i>
25	1.4.3.4	monoamine oxidase	8 α -(Cys)-FAD	NADP_Rossmann (Amino_oxidase)	mammals
26	1.4.3.-	amino acid oxidase, NikD	8 α -(Cys)-FAD	NADP_Rossmann (DAO)	<i>Streptomyces</i>
27	1.5.3.1	sarcosine oxidase (monomeric)	8 α -(Cys)-FAD	NADP_Rossmann (DAO)	<i>Bacillus</i>
28	1.5.3.6	sarcosine oxidase (heterotetrameric)	8 α -(N3-His)-FMN	α and β interface	<i>Corynebacterium</i>
29	1.5.3.7	(R)-6-hydroxynicotine oxidase	8 α -(N1-His)-FAD	FAD_PCMH (FAD_binding_4)	<i>Arthrobacter</i>
30	1.5.3.10	L-pipecolate oxidase	8 α -(Cys)-FAD?	-----	<i>Pseudomonas</i>
31	1.5.3.-	dimethylglycine oxidase	8 α -(N3-His)-FAD	NADP_Rossmann (DAO)	<i>Arthrobacter</i>
32	1.5.8.1	γ -N-methylaminobutyrate oxidase	8 α -(His)-FAD	-----	<i>Arthrobacter</i>
33	1.5.8.2	dimethylamine dehydrogenase	6-(Cys)-FMN	-----	<i>Hyphomicrobium</i>
34	1.5.99.1	trimethylamine dehydrogenase	6-(Cys)-FMN	TIM_barrel (Oxidored_FMN)	<i>Hyphomicrobium</i>
35	1.5.99.2	sarcosine dehydrogenase	8 α -(N3-His)-FAD	-----	ubiquitous
36	1.5.99.12	dimethylglycine dehydrogenase	8 α -(N3-His)-FAD	-----	ubiquitous
37	1.14.14.-	cytokinin dehydrogenase	8 α -(N1-His)-FAD	FAD_PCMH (FAD_binding_4)	plants
38	1.17.99.1	halogenase in chloramphenicol biosynthesis (CmlS)	8 α -(Asp)-FAD	NADP_Rossmann (Trp_halogenase)	<i>Streptomyces</i>
39*	1.21.3.3	4-cresol dehydrogenase (hydroxylating)	8 α -(O-Tyr)-FAD	FAD_PCMH (FAD_binding_4)	<i>Pseudomonas</i>
40	1.21.99.1	reticuline oxidase (berberine bridge enzyme)	8 α -(N1-His, 6-Cys)-FAD	FAD_PCMH (FAD_binding_4)	<i>Eschscholzia</i>
41*	1.-.-	β -cyclopirozate dehydrogenase	8 α -(N1-His)-FAD	-----	<i>Aspergillus</i>
42	-----	Δ^1 -tetrahydrocannabinolic acid synthase	8 α -(N1-His, 6-Cys)-FAD	FAD_PCMH (FAD_binding_4)	<i>Cannabis</i>
		redox driven ion pumps, RnfG and RnfD	ribitylphosphate- (O-Thr)-FMN	-----	<i>Vibrio</i>
		pollen allergens (BBE-like proteins)	8 α -(N1-His, 6-Cys)-FAD	FAD_PCMH (FAD_binding_4)	grasses

*predicted (Lefevink, N.G.H., Heuts, D.P.H.M., Fraaije, M.W., van Beekel, W.J.H.: The growing VAO flavoprotein family, Arch. Biochem. Biophys. 474:292-301, 2008)

^bpredicted from homology modeling (Gesell, A., Diaz Chavez, M.L., Kramell, R., Piotrowski, M., Macheroux, P., Kutchan, T.: Heterologous expression of two FAD-dependent oxidases with (S)-tetrahydroprotoberberine oxidase activity from *A. mexicana* and *B. wilsoniae*, Planta, 233:1185-1197, 2011)

The paradigm of bicovalent flavoenzymes: Berberine bridge enzyme (BBE) from *Eschscholzia californica*

BBE is a branch point enzyme in benzyloquinoline alkaloid biosynthesis [13]. It catalyzes the oxidative cyclization of (*S*)-reticuline to (*S*)-scoulerine and hence opens the way towards formation of protoberberine, protobine and benzophenanthridine alkaloids (Fig.1) [14, 15].

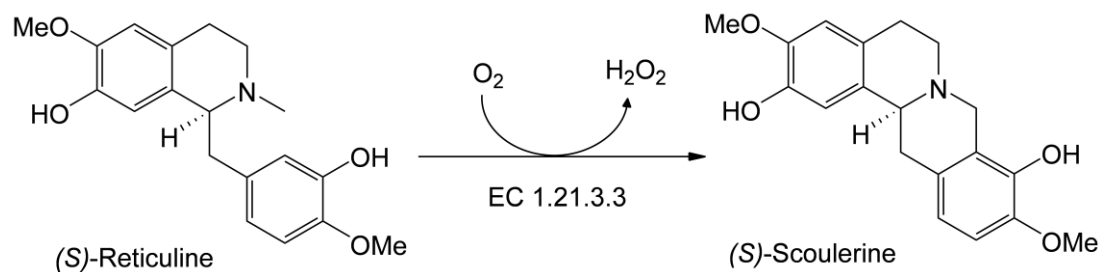


Figure 1: Overall reaction catalyzed by BBE.

The first isolation of the enzyme dates back to 1975, when Rink and Böhm reported the partial purification of BBE from *Macleaya microcarpa* cell cultures [16]. Subsequently Steffens *et al.* found BBE activity in 66 differentiated plants and cell suspension cultures, mainly from the families *Papaveraceae* and *Fumariaceae* [17]. Later the enzyme was successfully expressed in small amounts in insect cell culture and it was demonstrated that the FAD cofactor is covalently linked to a histidine residue via its 8 α -position [18]. During our studies with BBE, expressed in the methylotrophic host *Pichia pastoris*, we noticed that photoreduction of the enzyme yields 6-thio-FAD, a product known to form during photoreduction of 6-cysteinyl-flavins [19]. This observation prompted us to isolate the flavin-containing tryptic fragment and analyze its composition by amino acid sequencing and mass spectrometry [20]. This analysis clearly revealed that the FAD bears two peptides and we proposed that His104 and Cys166 forms a linkage to position 8 α and 6 of the flavin isoalloxazine ring system, respectively [20]. Later, the elucidation of the crystal structure confirmed our model of bicovalent cofactor attachment [14].

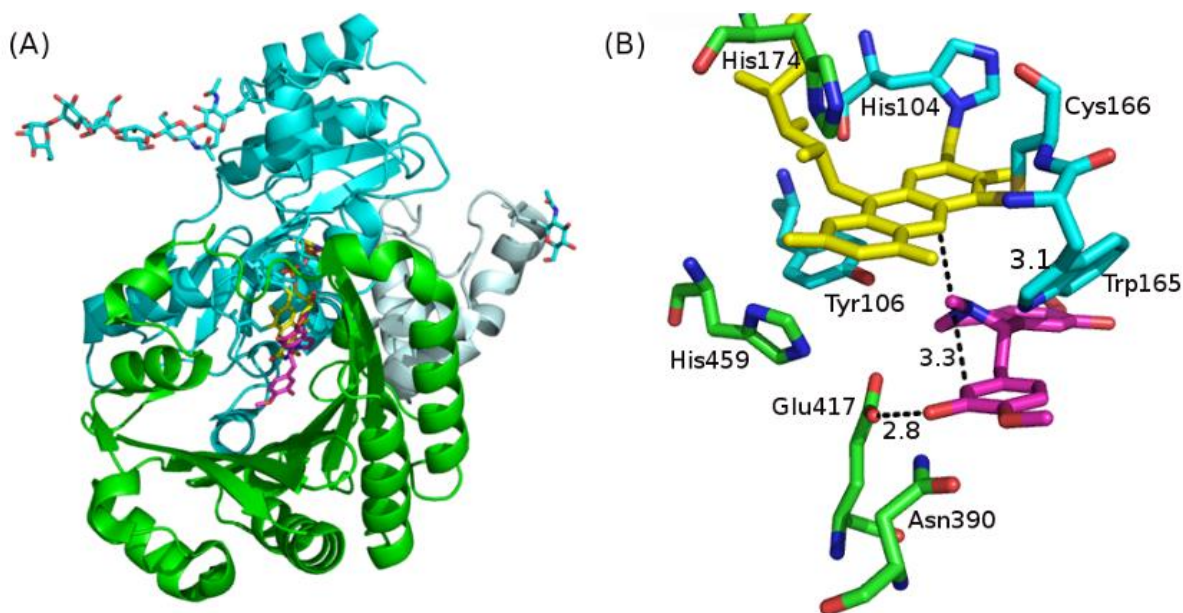


Figure 2: Schematic representation of the protein structure.

(A) Overall topology of BBE. The *N*-terminal FAD-binding subdomains are shown in cyan including the C-terminal α -helical stretch in pale blue. The central substrate binding domain is shown in green. N-linked sugar residues (blue), the FAD cofactor (yellow), and the substrate (*S*)-reticuline (magenta) are represented as stick models.

(B) Active site of BBE in complex with (*S*)-reticuline. The flavin cofactor is shown in yellow with its bicovalent linkage to His104 and Cys166. Important active site amino acid residues are drawn in stick representation. The substrate (*S*)-reticuline is shown in magenta. Distances are indicated in Å.

Not surprisingly, the structural topology turned out to be very similar to GOOX, which is also a member of the PCMH superfamily (clan FAD_binding_4). The structure is composed of a FAD and substrate binding domain, which is formed by a seven-stranded antiparallel β -sheet in an α/β domain [14] (Fig.2). It provided the ultimate proof for the bicovalent tethering of the flavin cofactor to His104 and Cys166 of the protein. The substrate (*S*)-reticuline is found in a relatively open substrate binding site sandwiched between the flavin cofactor and active site amino acid residues extending from the central β -sheet. The structure of BBE enabled a comprehensive mutagenesis program geared towards a better understanding of the mechanism for C-C bond formation. This program comprised the replacement of active site residues Glu417, Tyr106, and His459 with Gln, Phe, and Ala, respectively, and determination of kinetic parameters for all variant proteins (see Fig.2 for an active site representation of BBE) [14].

Eventually, these studies culminated in the formulation of a concerted reaction mechanism for the formation of the “berberine” bridge in the product (*S*)-scoulerine. In this mechanism, Glu417 acts as catalytic base by deprotonating the C3' hydroxy group of (*S*)-reticuline and thereby increases the nucleophilicity of the C2' atom, which further performs a S_N2- nucleophilic attack on the *N*-methyl group of the substrate. Thus the methylene bridge of (*S*)-scoulerine is formed and a hydride is transferred to the flavin cofactor (Fig.3) [14].

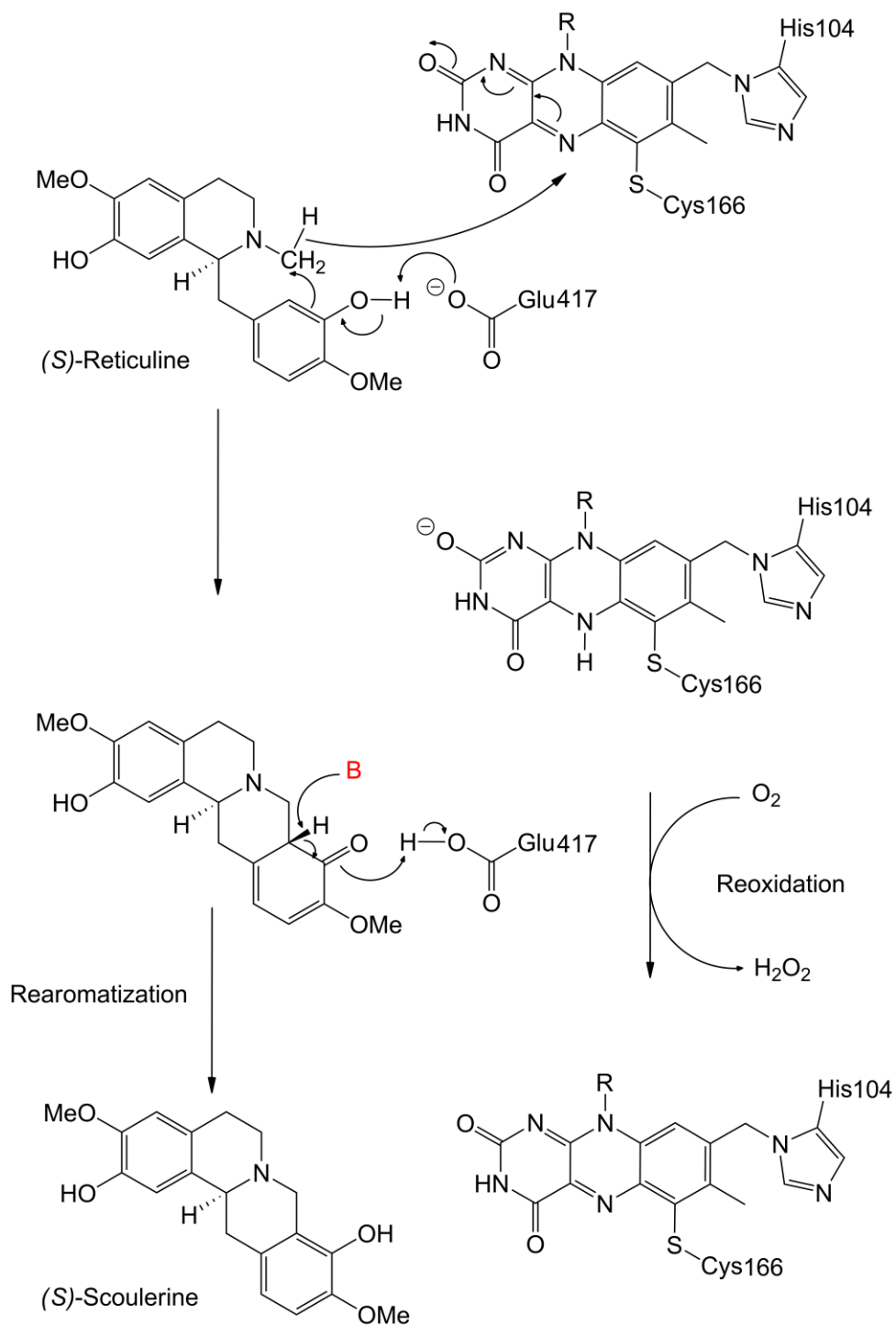


Figure 3: Concerted mechanism for BBE.

Single variant proteins with either His104 or Cys166 replaced by alanine were expressed and resulted in a decrease in midpoint potentials and k_{cat} -values compared to wild type BBE [12]. Thus bicovalent linkage in BBE increases the redox potential of the flavin cofactor and is crucial

for enzyme activity. Unfortunately, attempts to obtain the H104A/C166A double-variant failed presumably because covalent cofactor linkage is required for protein folding and/or stability [12].

Even before the first crystal structures of flavoproteins became available, the presence of a positive charge in vicinity to the N(1)-C(2)=O locus was suggested as a common feature of flavin-dependent oxidases [21-24]. Upon electron uptake the resulting negative charge at the N(1)-C(2)=O locus of the isoalloxazine ring system is stabilized by a positive environment [8, 25]. This property of flavin oxidases also leads to the stabilization of anionic flavin semiquinones, N(5)-sulfite adducts as well as the deprotonated forms of artificial flavins bearing an ionizable group at positions 6 or 8 (e.g. 6- or 8-mercaptoflavin) [21-23, 26-34, 34]. So far, investigations on different flavoproteins suggest that this charge can be supplied by either a positively charged amino acid residue, such as a histidine [35-37], lysine [27, 38-41], or arginine [42], or by the positive end of a helix dipole [8, 43-45]. BBE exhibits characteristic properties of flavoprotein oxidases, such as stabilization of the anionic semiquinone, or the ability to form N(5)-sulfite adducts, albeit with a dissociation constant that is notably higher than for other characterized flavin-dependent oxidases [46]. His174 was identified to be the respective amino acid in BBE supplying stabilization of transient negative charges. Interestingly, this residue does not directly interact with the N(1)-C(2)=O locus of the flavin, but forms a hydrogen bonding network via the C2' hydroxyl group of the ribityl side chain of the flavin. Exchange of His174 to Ala had a pronounced effect on the catalytic activity by decreasing k_{cat} 120-fold (Wallner *et al.* 2012 submitted).

Today, BBE is considered a paradigm of the entire family of enzymes as it is arguably one of the best characterized members. Our detailed understanding of the *E. californica* BBE has also led to the exploitation of the enzyme for the production of enantiomerically pure alkaloids with different pharmacological activities [47].

Recently Schrittwieser *et al.* applied BBE for the production of various (*S*)-berbines and (*R*)-benzylisoquinolines [48]. Berbines and benzylisoquinoline alkaloids are a related class of natural compounds [49] that share the isoquinoline heterocycle as a common structural feature (Fig.4).

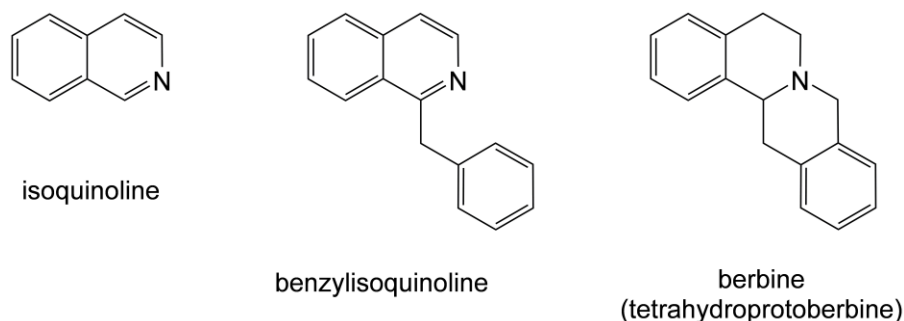


Figure 4: Structure of benzyloisoquinoline and berbine alkaloids.

Benzyloisoquinolines show a broad range of biological effects and are applied as pharmaceuticals with analgesic, sedative, hypnotic, antihypertensive, tranquilizing, or muscle relaxation activity [50-53]. Furthermore some 1-benzyl-1,2,3,4,-tetrahydroisoquinolines show *in vitro* anti-HIV activity making those compounds potential lead structures for the treatment of HIV patients [54]. Most berbine alkaloids show a relaxing effect on the central nervous system and hence are applied as potent sedatives [55]. Recently berbine derivatives are being investigated as drugs for the treatment of schizophrenia [56].

So far, there are several alkaloids with potential application as pharmaceuticals. However, the isolation of these alkaloids from their natural source is very time consuming and results in extremely low yields. Moreover, total organic synthesis of those chiral and complex alkaloids is inefficient and can not be accomplished with satisfactory enantiomeric excess [57-59].

Hence the biocatalytic approach of Schrittwieser *et al.* is an important step towards the production of enantiomerically pure (*S*)-berbines and (*R*)-benzyloisoquinolines [48]. A broad spectrum of substrates was investigated and it was shown that BBE accepts non-natural benzyloisoquinolines in (*S*)-configuration (Fig.5).

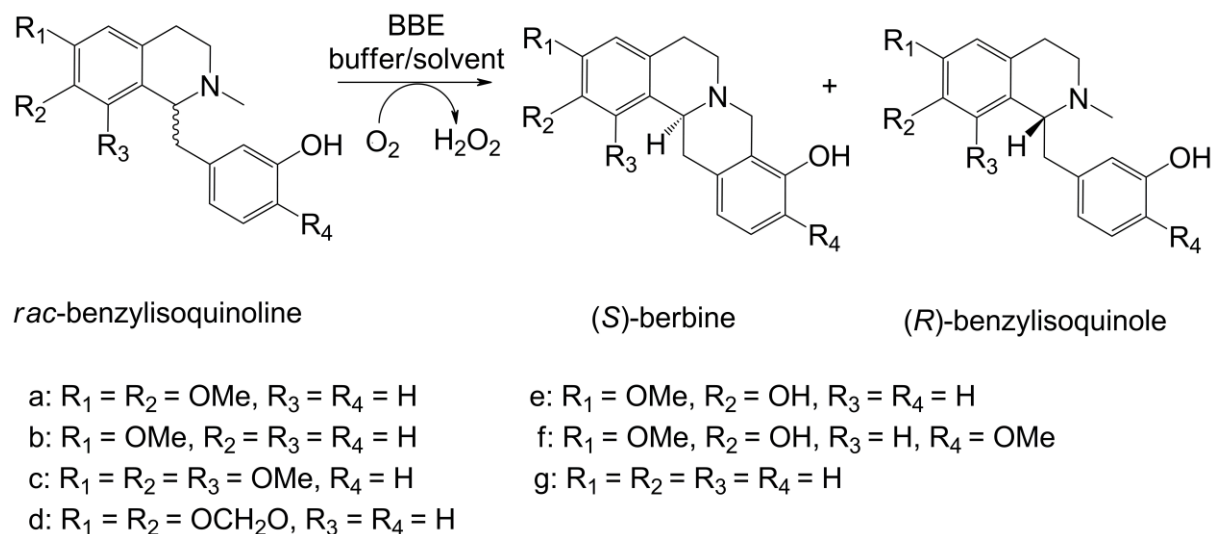


Figure 5: Kinetic resolution of racemic benzylisoquinolines catalysed by BBE.

Furthermore the reaction was optimized regarding pH, temperature and solvent [47, 60]. Due to the low solubility of benzylisoquinolines in aqueous buffer the use of cosolvents is required to allow substrate concentrations of at least 20 g L^{-1} . Interestingly, BBE exhibited an unexpectedly high tolerance towards different organic solvents with 70% v v^{-1} toluene being the best solvent concentration for efficient catalysis. High conversion rates can be achieved using pH values between 8 and 11 and a temperature from 30 to 50 °C. Using optimized reaction conditions the model reaction was performed in 500 mg scale with 50% conversion in 24 h giving enantiopure (*S*)-berbine ($ee > 97\%$) and (*R*)-benzylisoquinole ($ee > 97\%$) [60]. Moreover, the conversion of different racemic benzylisoquinolines was studied (Fig.5). In all cases the (*S*)-enantiomer of the respective benzylisoquinole was accepted as substrate resulting in the formation of (*S*)-berbines and (*R*)-benzylisoquinolines in optically pure form ($ee > 97\%$) and in good to excellent yield (22% - 50%).

It is noteworthy that BBE converts 1,2,3,4-tetrahydrobenzylisoquinolines mainly to 9-hydroxy functionalized products and not to the 11-hydroxy functionalized regioisomers. In a further study Resch *et al.* attempted to change regioselectivity of BBE by medium engineering and by blocking the “normal” reaction centre with a fluoro moiety. This proved to be an efficient strategy for completely changing regioselectivity leading to the formation of new 11-hydroxy functionalized products (Resch *et al.* 2012, submitted).

In conclusion, the studies with BBE as a potential industrial biocatalyst show that the enzyme can be successfully applied for the preparation of enantiomerically pure isoquinoline and berbine derivatives.

The family of BBE-like enzymes in the plant kingdom: how many and what for?

The group of BBE-like proteins is steadily increasing and sequence alignments provide strong evidence that a variety of plant proteins possess conserved histidine and cysteine residues for bivalent attachment of the cofactor. The availability of whole genomes for different plants enabled a targeted search of BBE-homologues in 26 plant species as shown in Tab.2. Using the Blast tool provided on the phytozome website (<http://www.phytozome.net/search.php>) many BBE-homologues could be identified in the available plant genomes. The highest number of BBE homologues was found in the poplar *Populus trichocarpa*, which possesses 57 BBE-like proteins. To our knowledge this plant does not accumulate complex alkaloids and hence BBE-like proteins in poplar seem to fulfil roles apart from alkaloid biosynthesis. Furthermore, our analysis revealed that a high number of BBE-homologues are also present in the orders of Fabales (e.g. soybean), Rutales (e.g. citrus fruits) and Brassicales (e.g. *Arabidopsis*), suggesting a high abundance of bivalent flavoproteins in the plant kingdom. Poales, such as rice, sorghum or maize, possess comparatively few BBE-homologue proteins, the same applies for grape. Finally, in mosses and algae BBE-like proteins seem to be rare (Tab.2).

Table 2: BBE-like proteins in various plant species & families.

Plant	Family	Common name	BBE-like homologues
<i>Populus trichocarpa</i>	<i>Salicaceae</i>	Western balsam poplar	57
<i>Glycine max</i>	<i>Fabaceae</i>	soybean	46
<i>Citrus clementina</i>	<i>Rutaceae</i>	clementine	39
<i>Prunus persica</i>	<i>Rosaceae</i>	peach	30
<i>Arabidopsis thaliana</i>	<i>Brassicaceae</i>	mouse-ear cress	28
<i>Arabidopsis lyrata</i>	<i>Brassicaceae</i>		27
<i>Eucalyptus grandis</i>	<i>Myrtaceae</i>	eucalyptus	27
<i>Mimulus guttatus</i>	<i>Scrophulariaceae</i>	common monkey-flower	25
<i>Citrus sinensis</i>	<i>Rutaceae</i>	orange	24
<i>Cucumis sativus</i>	<i>Cucurbitaceae</i>	cucumber	23
<i>Aquilegia coerulea</i>	<i>Ranunculaceae</i>	Rocky mountain columbine	18
<i>Medicago truncatula</i>	<i>Fabaceae</i>	barrel medic	18
<i>Manihot esculenta</i>	<i>Euphorbiaceae</i>	cassava (manioc)	17
<i>Zea mays</i>	<i>Poaceae</i>	maize	16
<i>Ricinus communis</i>	<i>Euphorbiaceae</i>	ricinus	15
<i>Setaria italica</i>	<i>Poaceae</i>	foxtail millet	13
<i>Sorghum bicolor</i>	<i>Poaceae</i>	sorghum	13
<i>Carica papaya</i>	<i>Caricaceae</i>	papaya	12
<i>Oryza sativa</i>	<i>Poaceae</i>	rice	11
<i>Brachypodium distachyon</i>	<i>Poaceae</i>	purple false brome	10
<i>Vitis vinifera</i>	<i>Vitaceae</i>	grape	5
<i>Physcomitrella patens</i>	<i>Funariaceae</i>		1
<i>Chlamydomonas reinhardtii</i>	<i>Chlamydomonadaceae</i>		0
<i>Selaginella moellendorffii</i>	<i>Selaginellaceae</i>		0
<i>Volvox carteri</i>	<i>Volvocaceae</i>		0

In addition to this bioinformatical analysis, there is also experimental evidence that flavoproteins from different plant sources possess both a covalent histidinyl- and cysteinyl- linkage of the cofactor [20, 61-65]. In plants bicovalent flavoproteins are involved in many different processes. They comprise oxidases in alkaloid biosynthesis (BBE, STOX) [20, 64], cannabinoid metabolism (THCA synthase) [66], or active plant defense (nectarin V, carbohydrate oxidases from *Helianthus annuus* and *Lactuca sativa*) [67, 68]. In the seaweed *Chondrus crispus* a BBE-like enzyme was found to catalyze the oxidation of a variety of hexose sugars [69-72]. A further group of bicovalently linked plant proteins is known to act as pollen allergens and is found in various grasses, such as timothy (Phl p 4) [65] or Bermuda grass (Cyn d 4, earlier referred to as BG60) [73].

In *Papaveraceae* bicovalently linked flavoproteins are reported to catalyze crucial oxidations in alkaloid biosynthesis. As discussed before, BBE catalyzes the oxidative formation of the methylene bridge of (*S*)-scoulerine in different poppy species [17, 74]. Moreover, (*S*)-tetrahydroprotoberberine oxidase (STOX) is described as a flavin containing oxidase accepting tetrahydroprotoberberines in (*S*)-configuration [75-77]. Due to the lack of a crystal structure of STOX there is no final evidence that the enzyme belongs to the family of bicovalent flavoproteins, however, homology modelling and a phylogenetic analysis strongly suggests that the flavin cofactor in STOX is also bicovalently bound [64]. The substrate specificity of STOX from *Argemone mexicana* and *Berberis wilsoniae* were investigated and both enzymes catalyze the oxidation of (*S*)-tetrahydropalmatine to palmatine (Fig.6) [64]. Additionally, (*S*)-scoulerine and (*S*)-canadine were accepted as substrates for STOX from *B. wilsoniae*, and STOX from *A. mexicana* converted (*S*)-coreximine, respectively [64]. Thus STOX is proposed to catalyze the oxidation of different tetrahydroprotoberberines in benzyloisoquinoline producing plants.

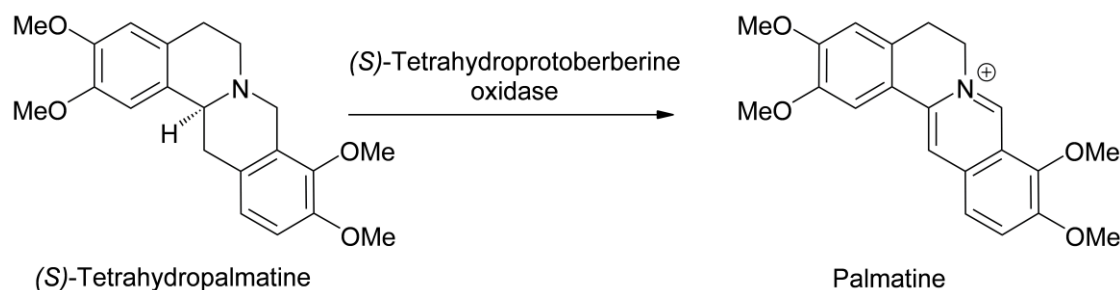


Figure 6: Conversion of (*S*)-tetrahydropalmatine by STOX.

Δ^1 -Tetrahydrocannabinolic acid (THCA) synthase was identified to be an important enzyme in controlling the psychoactivity of *Cannabis sativa* [66]. It catalyzes the oxidative cyclization of the monoterpene moiety of cannabigerolic acid (CBGA) into THCA, which further decarboxylates in a non-enzymatic fashion yielding THC as psychoactive compound (Fig.7) [66, 78]. Cannabinoids are exclusively found in *C. sativa* [79] and the pharmacological importance of these compounds [79-86] boosted investigations on THCA synthase [87]. Successful crystallization of THCA synthase was published in 2005 [61] and the elucidated structure clearly reveals that the enzyme belongs to the PCMH superfamily of flavoproteins with a bicovalent tethered cofactor as was already discussed previously for BBE (personal communication, R. Kuroki, Quantum Beam Science Directorate, Japan Atomic Energy Agency, Tokai, Japan).

THCA synthase catalyzes an oxidative ring closure reaction, which is similar to the berberine bridge formation. However, Shoyama *et al.* suggest a cationic mechanism for THCA synthase instead of the one-step concerted reaction found for BBE [61]. According to these authors, catalysis is initiated by a hydride transfer from the C-3 position of CBGA to the N-5 position of the isoalloxazine ring moiety of the FAD cofactor. The resulting carbocation then collapses to the product by nucleophilic attack of the oxyanion previously generated by proton abstraction. The reduced flavin is reoxidized by transferring a hydride to molecular oxygen resulting in the formation of hydrogen peroxide as a side product. (Fig.7) [66] So far, there is no evidence for the cationic mechanism and we rather suggest that the concerted mechanism of BBE might also be relevant for the C-C bond formation of Δ^1 -tetrahydrocannabinolic acid (THCA) synthase. It is noteworthy that BBE and THCA synthase exhibit substantial sequence similarities and that the crucial catalytic glutamate residue is present in both enzymes suggesting a similar path for catalysis in these two oxidases [14].

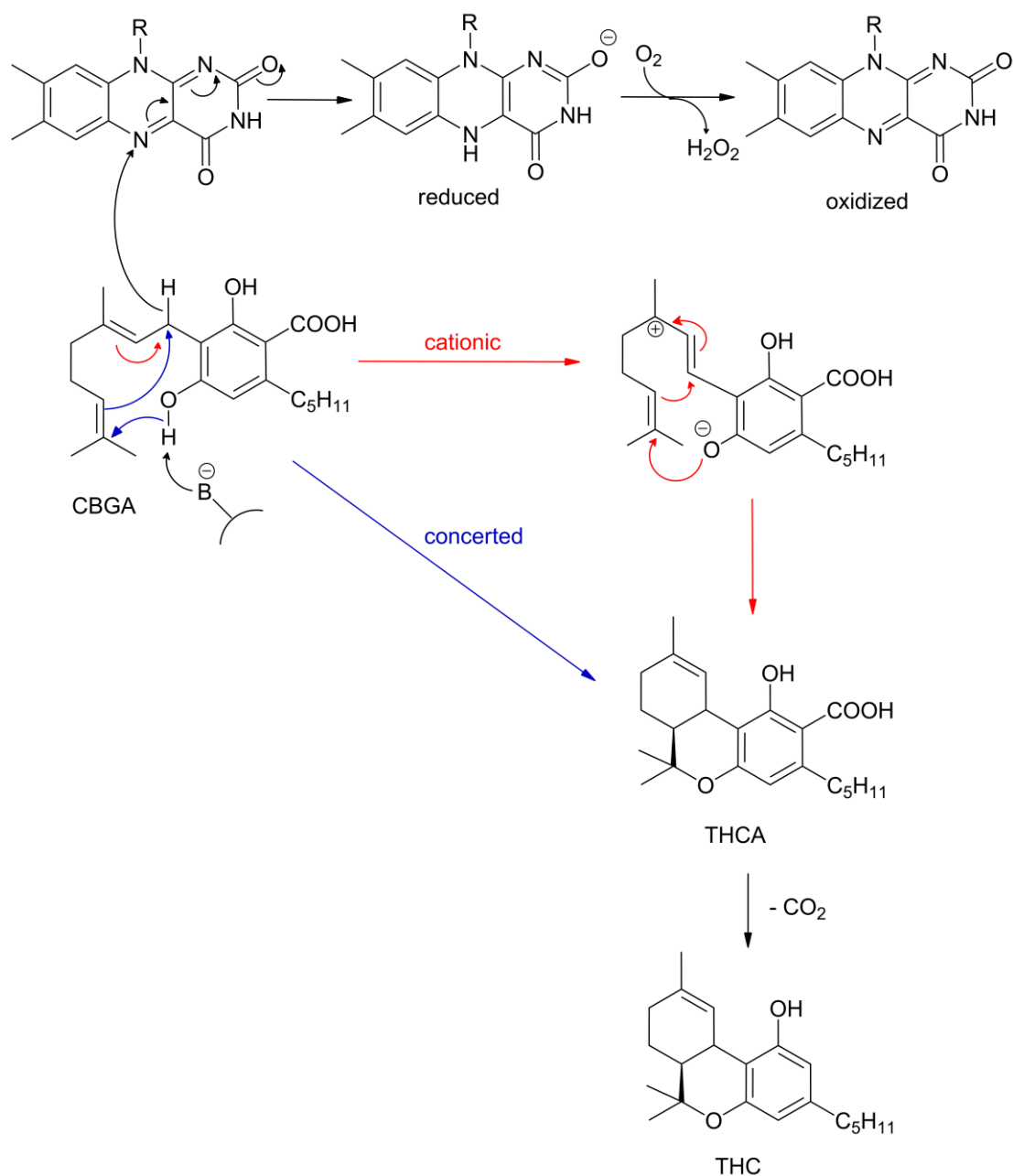


Figure 7: Proposed mechanism for THCA synthase. Two possible routes for THCA formation, which both are initiated by proton abstraction from CBGA. In the mechanism suggested by Sirikantaramas *et al.* (red arrows) a cationic intermediate is formed, which further cyclizes yielding THCA, which further undergoes non-enzymatic decarboxylations. We rather suggest a concerted mechanism (blue arrow) as was already reported for BBE. In both cases the reduced flavin is regenerated with molecular oxygen. [66]

Interestingly, not all bicovalent flavoproteins are involved in secondary metabolite production in plants. Nectarin V (NEC5) is a BBE-like enzyme and is expressed in the nectary gland of ornamental tobacco [62, 88]. The enzyme shows glucose oxidase activity by oxidizing glucose to

gluconolactone and hydrogen peroxide [62]. Hydrogen peroxide in turn seems to play a vital role in defense against microbial attack by preventing microbe contamination of the floral reproductive tract [67, 89-92]. There is also evidence that in contrast to the earlier discussed bicovalently flavinylated oxidases, NEC5 does not strictly depend on oxygen as electron acceptor for cofactor reoxidation. According to unpublished data of C. Carter and R.W. Thornburg mentioned in [67] dehydroascorbate is accepted instead of molecular oxygen resulting in flavin reoxidation and recycling of ascorbate from dehydroascorbate.

Enzymes involved in plant defense were also identified in other species, such as *H. annuus* (sunflower) or *L. sativa* (lettuce). Both plants express a carbohydrate oxidase with broad substrate specificity for the majority of mono- and disaccharides and with the production of H₂O₂ as a toxic reaction product [68].

Hexoses oxidase (HOX) from the seaweed *C. crispus* is another BBE-like enzyme accepting glucose as substrate [71]. However, this enzyme exhibits a broad substrate range compared to nectarin V. Besides glucose and galactose, HOX accepts various oligomeric sugars such as lactose, maltose, cellobiose and maltotriose as well as glucooligosaccharides with up to seven glucose units [71, 72].

For another group of BBE-like proteins no catalytic function could be identified up to now. These proteins are known to act as pollen allergens and they share the histidine and cysteine motifs for covalent flavinylation [65, 73]. Pollen allergens are generally found in different grasses and types of corn. BG60, later referred to as Cyn d 4, is described as a covalently flavinylated pollen allergen in Bermuda grass [73, 93]. Later, antigens with homology to BG60 were described to be present in celery (Api g 5) and in oilseed rape pollen [94-96]. Moreover, Phl p 4 was discovered in two isoforms in timothy grass [97] and later was identified as BBE-like protein [65]. The crystal structure of Phl p4 from *Phleum pratense* confirms the structural homology to BBE and bicovalent attachment of the FAD cofactor (pdb code 3tsh). Blast searches with the two experimentally determined full-length BBE-like pollen allergens BG60 and Phl p 4 resulted in the identification of four additional BBE-like proteins, namely Sec c 4, Hor v 5, Tri a 4 and Lol p 4 from rye, barley, wheat and perennial ryegrass, respectively. Except for Lol p 4 these proteins show almost the same size and show high sequence similarities.

These examples of characterized BBE-like enzymes already suggest that this group of bicovalently linked flavoproteins is involved in a variety of chemical reactions and biological functions. Thus it is obvious that specific enzyme functions cannot easily be predicted on the sole

basis of sequence homology and functional annotations should be performed carefully [98, 99]. This suggestion has been confirmed by various examples, where marginal or even single amino acid exchanges led to a distinct substrate specificity of the respective enzymes [100, 101]. For example, substrate specificity of ChitO from *F. graminearum* was completely changed by a single amino acid replacement in the active site of the enzyme leading to an increased acceptance of glucose and small oligosaccharides such as maltose or lactose [99]. However, we suggest that a comprehensive analysis of sequence homology and available biochemical data of already characterized bicovalent flavoproteins can result in reliable predictions of enzyme function, which can further be experimentally proven. One recent example for the practicability of a comprehensive theoretical analysis is the prediction of Gln268 in ChitO as active site residue involved in substrate recognition. Homology modelling of ChitO and a detailed comparison with the elucidated crystal structure of GOOX led to the correct identification of the respective residue [99]. Thus, here we present a detailed analysis of BBE homologues from *Arabidopsis thaliana*, which comprises both sequence homology and analysis of homology models in combination with structural and biochemical data available for BBE and GOOX.

To identify BBE-like enzymes in *A. thaliana* the sequence of BBE from *E. californica* was used for a Blastp search against the whole *Arabidopsis* genome. We found 28 BBE homologues in *A. thaliana*, which are encoded on chromosomes 1, 2, 4, and 5 (Tab.3). As a consequence of the identification of this unexpectedly high number of BBE homologues, the outstanding question has to be addressed whether *A. thaliana* can produce complex alkaloids or which alternative function these enzymes could adopt *in planta* (for a detailed review on this issue see [98]). It is known that *Arabidopsis* species accumulate simple alkaloids such as camalexin [102]. However, complex alkaloids have not been detected in this plant so far, which does not necessarily imply their absence in *Arabidopsis*. Toghe *et al.* describe the available chemical information regarding *Arabidopsis* metabolites as insufficient [103] and the recent discovery of volatile terpenoids in *A. thaliana* suggests the presence of a complex secondary metabolism thus lending credibility to the possible occurrence of yet undiscovered alkaloids in the plant [98, 104, 105]. Moreover, the identification of a plant efflux carrier with the ability for berberine transport [106] can be regarded as an indication for the presence of complex alkaloids in *Arabidopsis*.

Tab.3: Predicted active site residues in putative BBE-like proteins of *A. thaliana* through homology modelling.

Locus Name	Working Name	Accession Number	Comparison to Berberine Bridge Enzyme Active Site Residues								
			His104	Cys166	Glu417	Tyr106	His459	His174	Tyr456	Trp165	
AT1G01980.1	BBE-like 1	Q9LPC3	His	Cys	Gln	Tyr	Tyr	His	His	Tyr	Val
AT1G11770.1	BBE-like 2	Q9SA99	His	Cys	Gln	Tyr	Tyr	His	His	Tyr	Val
AT1G26380.1	BBE-like 3	Q9FZC4	His	Cys	Gln	Asn	Asn	His	His	Phe	Ile
AT1G26390.1	BBE-like 4	Q9FZC5	His	Cys	Gln	Tyr	Tyr	His	His	---	---
AT1G26400.1	BBE-like 5	Q9FZC6	His	Cys	Gln	Tyr	Tyr	His	His	Leu ^b	Val
AT1G26410.1	BBE-like 6	Q9FZC7	His	Cys	Gln	Asn	Asn	His	His	---	Val
AT1G26420.1	BBE-like 7	Q9FZC8	His	Cys	Gln	Leu	Leu	His	His	---	Val
AT1G30700.1	BBE-like 8	Q9SA85	His	Cys	Gln	Tyr	Tyr	His	His	Phe	Ile
AT1G30710.1	BBE-like 9	Q9SA86	His	Cys	Gln	Tyr	Tyr	His	His	---	Ile
AT1G30720.1	BBE-like 10	Q9SA87	His	Ser	Glu	Phe	Phe	His	His	---	Leu
AT1G30730.1	BBE-like 11	Q9SA88	His	Cys	Glu	Phe	Phe	His	His	---	Leu
AT1G30740.1	BBE-like 12	Q9SA89	His	Cys	Gln	Tyr	Tyr	His	His	Tyr	Val
AT1G30760.1	BBE-like 13	Q93ZA3	His	Cys	Gln	Tyr	Tyr	His	His	Tyr	Leu
AT1G34575.1	BBE-like 14	Q9LNL9	His	Cys	Gln	Tyr	Tyr	His	His	---	Ile
AT2G34790.1	BBE-like 15	O64743	His	Cys	Gln	Tyr	Tyr	His	His	---	Leu
AT2G34810.1	BBE-like 16	O64745	His	Cys	Glu	Tyr	Tyr	His	His	Phe	Val
AT4G20800.1	BBE-like 17	Q9SVG7	His	Cys	Gln	Tyr	Tyr	His	His	Phe	Val
AT4G20820.1	BBE-like 18	Q9SVG5	His	Cys	Gln	Tyr	Tyr	His	His	Leu	Val
AT4G20830.1 ^c	BBE-like 19	Q9SVG4	His	Cys	Gln	Tyr	Tyr	His	His	Tyr	Val
AT4G20830.2 ^c	BBE-like 20	Q9SVG4	His	Cys	Gln	Tyr	Tyr	His	His	Tyr	Val
AT4G20840.1	BBE-like 21	Q9SVG3	His	Cys	Gln	Tyr	Tyr	His	His	Tyr	Val
AT4G20860.1	BBE-like 22	Q9SUC6	His	Cys	Gln	Tyr	Tyr	His	His	---	Ile
AT5G44360.1	BBE-like 23	Q9FKV2	His	Cys	Gln	Tyr	Tyr	His	His	Tyr	Thr
AT5G44380.1	BBE-like 24	Q9FKV0	His	Cys	Leu	Phe	Phe	Tyr	Tyr	Tyr	Leu
AT5G44390.1	BBE-like 25	Q9FKU9	His	Tyr	Gln	Tyr	Tyr	His	His	Tyr	Val
AT5G44400.1	BBE-like 26	Q9FKU8	His	Cys	Gln	Tyr	Tyr	His	His	Tyr	Leu
AT5G44410.1	BBE-like 27	Q9FI25	His	Tyr	Gln	Tyr	Tyr	His	His	Phe	Leu
AT5G44440.1	BBE-like 28	Q9FI21	His	His	Gln	Tyr	Tyr	Gln	Gln	Phe	Ile

^a prediction of the respective active site residue not feasible due to different secondary structure elements in berberine bridge enzyme and the modelled homologue

^b prediction is not accurate since homology model of BBE-like 5 shows different secondary structure and is rather imprecise in the respective area

^c AT4G20830.1 and AT4G20830.2 represent two isoforms of the respective BBE-like protein in *A. thaliana*

We analyzed the 28 homologous proteins of *A. thaliana* using the YASARA modelling tool. These BBE homologues all possess a conserved histidine residue on the site corresponding to His104 of BBE, indicating a covalent 8 α -histidinyl linkage of the cofactor. Moreover, 24 out of 28 BBE homologues additionally possess the conserved cysteine residue for 6-*S*-cysteinylation; hence it appears that *A. thaliana* possesses 24 bicovalent flavoenzymes! The remaining four BBE homologous (BBE-like 10, 25, 27, and 28) feature a serine, tyrosine, or histidine residue at the position corresponding to Cys166 of BBE. So far, only 6-*S*-cysteinylation was reported for bicovalently linked flavoproteins; however, other modes of covalent cofactor tethering can not be ruled out. Whether these residues are capable of forming a covalent bond to C6 of the flavin cofactor in the respective protein has to be seen.

Moreover, the homology models were scanned for BBE active site residues, such as Glu417, which is the catalytic base necessary for carbon-carbon bond formation in BBE [14]. Tab.3 shows a compilation of predicted active site residues in the 28 BBE-like *Arabidopsis* proteins.

Interestingly, only three BBE-homologues, BBE-like proteins 10, 11 and 16, possess a glutamate residue at the respective site of Glu417 in BBE. Consequently, these proteins could possibly be involved in ring-closure reactions initiated by proton abstraction from the substrate by the catalytic glutamate residue. BBE-like 11 and BBE-like 16 show overall active site architectures which are highly similar to the structural environment in BBE suggesting that these enzymes could be involved in similar enzymatic reactions. BBE-like 10, however, possesses a serine residue in place of the cysteine required for cofactor attachment. Hence this serine residue could possibly influence the flavin cofactor in BBE-like 10 and modulate the redox potential for efficient catalysis by forming a hitherto uncharacterized novel covalent linkage or by influencing the electronic environment of the cofactor without covalent tethering.

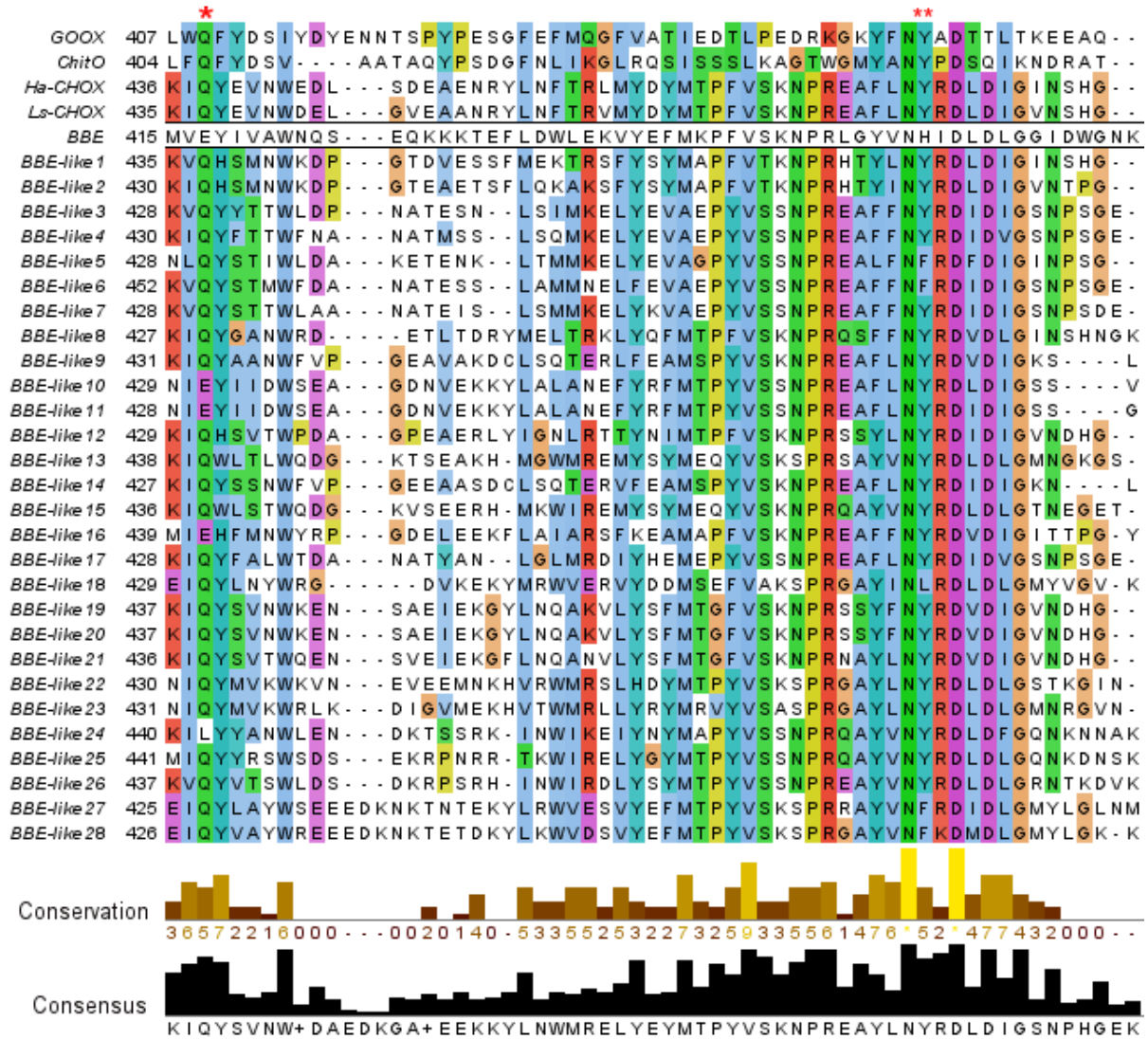


Figure 8: Multiple sequence alignment of characterized bicovalently flavinylated oxidases and 28 predicted BBE-like proteins from *A. thaliana* using ClustalW.

The sequence of BBE is displayed without colouring and the position of glutamate 417 is indicated (*). The conserved tyrosine residue in carbohydrate oxidases is indicated with **. Conserved amino acid residues are highlighted in coloured boxes. The amino acid sequences of following characterized oxidases were used: GOOX from *A. strictum* (AAS79317), ChitO from *F. graminearum* (XP_391174), carbohydrate oxidases from sunflower (AAL77103) and from lettuce (AAL77102) and BBE from *E. californica* (AC39358).

Except BBE-like 24 the remaining BBE-like proteins exhibit a glutamine residue at the position of Glu417 in BBE (Tab.3, Fig.8). Interestingly, multiple sequence alignments revealed that this active site glutamine residue is also present in characterized carbohydrate oxidases, such as GOOX (AAS79317), ChitO (XP_391174) and the carbohydrate oxidases from sunflower

(AAL77103) and lettuce (AAL77102). The proposed mechanism of GOOX suggests an active site tyrosine residue (Tyr429) as general base for catalysis, which initiates substrate conversion by proton abstraction from the OH¹ group of the sugar moiety [7, 107]. Multiple sequence alignments performed with ClustalW [108, 109] and analyzed in Jalview 2.7 [110] resulted in the finding that this tyrosine residue is strictly conserved in carbohydrate oxidases and hence might be a reliable predictor for enzymatic function. 23 out of 28 BBE homologues from *A. thaliana* possess this conserved tyrosine residue (Fig.8), which supports the idea that some BBE homologues in *A. thaliana* are in fact carbohydrate oxidases. In plants, carbohydrate oxidases seem to play a vital role in active plant defense due to their ability to form hydrogen peroxide as a product of enzymatic turnover [67, 68]. Thus it is conceivable that a portion of the BBE homologues in *Arabidopsis* acts as carbohydrate oxidases involved, for example in floral defense against pathogen attack (see before).

The occurrence of BBE-like enzymes in fungi

BBE-like enzymes are not restricted to the plant kingdom and are also found in fungi and bacteria. Elucidation of the crystal structure of GOOX from the fungus *Acremonium strictum* provided the first example of a bicovalently flavinylated oxidase [7] and ChitO from *F. graminearum* is a further well-investigated fungal BBE-like enzyme [10].

GOOX was first isolated from wheat bran cultures of *A. strictum* T1 by Lin *et al.* during screening experiments for novel glucooligosaccharide oxidases for application as industrial biocatalysts or diagnostic reagents for alternative carbohydrate assays [111, 112]. The enzyme was described as a flavoprotein catalyzing the oxidation of a variety of carbohydrates like glucose, maltose, lactose, and a variety of oligosaccharides composed of 1,4-linked D-glucopyranosyl residues [107, 111, 113]. The availability of the crystal structure of GOOX led to the discovery of the first bicovalent cofactor attachment. Moreover, it enabled the formulation of a reaction mechanism for GOOX and led to a deeper insight in the mode of substrate binding and substrate specificity [7]. As discussed previously for BBE, GOOX also belongs to the PCMH superfamily of flavoproteins and comprises a flavin- and a substrate-binding domain with an open carbohydrate binding groove allowing bulky oligosaccharide substrates to access the active site. The FAD cofactor is bicovalently attached to His70 and Cys130 of the enzyme and for GOOX this mode of cofactor linkage was reported to tune the redox potential for efficient catalysis, to contribute to flavin and substrate binding, and to increase protein stability [7, 11].

Tyr429 is activated by Asn355 through water-mediated hydrogen bonding and acts as general active site base crucial for catalysis [7, 107]. It initiates oxidation by subtracting a proton from the substrate thereby causing a direct transfer of a hydride to N(5) of the flavin isoalloxazine ring resulting in the formation of a lactone and reduced flavin [7]. The intermediate lactone spontaneously hydrolyses to the corresponding acid. Stabilization of the negative charge at the N(1)-C(2)=O locus of the isoalloxazine ring could be achieved by His138, Tyr426 and the backbone NH of Tyr144 [7]. The reduced flavin cofactor is reoxidized in a reaction with molecular oxygen (Fig.9).

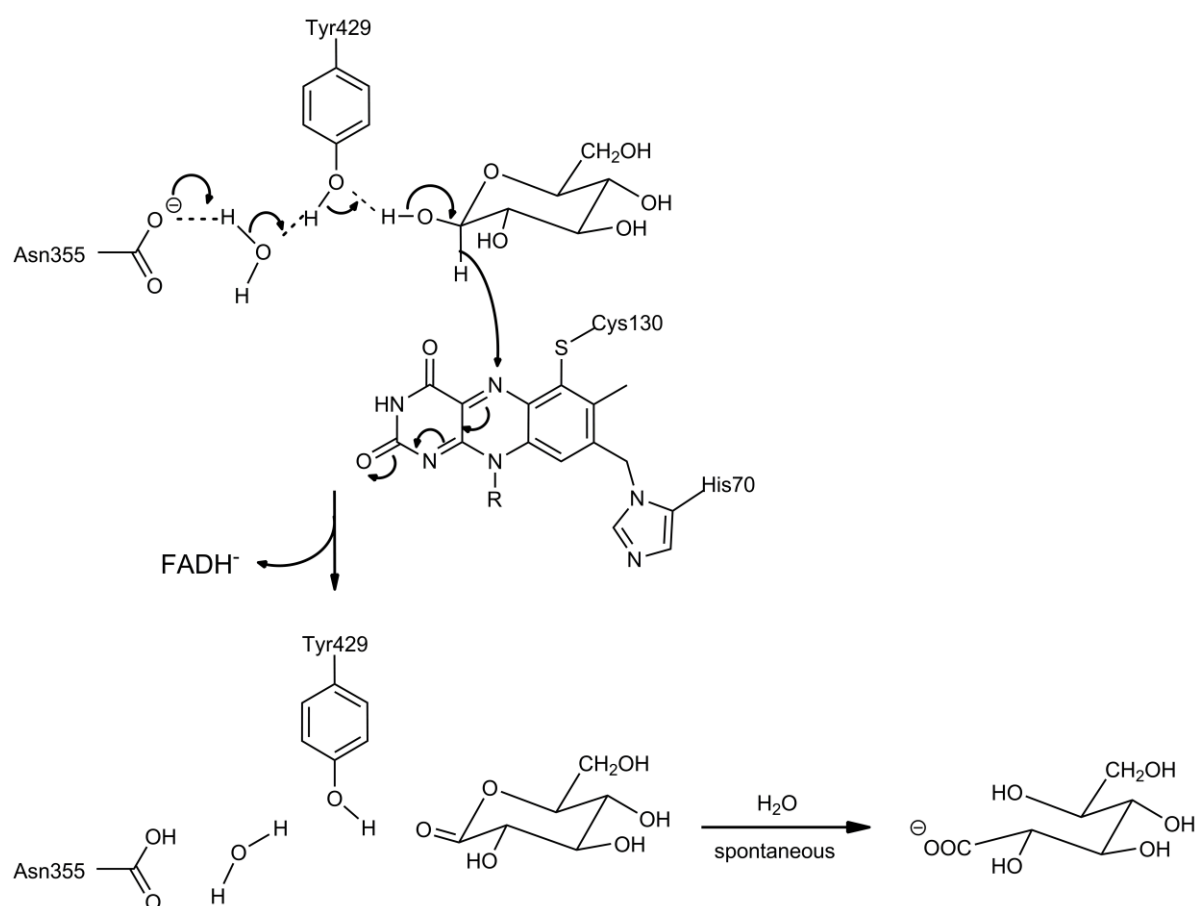


Figure 9: Proposed mechanism for GOOX.

Tyr429, which is activated by Asn355 via water mediated hydrogen bonding, subtracts a proton from the OH¹ group of the substrate thereby causing a direct transfer of a hydride to the N(5) atom of the flavin isoalloxazine ring. The resulting glucono-1,5-lactone spontaneously hydrolyzes to gluconic acid. The reduced flavin cofactor gets reoxidized by molecular oxygen. Fig.9 was modified according to [7].

Recently Foumani *et al.* reported the successful expression of a GOOX variant (GOOX-VN) from a different strain of *A. strictum* with altered substrate specificity [114]. This variant comprises fifteen amino acid substitutions compared to GOOX from *A. strictum* T1 leading to an improved substrate acceptance. Additionally to glucose, maltose, lactose, and oligosaccharides composed of 1,4-linked D-glucopyranosyl residues, GOOX-VN accepts galactose, and xylo-oligosaccharides with similar catalytic efficiency as for cello-oligosaccharides. This indicates that directed evolution on GOOX could lead to improved biocatalysts for oxidative modification of cello- and xylo-oligosaccharides [114].

Moreover, GOOX is of special interest since many hypothetical bicovalently linked flavoproteins show a tyrosine residue at the position corresponding to the catalytic Tyr429 in GOOX. Hence it is likely that these hypothetical proteins are carbohydrate oxidases with various functions in the respective organism (see discussion in previous section).

Blast searches against the non redundant protein sequence database on NCBI with GOOX or BBE as query resulted in the identification of a great number of putative bicovalently linked flavoprotein oxidases in fungi. Especially moulds and pathogenic fungi which affect plants or insects, were found to possess proteins homologous to BBE and GOOX. Blastp searches clearly revealed the high abundance of putative bicovalently flavinylated proteins among Ascomycota and Basidiomycota. Different *Aspergillus* species, such as *Aspergillus niger* or *Aspergillus oryzae*, and the basidiomycete *Melampsora laricis* possess with 9, 7, and 10 BBE-homologs the highest number of hypothetical bicovalently linked flavoproteins.

Heuts *et al.* identified six new glucooligosaccharide oxidase homologues with altered substrate preference [99, 107]. From these homologues a putative oxidase (XP_391174) from *F. graminearum* was selected for detailed investigations [10, 99]. Surprisingly, the new oxidase displayed a distinct substrate preference as compared to known oligosaccharide oxidases and catalyzed the regioselective oxidation of *N*-acetylated oligosaccharides leading to the name chitooligosaccharide oxidase. ChitO is a bicovalently linked flavoprotein belonging to the same structural class as GOOX or BBE. For ChitO, a glutamine (Gln268) was identified as active site residue responsible for recognition of the *N*-acetyl moiety. Thus, a Q268R mutant protein was prepared with Gln268 replaced with arginine, the amino acid found on the corresponding position in GOOX. Interestingly, this amino acid replacement had a drastic effect on the K_M value for all substrates leading to an increased acceptance of cello-oligosaccharides and a reduced conversion

rate for ChitO, which again suggests a possible application of site-directed mutagenesis for the production of improved oligosaccharide oxidases with tailored substrate specificity.

BBE-like enzymes in bacteria: oxidative power for the biosynthesis of antibiotics

In recent years the number of flavoenzymes possessing a bicovalently attached flavin cofactor has steadily risen in bacteria [70, 115-120]. In contrast to plants, none of the bacterial enzymes known so far are involved in cyclization reactions. Instead, the enzymes typically catalyze the oxidation of primary or secondary alcohol groups and the substrates are complex and bulky molecules. Furthermore, the reactions catalyzed by the enzymes are in biosynthetic pathways leading to antibiotics, such as aclacinomycin from *Streptomyces galileus* [115], glycopeptide A40926 (a teicoplanin homologue) from *Nonomuraea* sp. [117], tirandamycin [116, 118] and gilvocarcin V from *Streptomyces* sp. (Fig.10) [119, 121]. The first two reactions comprise a four electron oxidation, *i. e.* the FAD cofactor runs twice through the catalytic cycle of two electron reduction and reoxidation by molecular oxygen in the course of the reaction. Aclacinomycin oxidoreductase (AknOx) first oxidizes the alcohol group at C-4 of the terminal pyranose ring and in the second round of oxidation a C-C double bond is introduced between C-2 and C-3 thus yielding a α,β -unsaturated ketone (Fig.10, a). On the other hand, the reaction catalyzed by the hexose oxidase Dbv29 is a four electron oxidation of a primary alcohol group to a carboxylic acid at C-6 of the sugar moiety (Fig.10, b). In both cases, the enzyme acts on the carbohydrate moiety of the molecule rather than its aglycone. This is in contrast to the reactions in tirandamycin and gilvocarcin V biosynthesis where the oxidation concerns a secondary alcohol group. In the latter case, the oxidation yields a lactone in a complex polyketide molecule whereas the former reaction leads to a ketone group in the bicyclic ketal moiety of the antibiotic (Fig.10, c and d). It is noteworthy that in all of the reactions considered here, the flavoenzyme catalyzes one of the terminal reactions in the biosynthetic pathways, *i. e.* occurs at a stage where the skeleton of the target molecule is already established. This contrasts to the reactions catalyzed by BBE from *E. californica* and THCA synthase from *C. sativa* where the oxidation reaction is central to the generation of the carbon skeleton of the natural compound produced by these plants (compare Fig.1 and Fig.7).

Similarity searches against the non redundant protein database on NCBI resulted in the discovery of many putative BBE homologues in the bacterial kingdom. In various *Streptomyces* species BBE homologues are found, which according to sequence alignments possess the

conserved cysteine and histidine residue for bicovalent flavin attachment. These enzymes are suggested to be potential oxidoreductases, berberine bridge enzymes, FAD binding proteins, twin-arginine translocation pathway signal proteins and interestingly a relatively large number of BBE homologues in *Streptomyces* is defined as lipoproteins. A sequence alignment of these putative lipoproteins shows high sequence identity of these enzymes in different *Streptomyces* species. A similar search in the genomes of *Pseudomonas* failed to detect BBE homologues. Hence BBE-like enzymes are not uniformly distributed in eubacteria but appear to be present only in distinct genera. Apart from *Streptomyces*, BBE-like proteins were also found in *Bacillus*, *Mycobacterium*, *Ruegeria* and *Frankia* species.

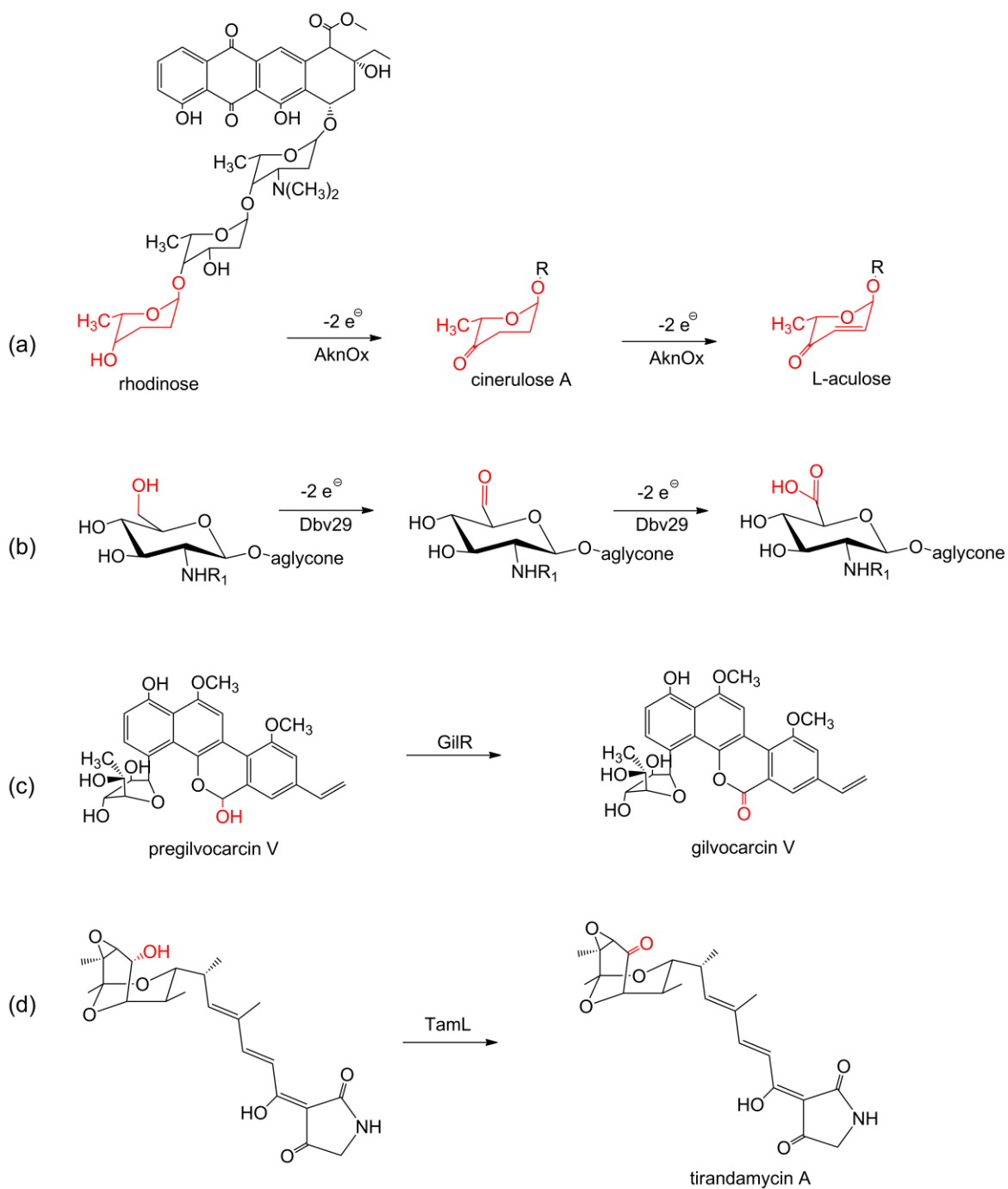


Figure 10: Reactions catalyzed by bicovalent flavoenzymes in the bacterial kingdom. Reactions catalyzed by (a) AknOx, aclacinomycin reductase from *Streptomyces galileus*, (b) Dbv29 from *Nonomuraea* sp., (c) GilR, pregilvocarcin V dehydrogenase from *Streptomyces*, and (d) TamL, 10-hydroxy-dehydrogenase in tirandamycin biosynthesis from *Streptomyces*.

Conclusions

In the last five years, bicovalent flavinylation has emerged as a novel mode of cofactor linkage. Currently, ~ 25% of covalently linked flavoenzymes feature bicovalent flavinylation, with a large number of bacterial, fungal and plant genes predicted to belong to this family of “BBE-like proteins”. So far, bicovalent flavin attachment is confined to bacteria, fungi, and plants, where some genera seem to be rich in bicovalent flavoproteins and others appear to have only a few members of this family. Bicovalent flavoproteins are totally absent from archaea and the animal kingdom. In nature, these enzymes adopt different roles in the metabolism of plants, fungi, and bacteria. In plants, bicovalent flavoenzymes catalyze complex cyclization reactions in natural product biosynthesis, such as alkaloids and terpenes. Moreover, these enzymes act as sugar and alcohol oxidases and thus fulfil different roles in the respective organism. As sugar oxidases bicovalent flavoproteins are involved in plant or fungal defense against pathogens and as alcohol oxidases they catalyze the final step(s) in antibiotic biosynthesis in bacteria. Hence these enzymes catalyze promising reactions with the potential to produce novel natural products and antibiotics in a biocatalytic setting.

References

- ADDIN RW.BIB**[1] Macheroux P, Kappes B, Ealick SE. Flavogenomics - a genomic and structural view of flavin-dependent proteins. *FEBS J* 2011;278:2625-34.
- [2] Singer TP, Kearney EB. *Biochem Biophys Acta* 1956;15:151.
- [3] Salach J, Walker WH, Singer TP, et al. Studies on succinate dehydrogenase. Site of attachment of the covalently-bound flavin to the peptide chain. *Eur J Biochem* 1972;26:267-78.
- [4] Kearney EB, Salach JI, Walker WH, et al. The covalently-bound flavin of hepatic monoamine oxidase. 1. Isolation and sequence of a flavin peptide and evidence for binding at the 8 α position. *Eur J Biochem* 1971;24:321-7.
- [5] McIntire W, Edmondson DE, Hopper DJ, Singer TP. 8 α -(O-tyrosyl)flavin adenine dinucleotide, the prosthetic group of bacterial *p*-cresol methylhydroxylase. *Biochemistry* 1981;20:3068-75.
- [6] Mewies M, McIntire WS, Scrutton NS. Covalent attachment of flavin adenine dinucleotide (FAD) and flavin mononucleotide (FMN) to enzymes: The current state of affairs. *Protein Science* 1998;7:7-20.
- [7] Huang CH, Lai WL, Lee MH, et al. Crystal structure of glucooligosaccharide oxidase from *Acremonium strictum*: A novel flavinylation of 6-S-cysteinyl, 8 α -N1-histidyl FAD. *J Biol Chem* 2005;280:38831-8.
- [8] Heuts DPHM, Scrutton NS, McIntire WS, Fraaije MW. What's in a covalent bond?: On the role and formation of covalently bound flavin cofactors. *FEBS J* 2009;276:3405-27.
- [9] Winkler A, Kutchan TM, Macheroux P. 6-S-cysteinylation of bi-covalently attached FAD in berberine bridge enzyme tunes the redox potential for optimal activity. *J Biol Chem* 2007;282:24437-43.
- [10] Heuts DPHM, Winter RT, Damsma GE, Janssen DB, Fraaije MW. The role of double covalent flavin binding in chito-oligosaccharide oxidase from *Fusarium graminearum*. *Biochem J* 2008;413:175-83.
- [11] Huang CH, Winkler A, Chen CL, et al. Functional roles of the 6-S-cysteinyl, 8 α -N1-histidyl FAD in glucooligosaccharide oxidase from *Acremonium strictum*. *J Biol Chem* 2008;283:30990-6.
- [12] Winkler A, Motz K, Riedl S, Puhl M, Macheroux P, Gruber K. Structural and mechanistic studies reveal the functional role of bicovalent flavinylation in berberine bridge enzyme. *J Biol Chem* 2009;284:19993-20001.
- [13] Kutchan TM. Molecular genetics of plant alkaloid biosynthesis. In: Cordell GA, ed. *The Alkaloids: Chemistry and Biology*. San Diego, CA, USA: Academic Press, 1998;50:257-316.

- [14] Winkler A, Łyskowski A, Riedl S, et al. A concerted mechanism for berberine bridge enzyme. *Nat Chem Biol* 2008;4:739-41.
- [15] Liscombe DK, Facchini PJ. Evolutionary and cellular webs in benzyloisoquinoline alkaloid biosynthesis. *Curr Opin Biotechnol* 2008;19:173-80.
- [16] Rink E, Bohm H. Conversion of reticuline into scoulerine by a cell free preparation from *Macleaya microcarpa* cell suspension cultures. *FEBS Lett* 1975;49:396-9.
- [17] Steffens P, Nagakura N, Zenk MH. Purification and characterization of the berberine bridge enzyme from *Berberis beaniana* cell cultures. *Phytochem* 1985;24:2577-83.
- [18] Kutchan TM, Dirtrich H. Characterization and mechanism of the berberine bridge enzyme, a covalently flavinylated oxidase of benzophenanthridine alkaloid biosynthesis in plants. *J Biol Chem* 1995;270:24475-81.
- [19] Ghisla S, Kenney WC, Knappe WR, McIntire W, Singer TP. Chemical synthesis and some properties of 6-substituted flavins. *Biochemistry* 1980;19:2537-44.
- [20] Winkler A, Hartner F, Kutchan TM, Glieder A, Macheroux P. Biochemical evidence that berberine bridge enzyme belongs to a novel family of flavoproteins containing a bi-covalently attached FAD cofactor. *J Biol Chem* 2006;281:21276-85.
- [21] Massey V, Ghisla S, Moore EG. 8-Mercaptoflavins as active site probes of flavoenzymes. *J Biol Chem* 1979;254:9640-50.
- [22] Fitzpatrick PF, Massey V. The reaction of 8-mercaptoflavins and flavoproteins with sulfite. Evidence for the role of an active site arginine in D-amino acid oxidase. *J Biol Chem* 1983;258:9700-5.
- [23] Massey V, Muller F, Feldberg R, et al. The reactivity of flavoproteins with sulfite. Possible relevance to the problem of oxygen reactivity. *J Biol Chem* 1969;244:3999-4006.
- [24] Massey V, Hemmerich P. Active-site probes of flavoproteins. *Biochem Soc Trans* 1980;8:246-57.
- [25] Fraaije MW, Mattevi A. Flavoenzymes: diverse catalysts with recurrent features. *Trends Biochem Sci* 2000;25:126-32.
- [26] Macheroux P, Kieweg V, Massey V, Soderlind E, Stenberg K, Lindqvist Y. Role of tyrosine 129 in the active site of spinach glycolate oxidase. *Eur J Biochem* 1993;213:1047-54.
- [27] Wagner MA, Trickey P, Che ZW, Mathews FS, Jorns MS. Monomeric sarcosine oxidase: 1. Flavin reactivity and active site binding determinants. *Biochemistry* 2000;39:8813-24.
- [28] Ohta-Fukuyama M, Miyake Y, Emi S, Yamano T. Identification and properties of the prosthetic group of choline oxidase from *Alcaligenes* sp. *J Biochem* 1980;88:197-203.

- [29] Gomez-Moreno C, Choy M, Edmondson DE. Purification and properties of the bacterial flavoprotein: thiamin dehydrogenase. *J Biol Chem* 1979;254:7630-5.
- [30] Bruhmuller M, Mohler H, Decker K. Covalently bound flavin in D-6-hydroxynicotine oxidase from *Arthrobacter oxidans*. *Z Naturforsch* 1972;27:1073-4.
- [31] Gadda G, Wels G, Pollegioni L, et al. Characterization of cholesterol oxidase from *Streptomyces hygroscopicus* and *Brevibacterium sterolicum*. *Eur J Biochem* 1997;250:369-76.
- [32] Muller F, Massey V. Flavin-sulfite complexes and their structures. *J Biol Chem* 1969;244:4007-16.
- [33] Gadda G, Fitzpatrick PF. Biochemical and physical characterization of the active FAD-containing form of nitroalkane oxidase from *Fusarium oxysporum*. *Biochemistry* 1998;37:6154-64.
- [34] Ghisla S, Massey V, Yagi K. Preparation and some properties of 6-substituted flavins as active site probes for flavin enzymes. *Biochemistry* 1986;25:3282-9.
- [35] Ghanem M, Gadda G. Effects of reversing the protein positive charge in the proximity of the flavin N(1) locus of choline oxidase. *Biochemistry* 2006;45:3437-47.
- [36] Hecht HJ, Kalisz HM, Hendle J, Schmid RD, Schomburg D. Crystal structure of glucose oxidase from *Aspergillus niger* refined at 2.3 Å resolution. *J Mol Biol* 1993;229:153-72.
- [37] Wohlfahrt G, Witt S, Hendle J, Schomburg D, Kalisz HM, Hecht HJ. 1.8 and 1.9 Å resolution structures of the *Penicillium amagasakiense* and *Aspergillus niger* glucose oxidases as a basis for modelling substrate complexes. *Acta Crystallogr D Biol Crystallogr* 1999;55:969-77.
- [38] Lindqvist Y, Branden CI. The active site of spinach glycolate oxidase. *J Biol Chem* 1989;264:3624-8.
- [39] Trickey P, Wagner MA, Jorns MS, Mathews FS. Monomeric sarcosine oxidase: Structure of a covalently flavinylated amine oxidizing enzyme. *Structure* 1999;7:331-45.
- [40] Muh U, Massey V, Williams Jr. CH. Lactate monooxygenase. I. Expression of the mycobacterial gene in *Escherichia coli* and site-directed mutagenesis of lysine 266. *J Biol Chem* 1994;269:7982-8.
- [41] Xia ZX, Mathews FS. Molecular structure of flavocytochrome b2 at 2.4 Å resolution. *J Mol Biol* 1990;212:837-63.
- [42] Efimov I, Cronin CN, Bergmann DJ, Kuusk V, McIntire WS. Insight into covalent flavinylation and catalysis from redox, spectral, and kinetic analyses of the R474K mutant of the flavoprotein subunit of *p*-cresol methylhydroxylase. *Biochemistry* 2004;43:6138-48.

- [43] Vrieling A, Lloyd LF, Blow DM. Crystal structure of cholesterol oxidase from *Brevibacterium sterolicum* refined at 1.8 Å resolution. *J Mol Biol* 1991;219:533-54.
- [44] Hallberg BM, Henriksson G, Pettersson G, Divne C. Crystal structure of the flavoprotein domain of the extracellular flavocytochrome cellobiose dehydrogenase. *J Mol Biol* 2002;315:421-34.
- [45] Mattevi A, Vanoni MA, Todone F, et al. Crystal structure of D-amino acid oxidase: a case of active site mirror-image convergent evolution with flavocytochrome b2. *Proc Natl Acad Sci U S A* 1996;93:7496-501.
- [46] Macheroux P, Massey V, Thiele DJ, Volokita M. Expression of spinach glycolate oxidase in *Saccharomyces cerevisiae*: purification and characterization. *Biochemistry* 1991;30:4612-9.
- [47] Schrittwieser JH, Resch V, Sattler JH, et al. Biocatalytic enantioselective oxidative C-C coupling by aerobic C-H activation. *Angew Chem Int Ed* 2011;50:1068-71.
- [48] Schrittwieser JH, Resch V, Wallner S, et al. Biocatalytic organic synthesis of optically pure (S)-scoulerine and berbine and benzyloisoquinoline alkaloids. *J Org Chem* 2011;76:6703-14.
- [49] Bentley KW. The isoquinoline alkaloids. Amsterdam, NL: Harwood Academic Publishers, 1998.
- [50] Eisenreich WJ, Hofner G, Bracher F. Alkaloids from *Croton flavens* L. and their affinities to GABA-receptors. *Nat Prod Res* 2003;17:437-40.
- [51] Gao JM, Liu WT, Li ML, Liu HW, Zhang XC, Li ZX. Preparation and structural elucidation of (-)-tetrahydroberberine-(+)-2,3-di(*p*-toluyl) tartaric acid complex. *J Mol Struct* 2008;892:466-9.
- [52] Martin ML, Diaz MT, Montero MJ, Prieto P, San Roman L, Cortes D. Antispasmodic activity of benzyloisoquinoline alkaloids analogous to papaverine. *Planta Med* 1993;59:63-7.
- [53] Chulia S, Ivorra MD, Lugnier C, Vila E, Noguera MA, D'Ocon P. Mechanism of the cardiovascular activity of laudanosine: comparison with papaverine and other benzyloisoquinolines. *Br J Pharmacol* 1994;113:1377-85.
- [54] Kashiwada Y, Aoshima A, Ikeshiro Y, et al. Anti-HIV benzyloisoquinoline alkaloids and flavonoids from the leaves of *Nelumbo nucifera*, and structure-activity correlations with related alkaloids. *Bioorg Med Chem* 2005;13:443-8.
- [55] Yamahara J, Konoshima T, Sakakibara Y, Ishiguro M, Sawada T. Central depressant action of tetrahydroberberine and its derivatives. *Chem Pharm Bull* 1976;24:1909-12.
- [56] Li J, Jin G, Shen J, Ji R. 1-Chloroscoulerine mesylate. *Drugs Future* 2006;31:379-84.

- [57] Barton DH, Kirby GW, Steglich W, et al. Investigations on the biosynthesis of morphine Alkaloids. *J Chem Soc* 1965;65:2423-38.
- [58] Chrzanowska M, Rozwadowska MD. Asymmetric synthesis of isoquinoline alkaloids. *Chem Rev* 2004;104:3341-70.
- [59] Matulenko MA, Meyers AI. Total synthesis of (-)-tetrahydropalmatine via chiral formamidine carbanions: unexpected behavior with certain ortho-substituted electrophiles. *J Org Chem* 1996;61:573-80.
- [60] Resch V, Schrittwieser JH, Wallner S, Macheroux P, Kroutil W. Biocatalytic oxidative C-C bond formation catalysed by the berberine bridge enzyme: Optimal reaction conditions. *Adv Synth Catal* 2011;353:2377-83.
- [61] Shoyama Y, Takeuchi A, Taura F, et al. Crystallization of Δ^1 -tetrahydrocannabinolic acid (THCA) synthase from *Cannabis sativa*. *Acta Crystallogr Sect F Struct Biol Cryst Commun* 2005;61:799-801.
- [62] Carter CJ, Thornburg RW. Tobacco nectarin V is a flavin-containing berberine bridge enzyme-like protein with glucose oxidase activity. *Plant Physiol* 2004;134:460-9.
- [63] Nandy A, Petersen A, Wald M, et al. Primary structure, recombinant expression, and molecular characterization of Phl p 4, a major allergen of timothy grass (*Phleum pratense*). *Biochem Biophys Res Commun* 2005;337:563-70.
- [64] Gesell A, Chávez MLD, Kramell R, Piotrowski M, Macheroux P, Kutchan TM. Heterologous expression of two FAD-dependent oxidases with (*S*)-tetrahydroprotoberberine oxidase activity from *Argemone mexicana* and *Berberis wilsoniae* in insect cells. *Planta* 2011;233:1185-97.
- [65] Dewitt AM, Andersson K, Peltre G, Lidholm J. Cloning, expression and immunological characterization of full-length timothy grass pollen allergen Phl p 4, a berberine bridge enzyme-like protein with homology to celery allergen Api g 5. *Clin Exp Allergy* 2006;36:77-86.
- [66] Sirikantaramas S, Morimoto S, Shoyama Y, et al. The gene controlling marijuana psychoactivity. Molecular cloning and heterologous expression of Δ^1 -tetrahydrocannabinolic acid synthase from *Cannabis sativa* L. *J Biol Chem* 2004;279:39767-74.
- [67] Carter C, Thornburg RW. Is the nectar redox cycle a floral defense against microbial attack? *Trends Plant Sci* 2004;9:320-4.
- [68] Custers JH, Harrison SJ, Sela-Buurlage MB, et al. Isolation and characterisation of a class of carbohydrate oxidases from higher plants, with a role in active defence. *Plant J* 2004;39:147-60.
- [69] Hansen OC, Stougaard P. Hexose oxidase from the red alga *Chondrus crispus*. Purification, molecular cloning, and expression in *Pichia pastoris*. *J Biol Chem* 1997;272:11581-7.

- [70] Rand T, Qvist KB, Walter CP, Poulsen CH. Characterization of the flavin association in hexose oxidase from *Chondrus crispus*. FEBS J 2006;273:2693-703.
- [71] Poulsen C, Høstrup PB. Purification and characterization of a hexose oxidase with excellent strengthening effects in bread. Cereal Chem 1998;75:51-7.
- [72] Van der Lugt JP. Evaluation of methods for chemical and biological carbohydrate oxidation. Delft, NL: Delft University of Technology 1998:1-148.
- [73] Liaw SH, Lee DY, Chow LP, Lau GX, Su SN. Structural characterization of the 60-kDa Bermuda grass pollen isoallergens, a covalent flavoprotein. Biochem Biophys Res Commun 2001;280:738-43.
- [74] Steffens P, Nagakura N, Zenk MH. The berberine bridge forming enzyme in tetrahydroprotoberberine biosynthesis. Tetrahedron Lett 1984;25:951-2.
- [75] Amann M, Nagakura N, Zenk MH. (S)-tetrahydroprotoberberine oxidase the final enzyme in protoberberine biosynthesis. Tetrahedron Lett 1984;25:953-4.
- [76] Amann M, Nagakura N, Zenk MH. Purification and properties of (S)-tetrahydroprotoberberine oxidase from suspension-cultured cells of *Berberis wilsoniae*. Eur J Biochem 1988;175:17-25.
- [77] Chou WM, Kutchan TM. Enzymatic oxidations in the biosynthesis of complex alkaloids. Plant J 1998;15:289-300.
- [78] Taura F, Morimoto S, Shoyama Y, Mechoulam R. First direct evidence for the mechanism of Δ^1 -tetrahydrocannabinolic acid biosynthesis. J Am Chem Soc 1995;117 (38):9766-7.
- [79] Turner CE, Elsohly MA, Boeren EG. Constituents of *Cannabis sativa* L. XVII. A review of the natural constituents. J Nat Prod 1980;43:169-234.
- [80] Pertwee RG. Cannabinoid pharmacology: the first 66 years. Br J Pharmacol 2006;147 Suppl 1:S163-71.
- [81] Pertwee RG. Pharmacological actions of cannabinoids. Handb Exp Pharmacol 2005;168:1-51.
- [82] Pertwee RG. The pharmacology of cannabinoid receptors and their ligands: an overview. Int J Obes 2006;30 Suppl 1:13-8.
- [83] Pertwee RG. Cannabinoids and multiple sclerosis. Mol Neurobiol 2007;36:45-59.
- [84] Grotenhermen F. Cannabinoids. Curr Drug Targets CNS Neurol Disord 2005;4:507-30.
- [85] Guzman M. Cannabinoids: potential anticancer agents. Nat Rev Cancer 2003;3:745-55.

- [86] Baker D, Pryce G, Giovannoni G, Thompson AJ. The therapeutic potential of cannabis. *Lancet Neurol* 2003;2:291-8.
- [87] Taura F, Dono E, Sirikantaramas S, Yoshimura K, Shoyama Y, Morimoto S. Production of Δ^1 -tetrahydrocannabinolic acid by the biosynthetic enzyme secreted from transgenic *Pichia pastoris*. *Biochem Biophys Res Commun* 2007;361:675-80.
- [88] Carter C, Graham RA, Thornburg RW. Nectarin I is a novel, soluble germin-like protein expressed in the nectar of *Nicotiana* sp. *Plant Mol Biol* 1999;41:207-16.
- [89] Chamnongpol S, Willekens H, Moeder W, et al. Defense activation and enhanced pathogen tolerance induced by H₂O₂ in transgenic tobacco. *Proc Natl Acad Sci U S A* 1998;95:5818-23.
- [90] Bolwell GP, Wojtaszek P. Mechanisms for the generation of reactive oxygen species in plant defence - A broad perspective. *Physiol Mol Plant Pathol* 1997;51 (6):347-66.
- [91] Wu G, Shortt BJ, Lawrence EB, Levine EB, Fitzsimmons KC, Shah DM. Disease resistance conferred by expression of a gene encoding H₂O₂-generating glucose oxidase in transgenic potato plants. *Plant Cell* 1995;7:1357-68.
- [92] Wojtaszek P. Oxidative burst: an early plant response to pathogen infection. *Biochem J* 1997;322:681-92.
- [93] Liaw SH, Lee DY, Yang SY, Su SN. Crystallization and preliminary diffraction data of 60-kDa glycosylated pollen isoallergens from Bermuda grass. *J Struct Biol* 1999;127:83-7.
- [94] Ganglberger E, Radauer C, Grimm R, et al. N-terminal sequences of high molecular weight allergens from celery tuber. *Clin Exp Allergy* 2000;30:566-70.
- [95] Bublin M, Radauer C, Wilson IB, et al. Cross-reactive N-glycans of Api g 5, a high molecular weight glycoprotein allergen from celery, are required for immunoglobulin E binding and activation of effector cells from allergic patients. *FASEB J* 2003;17:1697-9.
- [96] Chardin H, Mayer C, Senechal H, Tepfer M, Desvaux FX, Peltre G. Characterization of high-molecular-mass allergens in oilseed rape pollen. *Int Arch Allergy Immunol* 2001;125:128-34.
- [97] Fischer S, Grote M, Fahlbusch B, Müller WD, Kraft D, Valenta R. Characterization of Phl p 4, a major timothy grass (*Phleum pratense*) pollen allergen. *J Allergy Clin Immunol* 1996;98:189-98.
- [98] Facchini PJ, Bird DA, St-Pierre B. Can *Arabidopsis* make complex alkaloids? *Trends Plant Sci* 2004;9:116-22.
- [99] Heuts DPHM, Janssen DB, Fraaije MW. Changing the substrate specificity of a chitoooligosaccharide oxidase from *Fusarium graminearum* by model-inspired site-directed mutagenesis. *FEBS Lett* 2007;581:4905-9.

- [100] Frick S, Kutchan TM. Molecular cloning and functional expression of *O*-methyltransferases common to isoquinoline alkaloid and phenylpropanoid biosynthesis. *Plant J* 1999;17:329-39.
- [101] Frey M, Chomet P, Glawischnig E, et al. Analysis of a chemical plant defense mechanism in grasses. *Science* 1997;277:696-9.
- [102] Tsuji J, Jackson EP, Gage DA, Hammerschmidt R, Somerville SC. Phytoalexin accumulation in *Arabidopsis thaliana* during the hypersensitive reaction to *Pseudomonas syringae* pv *syringae*. *Plant Physiol* 1992;98:1304-9.
- [103] Tohge T, Yonekura-Sakakibara K, Niida R, Watanabe-Takahashi A, Saito K. Phytochemical genomics in *Arabidopsis thaliana*: A case study for functional identification of flavonoid biosynthesis genes. *Pure Appl Chem* 2007;79:811-23.
- [104] Chen F, Tholl D, D'Auria JC, Farooq A, Pichersky E, Gershenzon J. Biosynthesis and emission of terpenoid volatiles from *Arabidopsis flowers*. *Plant Cell* 2003;15:481-94.
- [105] Aharoni A, Giri AP, Deuerlein S, et al. Terpenoid metabolism in wild-type and transgenic *Arabidopsis* plants. *Plant Cell* 2003;15:2866-84.
- [106] Li L, He Z, Pandey GK, Tsuchiya T, Luan S. Functional cloning and characterization of a plant efflux carrier for multidrug and heavy metal detoxification. *J Biol Chem* 2002;277:5360-8.
- [107] Lee MH, Lai WL, Lin SF, Hsu CS, Liaw SH, Tsai YC. Structural characterization of glucooligosaccharide oxidase from *Acremonium strictum*. *Appl Environ Microbiol* 2005;71:8881-7.
- [108] Larkin MA, Blackshields G, Brown NP, et al. Clustal W and Clustal X version 2.0. *Bioinformatics* 2007;23:2947-8.
- [109] Goujon M, McWilliam H, Li W, et al. A new bioinformatics analysis tools framework at EMBL-EBI. *Nucleic Acids Res* 2010;38:695-9.
- [110] Waterhouse AM, Procter JB, Martin DM, Clamp M, Barton GJ. Jalview Version 2 - a multiple sequence alignment editor and analysis workbench. *Bioinformatics* 2009;25:1189-91.
- [111] Lin SF, Yang TY, Inukai T, Yamasaki M, Tsai YC. Purification and characterization of a novel glucooligosaccharide oxidase from *Acremonium strictum* T1. *Biochim Biophys Acta* 1991;1118:41-7.
- [112] Lin SF, Hu HM, Inukai T, Tsai YC. Production of novel oligosaccharide oxidase by wheat bran solid-state fermentation. *Biotechnol Adv* 1993;11:417-27.
- [113] Fan Z, Oguntimein GB, Reilly PJ. Characterization of kinetics and thermostability of *Acremonium strictum* glucooligosaccharide oxidase. *Biotechnol Bioeng* 2000;68:231-7.

- [114] Foumani M, Vuong TV, Master ER. Altered substrate specificity of the gluco-oligosaccharide oxidase from *Acremonium strictum*. *Biotechnol Bioeng* 2011;108:2261-9.
- [115] Alexeev I, Sultana A, Mäntsälä P, Niemi J, Schneider G. Aclacinomycin oxidoreductase (AknOx) from the biosynthetic pathway of the antibiotic aclacinomycin is an unusual flavoenzyme with a dual active site. *Proc Natl Acad Sci U S A* 2007;104:6170-5.
- [116] Carlson JC, Li S, Gunatilleke SS, et al. Tirandamycin biosynthesis is mediated by co-dependent oxidative enzymes. *Nature Chem* 2011;3:628-33.
- [117] Li YS, Ho JY, Huang CC, et al. A unique flavin mononucleotide-linked primary alcohol oxidase for glycopeptide A40926 maturation. *J Am Chem Soc* 2007;129:13384-5.
- [118] Mo X, Huang H, Ma J, et al. Characterization of TrdL as a 10-hydroxy dehydrogenase and generation of new analogues from a tirandamycin biosynthetic pathway. *Org Lett* 2011;13:2212-5.
- [119] Noinaj N, Bosserman MA, Schickli MA, et al. The crystal structure and mechanism of an unusual oxidoreductase, GilR, involved in gilvocarcin V biosynthesis. *J Biol Chem* 2011;286:23533-43.
- [120] Abad S, Nahalka J, Bergler G, et al. Stepwise engineering of a *Pichia pastoris* D-amino acid oxidase whole cell catalyst. *Microb Cell Fact* 2010;9:24.
- [121] Kharel MK, Pahari P, Lian H, Rohr J. GilR, an unusual lactone-forming enzyme involved in gilvocarcin biosynthesis. *ChemBioChem* 2009;10:1305-8.

Chapter 2: Oxidation of monolignols by members of the berberine bridge enzyme family suggests a role in plant cell wall metabolism

Bastian Daniel,¹ Tea Pavkov-Keller,^{2,3} Barbara Steiner,¹ Anđela Dordic,^{2,3} Alexander Gutmann,⁴ Bernd Nidetzky,⁴ Christoph W. Sensen,⁵ Eric van der Graaff,⁶ Silvia Wallner,¹ Karl Gruber² and Peter Macheroux^{1*†}

¹From Graz University of Technology, Institute of Biochemistry, Graz, Austria

²University of Graz, Institute of Molecular Biosciences, Graz, Austria

³ACIB GmbH, Graz, Austria

⁴Graz University of Technology, Institute of Biotechnology and Biochemical Engineering, Graz, Austria

⁵Graz University of Technology, Institute of Molecular Biotechnology, Graz, Austria

⁶Copenhagen University, Copenhagen, Denmark

To whom correspondence should be addressed: Peter Macheroux, Graz University of Technology, Institute of Biochemistry, Petersgasse 12/II, A-8010 Graz, Austria, Tel.: +43-316-873 6450, Fax: +43-316-873 6952; Email: peter.macheroux@tugraz.at

This chapter was published in the Journal of Biological Chemistry:

Daniel, B. *et al.*: Oxidation of Monolignols by Members of the Berberine Bridge Enzyme Family Suggests a Role in Plant Cell Wall Metabolism. J Biol Chem ; 290(30), 18770-18781

Author contributions

B.D., K.G. and P.M. initiated and designed the research; B.D., B.S. and S.W. carried out biochemical research; A.G. and B.N. synthesized glycosylated monolignol derivatives; A.D., T.P.-K., B.D. and K.G. crystallised proteins and solved the X-ray crystal structure; B.D., C.S. and E.v.d.G performed phylogenetic analysis and evaluated the data; B.D. E.v.d.G., K.G. and P.M. wrote the manuscript.

Abstract

Plant genomes contain a large number of genes encoding for berberine bridge enzyme (BBE)-like enzymes. Despite the widespread occurrence and abundance of this protein family in the plant kingdom, the biochemical function remains largely unexplored. In this study we have expressed two members of the BBE-like enzyme family from *Arabidopsis thaliana* in the host organism *Komagataella pastoris*. The two proteins, termed *AtBBE*-like 13 and *AtBBE*-like 15, were purified and their catalytic properties were determined. In addition, *AtBBE*-like 15 was crystallized and structurally characterized by X-ray crystallography. Here, we show that the enzymes catalyze the oxidation of aromatic allylic alcohols, such as coumaryl-, sinapyl-, and coniferyl alcohol, to the corresponding aldehydes and that *AtBBE*-like 15 adopts the same fold as vanillyl alcohol oxidase as previously reported for berberine bridge enzyme and other FAD-dependent oxidoreductases. Further analysis of the substrate range identified coniferin, the glycosylated storage form of coniferyl alcohol, as a substrate of the enzymes whereas other glycosylated monolignols were rather poor substrates. A detailed analysis of the motifs present in the active sites of the BBE-like enzymes in *A. thaliana*, suggested that 13 out of 28 members of the family might catalyze similar reactions. Based on these findings, we propose a novel role of BBE-like enzymes in monolignol metabolism that was previously not recognized for this enzyme family.

Flavoproteins are a large and diverse protein family employing the FAD cofactor for catalysis. Among them the BBE (berberine bridge enzyme)-like proteins (pfam 08031) can be set apart due to their unusual bicovalent attachment of the FAD cofactor. The namesake of this protein family is berberine bridge enzyme (BBE) from *Eschscholzia californica* (California poppy) that catalyzes the formation of the so-called “berberine bridge” by oxidation of the *N*-methyl group of (*S*)-reticuline yielding (*S*)-scoulerine (1). This step constitutes a branch point in the biosynthesis of numerous isoquinoline alkaloids (2,3). In recent years, a large number of genes encoding BBE-like enzymes have been identified in plants and bacteria in the course of genome sequencing efforts. The number of BBE-like genes in individual plant species varies considerably from a single gene in the moss *Physcomitrella patens* to 64 in the western poplar (*Populus trichocarpa*) (4). In the model plant *Arabidopsis thaliana*, 28 BBE-like genes were identified (termed *AtBBE*-like 1-28, (4)). However, the role of these BBE homologs in *A. thaliana* and most of the other plants is unknown, as most do not synthesize alkaloids of the benzyloisoquinoline family. Examination of microarray data (<http://bar.utoronto.ca/efp/cgi-bin/efpWEB.cgi> (5)) revealed the expression of *AtBBE*-like genes during certain developmental stages, such as root elongation and maturation, proliferation as well as embryonal development (Table 1). Similarly, osmotic stress and pathogen attack were shown to cause up-regulation of *AtBBE*-likes by up to 400-fold. This up-regulation was also seen in other plants, such as citrus fruit and poplar (6,7). The role in pathogen defense appears to be related to a carbohydrate oxidase activity that was reported previously for tobacco (nectarin V), sunflower and lettuce (8,9). Similar oxidation reactions occur in the biosynthesis of antibiotics generated in various bacterial species, such as *Streptomyces* (10-12). However, the role of BBE-homologs in plant development remains enigmatic.

Table 1: Expression of *AtBBE*-homologs *in planta*. Data was retrieved from the Arabidopsis eFP-browser

Subgroup	Name	Most significant expression value / up-regulation	Second significant expression value / up-regulation	Localization: MS/MS	Locus
1	<i>AtBBE</i> -like 18	822 seed linear cotyledon		unknown	AT4G20820.1
1	<i>AtBBE</i> -like 27	1117 root		unknown	AT5G44410.1
1	<i>AtBBE</i> -like 28	6000 shift dark to light	927 quiescent center root	extracellular	AT5G44440.1
2	<i>AtBBE</i> -like 3	2457 / 438 fold osmotic stress seedling	2318 / 457 fold infection <i>P. infestans</i>	Endoplasmic reticulum	AT1G26380.1
2	<i>AtBBE</i> -like 4	2070 / 78 fold infection <i>P. syringae</i>	391 root regeneration	unknown	AT1G26390.1
2	<i>AtBBE</i> -like 5	665 cotyledon	475 cotyledon greens	unknown	AT1G26400.1
2	<i>AtBBE</i> -like 6	604 / 42 fold osmotic stress	278 / 36 fold infection <i>P. syringae</i>	unknown	AT1G26410.1
2	<i>AtBBE</i> -like 7	1562 / 412 fold osmotic stress	800 / 163 fold mock infection	unknown	AT1G26420.1
2	<i>AtBBE</i> -like 17	7772 mycophylar endosperm		unknown	AT4G20800.1
3	<i>AtBBE</i> -like 10	4899 lateral root cap	912 / 57 fold mock infection	unknown	AT1G30720.1
3	<i>AtBBE</i> -like 11	4988 root epidermis	762 / 10 fold infection <i>P. syringae</i>	extracellular	AT1G30730.1
4	<i>AtBBE</i> -like 9	7582 mature pollen		unknown	AT1G30710.1
4	<i>AtBBE</i> -like 14	50 seed		unknown	AT1G34575.1
4	<i>AtBBE</i> -like 16	3682 root maturation zone	1537 stigma and ovaries	unknown	AT2G34810.1
5	<i>AtBBE</i> -like 1	11626 pollen	5509 mature pollen	plasma membrane, Golgi	AT1G01980.1
5	<i>AtBBE</i> -like 2	5088 pollen	2000 pollen tubes	unknown	AT1G11770.1
5	<i>AtBBE</i> -like 8	2557 root maturation zone	1157 / 246 fold infection <i>P. syringae</i>	unknown	AT1G30700.1
5	<i>AtBBE</i> -like 12	642 endosperm		unknown	AT1G30740.1
5	<i>AtBBE</i> -like 20	4000 root elongation zone	1394 / 10 fold infection <i>P. syringae</i>	extracellular, plasma membrane	AT4G20830.2
5	<i>AtBBE</i> -like 21	973 root elongation zone		plasma membrane	AT4G20840.1
6	<i>AtBBE</i> -like 13	2144 lateral root initiation	1594 xylem root maturation zone	unknown	AT1G30760.1
6	<i>AtBBE</i> -like 15	4927 xylem root	439 seed stage 8 curled	extracellular, plasma membrane	AT2G34790.1
6	<i>AtBBE</i> -like 24	32075 lateral root cap	1412 cotyledon	extracellular	AT5G44380.1
6	<i>AtBBE</i> -like 25	491 procambium root	164 / 5 fold infection <i>P. syringae</i>	extracellular	AT5G44390.1
6	<i>AtBBE</i> -like 26	604 / 5 fold osmotic stress root	250 / 3 fold infection <i>P. syringae</i>	extracellular	AT5G44400.1
7	<i>AtBBE</i> -like 22	1641 lateral root initiation	1427 / 13 fold infection <i>P. syringae</i>	plasma membrane, cytosol	AT4G20860.1
7	<i>AtBBE</i> -like 23	824 root	649 seed cotyledon heart stage	unknown	AT5G44360.1

For the present study, we have chosen *AtBBE*-like 15 (At2g34790) for further studies into the role of the BBE-like enzyme family in plants because gene disruption resulted in defects in female gametophyte development (*i.e.* unfused polar nuclei and endosperm development arrest) (13). Furthermore, mass spectrometric analysis has shown that *AtBBE*-like 15 is located in the

cell wall and thus might participate in as yet undefined reactions relevant for the formation of the cell wall (14). In addition, we have selected *AtBBE*-like 13 (At1g30760) for further analysis due to its close sequence relationship of 81% identity to *AtBBE*-like 15.

Structural analysis of recombinant *AtBBE*-like 15 by X-ray crystallography confirmed a topology similar to that of berberine bridge enzyme from *Eschscholzia californica* (*EcBBE*) and Δ^1 -tetrahydrocannabinolic acid synthase (THCA-synthase) from *Cannabis sativa* (15,16). However, composition and architecture of the active site of *AtBBE*-like 15 indicated distinct catalytic properties. To identify potential substrates we screened a small compound library with regard to its effect on the protein's thermal stability. This approach produced several hits and allowed the identification of cinnamyl alcohol as a lead structure. Further analysis showed that the *p*-hydroxylated derivatives of cinnamyl alcohol, *i.e.* the monolignols *p*-coumaryl-, coniferyl- and sinapyl alcohol are rapidly oxidized to their corresponding aldehydes. Furthermore, the β -*O*-glycosylated form of coniferyl alcohol (coniferin) is also accepted as a substrate. Since monolignols and their β -glycosylated derivatives (coniferin, syringin and *p*-coumaryl- β -glycoside) are important building blocks and monolignol storage forms, respectively, the catalytic reactions performed by *AtBBE*-like 13 and *AtBBE*-like 15 constitute a novel link between the phenylpropanoid pathway and the formation of plant polymerization products, such as lignin and suberin. The characteristic active site found in *AtBBE*-like 13 and *AtBBE*-like 15 is conserved in the majority of BBE-like enzymes in *A. thaliana* (14 out of 28) suggesting that they either exhibit different substrate preferences or have distinct spatial (*e.g.* different plant tissues) or temporal (*e.g.* in response to pathogens or herbivores) functions *in planta*.

Experimental Procedures

Chemicals

All chemicals were from Sigma Aldrich (St. Louis, MO, USA) and were of the highest grade commercially available. Restriction enzymes were obtained from Fermentas (Waltham, MA, USA). Ni Sepharose 6 Fast Flow column material was from GE Healthcare (Little Chalfont, U.K.). Synthetic genes coding for *AtBBE*-like 15 and *AtBBE*-like 13 were obtained from Life Technologies (Carlsbad, CA, USA) with codon usage optimized for *Komagataella pastoris*.

Molecular cloning

The proteins were expressed using *Komagataella pastoris* as expression host, according to the EasySelect™ *Pichia* Expression Kit provided by Invitrogen (Waltham, MA, USA). The genes were adapted to the *K. pastoris* codon usage and a C-terminal His-tag was added. SignalP was used to identify the native signal sequence of 30 and 27 amino acids for *AtBBE*-like 13 and *AtBBE*-like 15, respectively (17). The genes lacking the signal sequence were cloned into pPICZα vector® (Invitrogen) using standard techniques. *K. pastoris* strain KM71H was transformed with the pPICK-PDI vector harboring the gene for the protein disulfide isomerase from *Saccharomyces cerevisiae*. The modified KM71H strain was transformed with the linearized [pPICZα-*AtBBE*-like 13] or [pPICZα-*AtBBE*-like 15] construct using electroporation. Optimal expression strains were identified using the method proposed by Weis *et al.* (18).

Protein expression and purification

Expression was carried out using a BBI CT5-2 fermenter (Sartorius, Göttingen, Germany) using a basal salt minimal medium as described by Schrittwieser *et al.* (19). After 96 h of methanol induction the pH was set to 8.0 with sodium hydroxide and imidazole was added to a final concentration of 10 mM. The cells were removed by centrifugation at 4000 rpm at 4 °C for 30 min. The supernatant was incubated with 50 mL Ni Sepharose 6 Fast Flow material at 4 °C for 45 min. Then the affinity material was packed into a column and washed with five column volumes of 50 mM phosphate buffer pH 8.0 containing 150 mM NaCl and 20 mM imidazole. The protein was eluted using 50 mM phosphate buffer pH 8.0 containing 150 mM NaCl and 150 mM

imidazole. Fractions containing *AtBBE*-like 15 were concentrated using Amicon Ultra centrifugal filter units and subsequently loaded on a Superdex 200 gel filtration column using an Äkta system and separated using 50 mM Tris buffer pH 8.0 containing 150 mM sodium chloride. The purity of purified protein was monitored by SDS-PAGE. The final yield from 3.5 L fermentation supernatant was 520 mg of purified protein. The large-scale expression of *AtBBE*-like 13 was conducted as described for *AtBBE*-like15. In contrast to *AtBBE*-like 15, *AtBBE*-like 13 was not secreted and hence the protein was isolated from cells and not the cultivation medium. Briefly, the cell pellet was harvested and redissolved (1:3 w/v) in cell lysis buffer (50 mM NaH₂PO₄, 300 mM NaCl, 20 mM imidazole, pH 8.0), disrupted by Zirconia/Silica beads using a Merckenschlager homogenizer. The lysate was separated from the cell debris by centrifugation (18000 rpm, 30 min, 4 °C), filtered and incubated with Ni-sepharose 6 Fast Flow material (GE Healthcare, Little Chalfont, U.K.). The column was packed with the sepharose material and after extensive washing (50 mM NaH₂PO₄, 300 mM NaCl, 50 mM imidazole, pH 8.0) the protein was eluted with elution buffer containing 500 mM imidazole. Subsequent purification was performed as described for *AtBBE*-like 15.

Site-directed mutagenesis: Generation of the L182V variant

Site-directed mutagenesis was performed according to the instructions of the QuickChange XL kit (Stratagene, La Jolla, CA, USA) for site-directed mutagenesis. The pPICZ α -*AtBBE*-like 15 vector was used as template for the polymerase chain reaction. The introduction of the desired codon causing a change of leucine in position 182 to valine was verified by sequencing. Transformation of the gene was performed as described before. Expression of the mutated gene and purification of the *AtBBE*-like 15 L182V variant was performed as described for wild-type *AtBBE*-like 15.

Crystallization

Initial crystal screening of *AtBBE*-like 15₍₂₇₋₅₃₂₎ was performed with an Oryx8 robot (Douglas Instruments, Berkshire, UK) using commercially available Index (Hampton Research, Aliso Viejo, CA, USA) and JCSG+ (Molecular Dimensions, Suffolk, UK) screens. Screening was performed in Swissci triple well plates (Molecular Dimensions) using the sitting drop method

with a reservoir volume of 33 μL . Drops of 1 μL were pipetted in 1:1 ratio of protein and reservoir solution with two different protein stock solutions: 22 and 50 mg/mL in 50 mM Tris buffer pH 8.0 containing 150 mM sodium chloride, respectively. Plates were sealed with the thermal seal A sealing films (Sigma-Aldrich, St. Louis, MA, USA) and were incubated at 289 K. First crystals appeared after one week in JCSG+ screen condition #1-14 (0.2 M sodium thiocyanate and 20 % w/v PEG 3350) with the higher protein concentration. Crystals from this drop were pipetted out and crushed in 100 μL of the original #1-14 solution and used as a seeding stock. Cross seeding setups (20) were performed in the same manner as initial screening with drops consisting of 0.5 μL of protein stock solution (37 mg/mL), 0.2 μL of the seeding stock and 0.5 μL of the JCSG+ screen solutions from the reservoir. The best diffracting crystals appeared after four and a half weeks in a serial dilution setup done manually in Crystal clear duo plates for sitting drop (Douglas Instruments). The 1.2 μL drops consisted of 0.5 μL of protein stock solution (36 mg/mL), 0.2 μL of the seeding stock and 0.5 μL of the JCSG+ screen condition #2-33 (0.1 M potassium thiocyanate and 30 % w/v PEG 2000 MME) from the reservoir.

Data collection and processing

X-ray diffraction data were collected at 100 K at Elettra (Trieste) without additional cryoprotectant. Data processing was performed with the XDS program package (21). Unit cell parameters and assigned space groups as well as data statistics for both crystal forms are shown in Table 3. The solvent content was estimated based on the calculated Matthews coefficient (22). Molecular replacement was performed with Phaser (23) using the structure of *EcBBE* as the search template. Structure refinement was done with Phenix (24) followed by manual inspection and model rebuilding in Coot (25). The program Reckon! (included in Phenix) was used to generate restraints for metal coordination and the PEG-fragment included in the refinement. In total three sodium and one potassium ion were found to bind to the protein surface without structural impact. The TLSMD server was used to generate partitioning groups (three for chain A and four for chain B) to improve refinement (26). Several refinement cycles were done until all visible residues were assigned and no significant changes in R and R_{free} were observed. Structure validation was performed using MolProbity (27).

Chain A of the model consists of residues Ser27 to Gly532. Chain B starts with residue Gln30 and extends to Gly532. Some residues at the N-terminal part could not be modeled into the

electron density most likely due to their high flexibility (Val43 and Ser44 in chain A as well Gln40, Ser41 and Asp42 in chain B). In addition, no clear electron density was visible for a loop region (residues 301 to 305) in both chains.

Thermofluor experiments

Thermofluor experiments were performed using a Biorad® CFX Connect Real time PCR system (BioRad, Hercules, CA, USA). The experiments were performed using Sypro® Orange as fluorescent dye in 50 mM MES buffer pH 7.0. Stock solutions of all substrates were prepared in water with a concentration of 10 mg/mL. For substrates with a lower solubility a saturated solution was used. The total volume in each well was 25 μ L with a protein concentration of 0.4 mg/mL and 2 mg/mL substrate. The starting temperature of 20 °C was kept for 5 min and then the temperature was increased at a rate of 0.5 °C/min to 95 °C. Melting temperatures were determined using the program Biorad CFX Manager 3.0.

Rapid reaction kinetics using stopped flow spectrophotometry

Reductive and oxidative half reactions were determined with a stopped-flow device (SF-61DX2, TgK Scientific, U.K.) at 25 °C under anoxic conditions in a glove box (Belle Technology, Weymouth, U.K.). Oxygen was removed from the sample by flushing with nitrogen and subsequent incubation of the samples in the glove box for 1 h. Spectral changes of the flavin cofactor were followed at a wavelength of 450 nm using a KinetaScanT diode array detector (MG-6560, Hi-Tech) employing the Kinetic Studio Software (TgK Scientific, U.K.). Reductive half reactions were assayed by mixing 60 μ M *AtBBE*-like 15 or 13 in 50 mM potassium phosphate buffer pH 7.0 with various substrate concentrations. The observed rate constants at different substrate concentrations (k_{obs}) were determined using the Kinetic Studio Software by fitting the data to an exponential function. If suitable the dissociation constant was determined performing a sigmoidal fit of the observed rate constants employing Origin 7 (OriginLab Corporation, Northampton, USA). The oxidative half reaction was determined by mixing oxygen free photo-reduced 60 μ M *AtBBE*-like 15 or 13 with air-saturated buffer. Photoreduction was carried out according to Massey *et al.* (28).

Product identification

Products resulting from the conversion of monolignols and their glycosides were separated and identified using HPLC. Reactions were performed in 1.5 mL reaction vials in 50 mM potassium phosphate buffer pH 7.0 at 30 °C and 700 rpm. Substrates were used at a concentration of 2.5 mM and 30 µg/mL of *At*BBE-like 15. After 24 h the reaction was quenched by mixing 500 µL sample with 500 µL methanol. Samples were spun for 10 min at 9400 g in a bench-top centrifuge before the clear supernatant was applied to the HPLC. The products were identified by retention time and by comparing their UV-absorption spectra with authentic standards. HPLC analyses were done using a Dionex UltiMate 3000 HPLC (Thermo Fisher Scientific, Waltham, MA, USA) equipped with an Atlantis® dC18 5µM (4.6 x 250 mm) column. Separation of all compounds was achieved using a linear gradient with water with 0.1% TFA as solvent A and acetonitrile with 0.1 TFA as solvent B and a flow rate of 0.5 mL/min. Separations were started with a mobile phase of 80% solvent A and 20% solvent B. The concentration of solvent B was increased to 50% within 20 min followed by a steep ramp to 100% solvent B in 10 min. At the end of the protocol the concentration of solvent B was again decreased to 20% over 5 min. Retention times of authentic standard compounds were determined using the described protocol. Under these experimental conditions, the following retention times were observed: coniferyl alcohol, 16.06 min; coniferyl aldehyde, 21.39 min; ferulic acid, 18.27 min; coumaryl alcohol, 15.52 min; coumaryl aldehyde, 21.07 min; *p*-coumaric acid, 17.67 min; sinapyl alcohol, 15.40 min; sinapyl aldehyde, 21.01 min and sinapic acid, 17.76 min.

Synthesis of monolignol glycosides

A glucosyltransferase from apple (UGT71A15, *Malus x domestica*), was used for the synthesis of 4-*O*-β-D-glucopyranosides of the monolignols (29). Heterologous expression in *E. coli* and purification of the glucosyltransferase will be published elsewhere. Briefly, glucosylation of the aglyca (5 mM) from 7.5 mM uridine 5'-diphosphate (UDP)-glucose was performed in 50 mM Tris/Cl buffer (pH 7.5) containing 50 mM MgCl₂, 0.13% BSA and 10% DMSO in the presence of 6 µM UGT71A15.

Phylogenetic tree construction

M-Coffee was used to create a multiple sequence alignment including all 28 *AtBBE*-like family members (30). The alignment was edited by hand using Jalview (31). The PHYLIP package (PHYLIP 3.69) was used to create a bootstrapped phylogenetic tree using the programs SEQBOOT, PROTDIST, FITCH and CONSENSE (32). We created 1000 Jackknife sub-alignments with SEQBOOT, which were subsequently subjected to a bootstrapped protein-distance analysis. We chose *EcBBE* as the outgroup sequence. The tree shown in supplementary Figure S1 was visualized using Figtree (Tree Figure Drawing Tool, version 1.4.0 by Andrew Rambaut; <http://tree.bio.ed.ac.uk/>). The accession codes for the sequences used for the analysis are given in the legend of supplementary Figure S1.

Docking

Docking of coniferyl alcohol was performed using AutoDock Vina using the default docking parameters (33,34). Point charges were assigned according to the AMBER03 force field (35). The setup of the receptor was done with the YASARA molecular modeling program (36). Twentyfive Vina docking runs were performed and after clustering all runs, four distinct complex conformations with a binding energy of -6.4, -6.1, -5.0 and -4.6 kJ mol⁻¹ were found. The complex with a binding energy of -6.4 kJ mol⁻¹ and a conformation that is in agreement with the catalytic activity found for *AtBBE*-like 15 is shown in Figure 3. 8% of the docks cluster in this top pose.

Results

Enzymatic properties and identification of substrates of AtBBE-like 13 and AtBBE-like 15

AtBBE-like 13 and *AtBBE*-like 15 were expressed in *Komagataella pastoris* and purified from the culture medium by Ni-Sepharose affinity chromatography and subsequent gel filtration yielding ca. 10 mg and 150 mg of protein from 1 liter of fermentation culture, respectively. In order to identify potential substrates, we inspected the chemical nature of substrates recently identified for vanillyl alcohol oxidase (VAO) superfamily members. This revealed that oxidation

of primary and secondary alcohol groups is a prevailing feature in all of these reactions (4). In view of this recurring motif, we have assembled a library comprising predominantly compounds with one or more hydroxyl groups (see supplementary Table S1). Since strong protein-ligand interactions are known to increase the thermal stability of proteins, we first screened our library with regard to an increase in the melting temperature of *AtBBE*-like 15 using the *Thermofluor* method (37). This approach produced a number of promising hits, yielding a substantial increase of the melting temperature (up to 17 °C, for a complete list see supplementary Table S1). The compounds with the strongest effect on the thermal stability were tested as substrates revealing that cinnamyl alcohol was oxidized to cinnamyl aldehyde by *AtBBE*-like 15. Using cinnamyl alcohol as a lead structure, we tested several other naturally occurring aromatic alcohols as putative substrates and found that *AtBBE*-like 15 oxidizes the monolignols *p*-coumaryl-, coniferyl- and sinapyl alcohol to their corresponding aldehydes. In order to gain more detailed information on substrate specificity and kinetic parameters reductive half-reactions were studied using stopped-flow spectrophotometry (a summary of kinetic parameters is given in Table 2). Reduction of *AtBBE*-like 15 and 13, using either coniferyl or sinapyl alcohol, was very fast and essentially complete within the dead time of the instrument (ca. 5 ms) indicating that the rate of reduction exceeds 500 s⁻¹. In the case of *p*-coumaryl alcohol, the rate of reduction could be analyzed as a function of substrate concentration, yielding a dissociation constant of 700 μM and a limiting rate of 332 s⁻¹. Since monosaccharides, such as D-glucose, had such a profound effect on the protein's thermal stability, we also analyzed the β-*O*-glycosylated derivatives of the monolignols and found that coniferin was accepted as a substrate exhibiting a dissociation constant of 660 μM and a limiting rate of reduction of 171 s⁻¹. However, the β-*O*-glycosylated derivatives of *p*-coumaryl- and sinapyl alcohol (syringin) were relatively poor substrates of the enzyme. An equivalent set of experiments was conducted with *AtBBE*-like 13 demonstrating similar catalytic properties (summarized in Table 2). The observed rate constants for selected substrates determined for *AtBBE*-like 15 and 13 are shown in Figure 1 A and B. Thus we propose that *AtBBE*-like 13 and *AtBBE*-like 15 are in fact monolignol oxidoreductases.

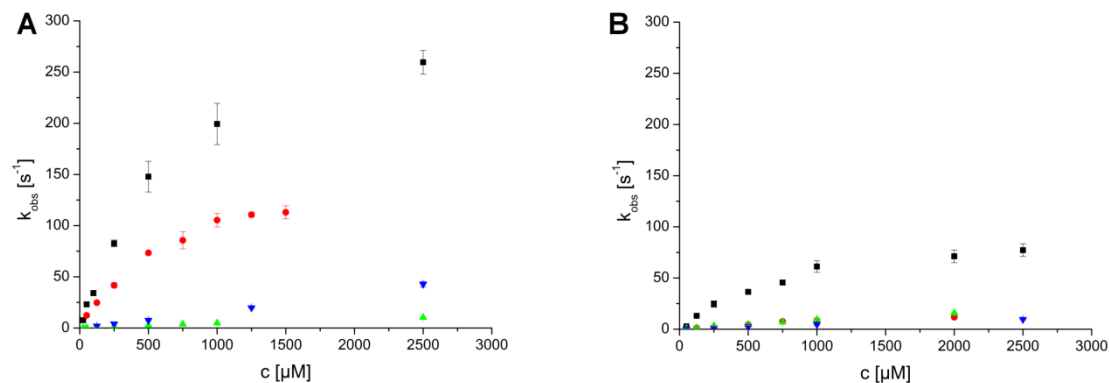
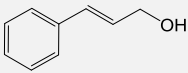
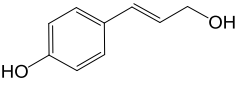
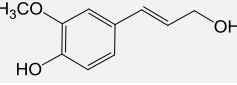
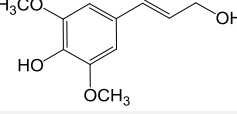
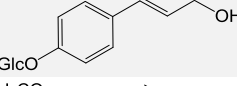
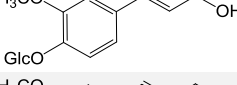
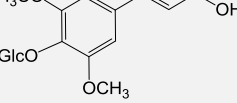


Figure 1: Rate constants observed for the reductive half reaction of *AtBBE*-like 15 (A) and *AtBBE*-like 13 (B). A stopped flow device was used to determine the rate constants of the reductive half reaction of *AtBBE*-like 15 and 13 with *p*-coumaryl alcohol (■), cinnamyl alcohol (▲), coniferyl alcohol β-glycoside (●) and sinapyl alcohol β-glycoside (▼). The course of the reaction was determined by following the absorption of the oxidized flavin at 450 nm. As the reactions follow pseudo first order kinetics, rates were calculated from a mono exponential fit.

Table 2: Chemical structures of substrates and their kinetic parameters for *AtBBE*-like 13 and *AtBBE*-like 15. Dissociation constants and observed rates of reduction of *AtBBE*-like 13 and *AtBBE*-like 15 with different monolignols and their glycosylated derivatives.

Substrate	<i>AtBBE</i> -like 15 K_d [μM]	<i>AtBBE</i> -like 13 K_d [μM]	<i>AtBBE</i> -like 15 k_{obs} at 500 μM [s^{-1}]	<i>AtBBE</i> -like 13 k_{obs} at 500 μM [s^{-1}]
cinnamyl alcohol 	n.a.*	n.a.*	2.6 ± 0.1	4.4 ± 0.4
<i>p</i> -coumaryl alcohol 	700 ± 120	867 ± 123	156 ± 8	36.5 ± 1
coniferyl alcohol 	n.a.**	n.a.**	$> 500^{**}$	$> 500^{**}$
sinapyl alcohol 	n.a.**	n.a.**	$> 500^{**}$	$> 500^{**}$
<i>p</i> -coumaryl alcohol β-glycoside 	n.a.*	n.a.*	0.01 ± 0.001	0.01 ± 0.001
coniferyl alcohol β-glycoside 	660 ± 100	1856 ± 624	73 ± 1	4.4 ± 1.1
sinapyl alcohol β-glycoside 	n.a.*	n.a.*	7.5 ± 0.7	2.4 ± 0.2

* not determined due to solubility limitation

** reaction too fast to be measured

Reoxidation of photo-reduced *AtBBE*-like 13 and *AtBBE*-like 15 by molecular dioxygen was very slow yielding an oxidative rate constant of $3.3 \pm 0.6 \text{ M}^{-1} \text{ s}^{-1}$ and $27.5 \pm 1.4 \text{ M}^{-1} \text{ s}^{-1}$, respectively, thus indicating that the enzymes suppress the reduction of oxygen by the reduced FAD cofactor. Recently, we have reported that oxygen reactivity in the BBE family is controlled by the side chain of a gatekeeper residue in the “oxygen reactivity loop” on the *re*-side of the isoalloxazine ring. In the case of *AtBBE*-like 15, the gatekeeper residue is a leucine (L182) and thus oxygen reactivity is suppressed because the side chain blocks access to the oxygen pocket (38). Replacement of L182 to valine in *AtBBE*-like 15 increased the rate of reoxidation ca. 400-fold to $1 * 10^4 \text{ M}^{-1} \text{ s}^{-1}$, *i.e.* very similar to the rate found with *EcBBE* ($k_{\text{ox}} = 5 * 10^4 \text{ M}^{-1} \text{ s}^{-1}$) (39), which also possesses a valine residue in the gatekeeper position. Since the reaction of the reduced FAD with dioxygen is very slow, we assume that an alternative electron acceptor is required for reoxidation of the reduced FAD cofactor of *AtBBE*-like 13 and *AtBBE*-like 15 *in planta*.

Crystal structure of AtBBE-like 15

In order to better understand the enzymatic reaction mechanism and substrate binding to the active site we have elucidated the three-dimensional structure of *AtBBE*-like 15 by means of X-ray crystallography (pdb entry 4ud8). Protein crystals were obtained using sitting drop conditions yielding diffraction data to 2.1 Å. The structure was solved by molecular replacement using *EcBBE* (pdb entry: 3D2H) with two molecules in the asymmetric unit (data collection and statistics are given in Table 3). *AtBBE*-like 15 adopts the same fold as other BBE-like enzymes, *i.e.* the VAO-fold that is characterized by a FAD-binding and a substrate-binding domain (Figure 2C, shown in green and orange, respectively). The substrate binding domain consists of a seven-stranded antiparallel β -sheet, which is covered by α -helices. The substrate-binding pocket and the active site are formed by two short loops (termed loop β 2- β 3 and loop α L- α M), the “oxygen reactivity motif” consisting of loop α D- α E, helix α E and loop α E- β 6. Additionally, the three strands β 14, β 15 and β 16 contribute to the active site (Figure 2B, nomenclature of secondary structure elements according to (15)). The FAD cofactor is bicovalently linked to the peptide chain via a covalent bond of His115 to the 8 α -methyl group and of Cys179 to the C6-position of the isoalloxazine ring.

Table 3: Data acquisition and refinement parameters for X-ray crystallography

(JCSG+ #2-33)	
Beamline	Elettra XRD1
Wavelength (Å)	0.971670
Unit cell parameters (Å, °)	63.6, 94.7, 188.3, 90, 90, 90
Space group	P2 ₁ 2 ₁ 2 ₁
Resolution limits (Å)	50-2.09 (2.21-2.09)
R _{meas}	0.209 (0.865)
R _{merge}	0.191 (0.794)
Total number of observations	415743 (58987)
Total number unique	67102 (9501)
<I/σ(I)>	7.73 (2.23)
Completeness (%)	97.8 (87.0)
Redundancy	6.2
Wilson B factor (Å ²)	32.02
Matthews coefficient (Å ³ Da ⁻¹)	2.36
Molecules per ASU	2
Solvent content (%)	48
Refinement	
Resolution (Å)	47.37 – 2.09
R (%)	18.35
R _{free} (%)	22.09
R.m.s.d. stereochemistry	
Bond lengths (Å)	0.008
Bond angles (°)	0.825
No. of protein atoms	7946
No. of non-protein atoms	247
No. of water molecules	615
Average B factor (Å ²)	25.54
Ramachandran analysis	
Favoured (%)	95.96
Allowed (%)	3.94
Disallowed (%)	0.1
PDB code	4ud8

As hydride transfer from the substrate to the N5-locus of the flavin cofactor is a generally accepted mode of reduction, a sphere with a radius of 10 Å around this locus was examined for putative catalytic residues. As shown in Figure 2A, Y117 and Q438 are engaged in a hydrogen bond on the *si*-side of the isoalloxazine ring (2.6 Å). These residues are positioned between the active site and the binding pocket and thus must interact with the substrate when it enters the active site. Therefore these residues were defined as substrate coordination motif. The hydroxyl groups of Y117, Y479 and Y193 point towards the active site with distances to the N5-locus of 4.8 Å, 4.6 Å and 5.0 Å, respectively. The two phenolic hydroxyl groups of Y479 and Y193 are within hydrogen bond distance (2.4 Å, Figure 2A). The ε-amino group of K436 is located 3.1 Å above the plane of the aromatic ring of Y193 and engages in a cation-π interaction. This arrangement of Y479, Y193 and K436 presumably favors deprotonation of the phenolic hydroxyl group of Y193 and activates this residue as a putative active site base thus these residues were defined as catalytic base motif.

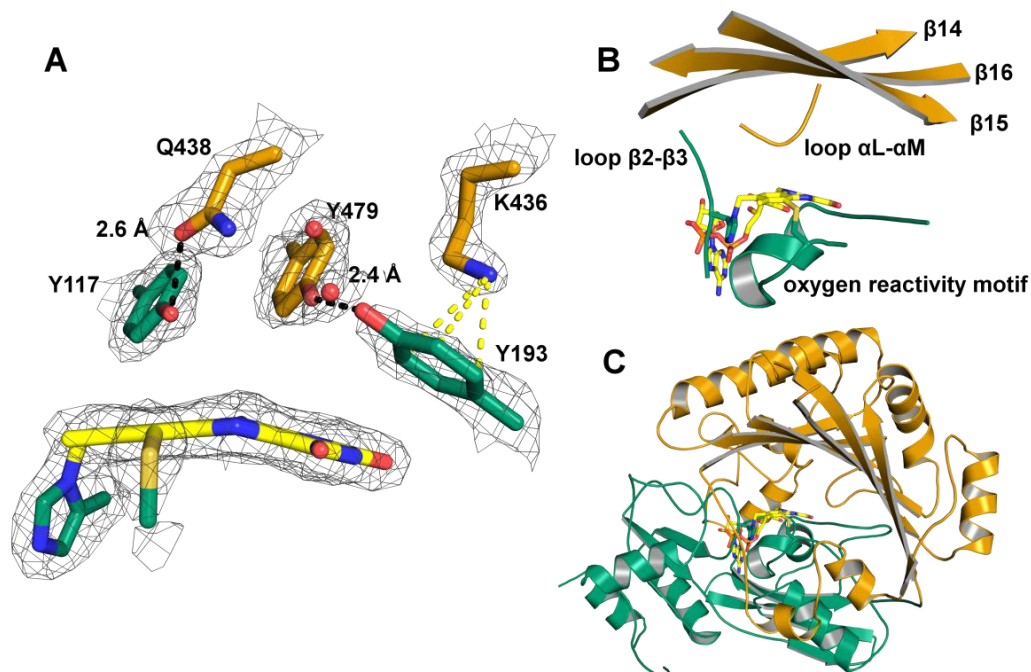


Figure 2: (A) Close-up view of the amino acids with a proposed role in substrate binding and catalysis. Y117 and Q438 form a hydrogen bond. K436 and Y193 are involved in a cation- π interaction and Y193 forms a hydrogen bond to Y479. Two well-defined water molecules are found in the active site (red spheres). The electron density was cut off at a sigma value of 1.5 Å. (B) Close-up view of the active site: Loop β 2- β 3 and the oxygen reactivity motif originate from the FAD binding domain and harbor H115 and C179, which form the two covalent linkages to the isoalloxazine ring of the FAD. Strands β 14, β 15, β 16 and loop α L- α M originate from the substrate-binding domain. They harbor amino acids defining the *si*-face near the N5-locus (<10 Å) that are putatively involved in the catalytic mechanism. (C) Overall topology of *AtBBE-like 15*: *AtBBE-like 15* adopts the VAO topology consisting of a FAD binding domain (green) and a substrate binding domain (orange). Furthermore, it features a bicovalently attached FAD typical for BBE-like proteins. The FAD cofactor is shown in stick representation in yellow.

Docking of substrates to the active site

Because co-crystallization with the identified substrates was unsuccessful we conducted docking experiments using coniferyl alcohol as a model substrate in order to gain further insights into the interaction of substrates with amino acid residues in the active site. At the *si*-side of the isoalloxazine ring a hydrophobic pocket is formed by residues F373, F377, L407, L440 and the dimethylbenzene moiety of the isoalloxazine ring. As shown in Figure 3, the substrate fits into this hydrophobic pocket (binding energy of -6.4 kJ mol⁻¹). The docking result suggests that the orientation of the allylic alcohol towards the proposed catalytic base Y193 is possible while the

aromatic ring is located in the hydrophobic pocket and thus this orientation is consistent with the productive catalysis found for *At*BBE-like 15 with this ligand.

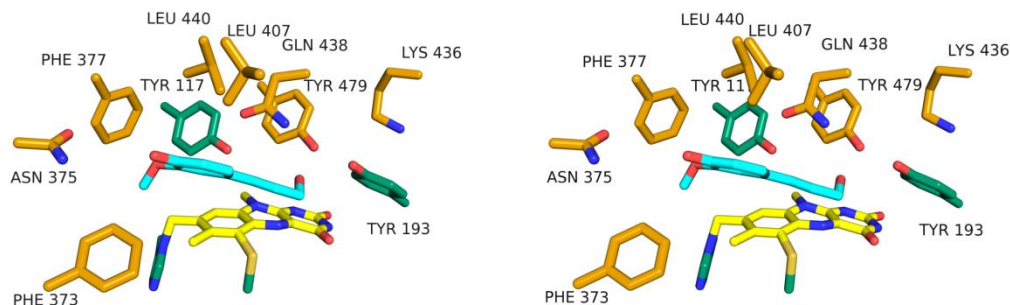


Figure 3: Substrate binding to *At*BBE-like 15. The substrate binding cavity and active site of *At*BBE-like 15 are shown in stereo view. The isoalloxazine ring is shown in yellow and conferyl alcohol in light blue as a stick model. Conferyl alcohol was docked into the cavity using YASARA. The aromatic moiety is located in the hydrophobic binding pocket formed by F377, F373, L407, L440, Y117 and the isoalloxazine ring while the allyl alcohol is facing the active site. All residues shown in this figure are conserved in *At*BBE-like 13.

Functional and structural characterisation of the BBE-like family in A. thaliana

The identification of critical active site residues with a role in substrate binding and catalysis in *At*BBE-like 15 raised the question whether these are conserved in all *At*BBE-like family members. To investigate this issue, we have constructed a protein distance tree (Figure 4, left). Seven distinct groups can be identified in the phylogenetic tree within the family of BBE-like enzymes in *A. thaliana*, in good agreement with previously published work (9). Based on these distinct groups we have created sequence logos for each of the elements forming the active site, *i.e.* the three strands at the ceiling of the active site cavity and the three loops in the vicinity of the isoalloxazine ring (Figure 4, right). The histidine residue (His115) in loop β 2- β 3 that forms the covalent bond to the $\delta\alpha$ -methyl group of the flavin isoalloxazine ring is conserved in all *At*BBE-like enzymes and thus it can be assumed that the covalent linkage is present in all family members. In contrast, the cysteine residue (Cys179) located in the “oxygen reactivity motif” is only conserved in phylogenetic groups 2, 4, 5 and 7 whereas the remaining groups feature other amino acids, such as histidine (group 1), serine (group 3) or tyrosine (group 1 and 6). We assume that these four *At*BBE-like enzymes possess a single covalent linkage whereas the remaining 24

feature a bicovalent linkage of the FAD cofactor as already shown for *Ec*BBE (40), Dbv29 (41), glucooligosaccharide oxidase (GOOX) (42), and THCA-synthase (15).

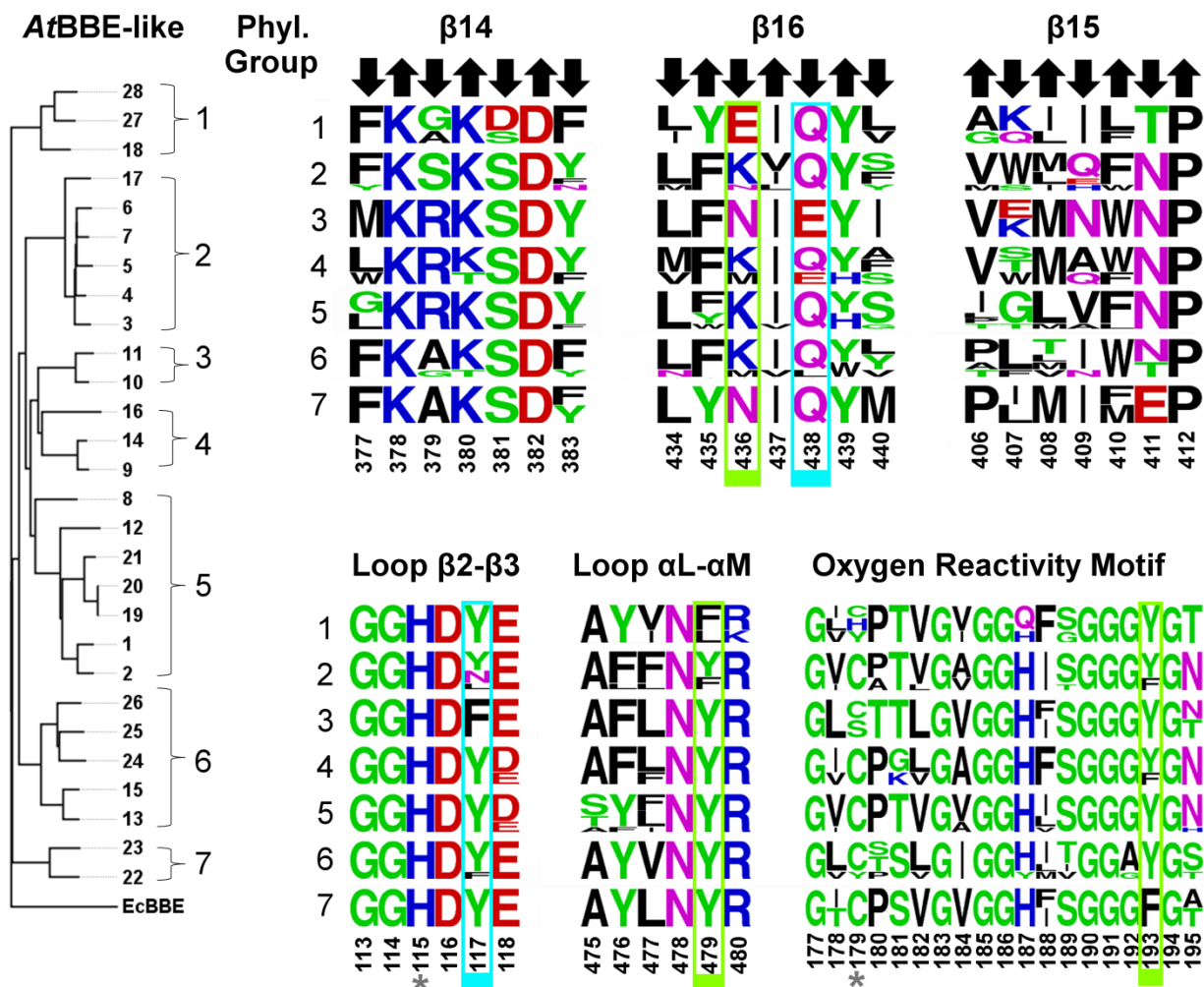


Figure 4: The chemical nature of the active sites present in different phylogenetic groups is represented by sequence logos of the active site forming secondary structure elements. Left: Protein distance tree of all BBE-like enzymes from *A. thaliana* with *Ec*BBE as outgroup. Right: Sequence logos representing the structural elements forming the active site of the seven phylogenetic groups reveal highly conserved motifs. Arrows indicate the orientation of the residues in the β -strands. An upward arrow indicates that the residue points away from the active site. These residues were found to be structurally relevant. A downward arrow indicates the residue points towards the active site and thereby contributes to the decoration. Residues highlighted in a green and cyan box define the substrate coordination and catalytic motif, respectively. Both motifs are putatively involved in the catalytic mechanism (see also Figure 5 and 6). Positions labeled with an asterisk highlight the two potential sites of covalent linkage.

Further analysis of the sequence logos generated for the three strands of the β -sheet provided important insights into the functions of amino acid side chains. Generally, amino acids oriented towards the α -helices (indicated by arrows pointing up) are conserved because they are important for the structural integrity of the protein. For example, Lys380 and Asp382 in strand β 14 form salt-bridges to Asp481 (2.7 Å) and Arg473 (3.3 Å), respectively. Thus, these amino acids are invariant in the whole family, because all of them adopt the same overall topology. In contrast, amino acid residues pointing towards the active site (indicated by arrows pointing down) are only conserved within certain phylogenetic groups, indicating that the composition of the active site differs markedly. In the case of *AtBBE*-like 15 (group 6 in Figure 4), the active site residues Y117, Y193, K436, Q438 and Y479 are important for substrate binding and catalysis (boxed residues in Figure 4 and shown as stick models in Figure 5, panel A). While residues Y193, Y479 and K436 concertedly act as an active site base (“catalytic motif”, shown in green), Y117 and Q438 appear to be involved in determining the substrate preference (“substrate coordination motif”, shown in cyan). Both motifs are strictly conserved in 14 members of the BBE-like enzymes in *A. thaliana* (see Table 4) indicating that their catalytic mechanism and substrate preference will be similar, *i.e.* oxidation of alcohols to their corresponding aldehyde products. This analysis was extended to other plants revealing that the active site signature found in *AtBBE*-like 13 and *AtBBE*-like 15 is conserved in soybean (*Glycine max*; 21 homologs out of 43 BBE-like enzymes), eucalyptus (*Eucalyptus grandis*; 18 out of 27), poplar (*Populus trichocarpa*; 17 out of 64) and potato (*Solanum tuberosum*; 6 out of 18). Interestingly, monocotyledonous species such as maize (*Zea mays*; 16 BBE-like enzymes) and rice (*Oriza sativa*, 11 BBE-like enzymes) appear to lack monolignol oxidoreductase activity, because the catalytic and substrate coordination motifs are not found in any of the BBE-like enzymes.

In contrast, major variations in the catalytic and/or substrate coordination motif are seen in groups one, three and seven. In group one, K436 in the catalytic motif is replaced by glutamic acid (Figure 4, strand β 16 and Figure 5, panel B) and Y479 by phenylalanine or leucine, respectively (Figure 4, α L- α M), while the substrate coordination motif is conserved. In group three, the substrate coordination motif (Y117 and Q438 are replaced by phenylalanine and glutamic acid, respectively) as well as the catalytic motif residues (K438 replaced by asparagine) are modified (Figure 5, panel C), while group seven features a conserved substrate coordination motif, but in the catalytic motif residues K436 and Y193 are replaced by asparagine and

phenylalanine, respectively (Figure 5, panel D). It is worthwhile noting that in all cases where the catalytic motif appears to be disrupted an alternative catalytic base is present, for example glutamic acid instead of K436 or N411 in group one and seven, respectively. Similarly, Q438 in group three is replaced by glutamic acid. Overall, we conclude that the BBE-like enzymes of these groups have distinct catalytic properties and act on different, however yet unidentified substrates. Interestingly, the presence of a catalytic active base appears to be an important feature in BBE-like enzymes, as it was also observed in *EcBBE* (16), *Dbv29* (41), *GilR* (43), *GOOX* (42) and *THCA-synthase* (15).

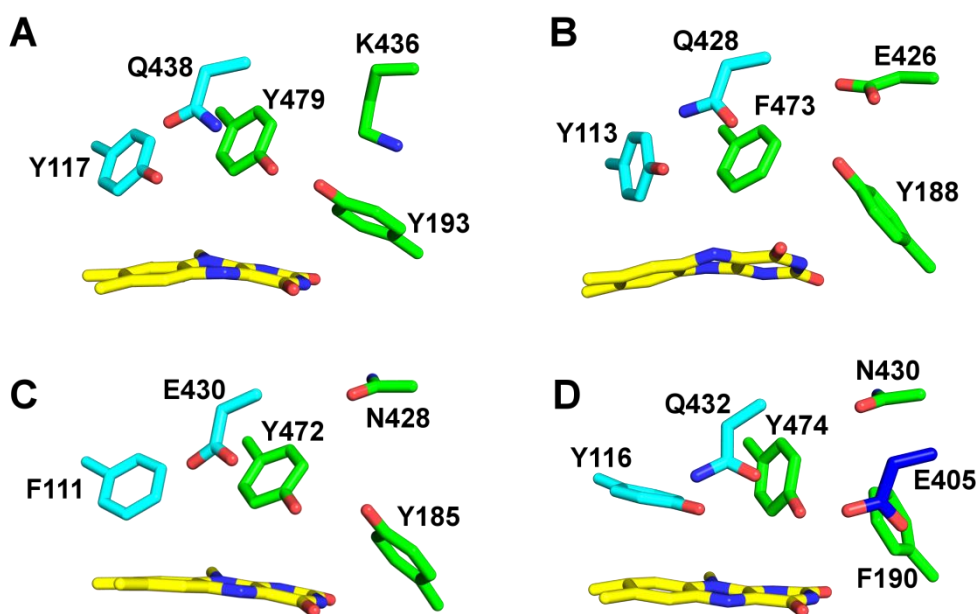


Figure 5: Active site composition predominantly present in different phylogenetic groups. The active site compositions shown in B, C and D were visualized using homology models created with YASARA. A: Active site composition of *AtBBE*-like 15 that is representative for groups 2, 4, 5 and 6. B: This active site composition is found in group 1 (numbering according to *AtBBE28*). The catalytic base as found in *AtBBE*-like 15 has been disrupted. K436 has been replaced by a glutamic acid that putatively can recover the catalytic base function. C: This active site composition is found in group 3 (numbering according to *AtBBE11*). The catalytic base motif is inconsistent, Q438 has been replaced by a glutamic acid what putatively recovers the catalytic base function. D: Active site composition as found in group 7 (numbering according to *AtBBE22*). In the catalytic base motif K436 has been replaced by an asparagine and F193 by a phenylalanine. In β 15 a glutamic acid can be found that putatively recovers the catalytic base function in this active site.

Table 4: Composition of the substrate coordination (Y117 and Q438) and catalytic motif (Y193, K436 and Y479)

	Phyl group	Y117	Q438	Y193	K436	Y479
AtBBE18	1	Y	Q	Y	E	L
AtBBE27	1	Y	Q	Y	E	F
AtBBE28	1	Y	Q	Y	E	F
<i>AtBBE3</i>	2	N	Q	Y	K	Y
<i>AtBBE4</i>	2	Y	Q	Y	K	Y
<i>AtBBE5</i>	2	Y	Q	F	N	F
<i>AtBBE6</i>	2	N	Q	F	K	F
<i>AtBBE7</i>	2	L	Q	Y	K	Y
<i>AtBBE17</i>	2	Y	Q	Y	K	Y
AtBBE10	3	F	E	Y	N	Y
AtBBE11	3	F	E	Y	N	Y
<i>AtBBE9</i>	4	Y	Q	Y	K	Y
<i>AtBBE14</i>	4	Y	Q	Y	K	Y
<i>AtBBE16</i>	4	Y	E	F	M	Y
AtBBE1	5	Y	Q	Y	K	Y
AtBBE2	5	Y	Q	Y	K	Y
AtBBE8	5	Y	Q	Y	K	Y
AtBBE12	5	Y	Q	Y	K	Y
AtBBE19	5	Y	Q	Y	K	Y
AtBBE20	5	Y	Q	Y	K	Y
AtBBE21	5	Y	Q	Y	K	Y
<i>AtBBE13</i>	6	Y	Q	Y	K	Y
<i>AtBBE15</i>	6	Y	Q	Y	K	Y
<i>AtBBE24</i>	6	F	L	Y	K	Y
<i>AtBBE25</i>	6	Y	Q	Y	M	Y
<i>AtBBE26</i>	6	Y	Q	Y	K	Y
AtBBE22	7	Y	Q	F	N	Y
AtBBE23	7	Y	Q	F	N	Y

Discussion

Catalytic mechanism of monolignol oxidation

Based on the crystallographic structure of *At*BBE-like 15 and the results obtained by substrate docking, we propose the following catalytic mechanism: Tyr193 is positioned such that the phenolic hydroxyl group points toward the substrate's alcohol group. Lys436 forms a cation- π interaction with the aromatic ring of Tyr193 thereby lowering the pK_a and thus stabilizing the deprotonated state. We also assume that Tyr479 stabilizes the deprotonated state of Tyr193 by hydrogen bonding (Figures 2 and 3). Thus these three amino acids make up the core catalytic machinery for deprotonation of the substrate's hydroxyl group that results in the concomitant transfer of a hydride from the C γ position to the N5 locus of the isoalloxazine ring of the flavin. A schematic reaction mechanism for the oxidation of monolignols by *At*BBE-like 15 is shown in Figure 6. To test this hypothesis we have initiated a site-directed mutagenesis study of the pertinent active site residues.

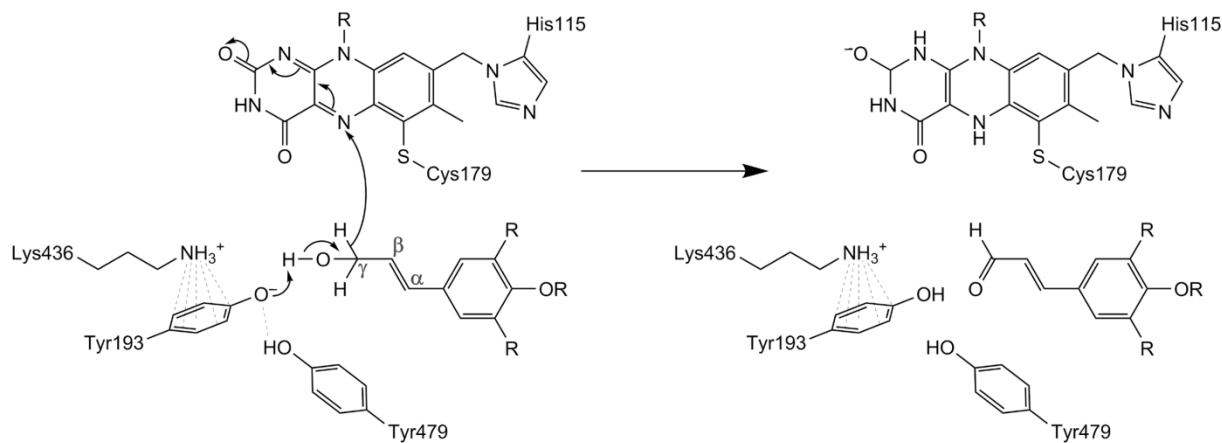


Figure 6: Proposed reaction mechanism for substrate oxidation. Y193, Y479 and K436 concertedly act as an active site base abstracting a proton from the alcohol with subsequent hydride transfer to the N5 of the isoalloxazine ring.

Structural comparison with other members of the VAO family

In recent years the structures of several other members of the VAO family were determined that share a high degree of structural similarity despite low similarity on the sequence level. Structural superposition of *At*BBE-like 15 with Dbv29, GOOX, AknOx and *Ec*BBE gives RMSD of 1.45 Å

(for 1652 backbone atoms), 1.36 Å (for 1556 backbone atoms), 1.47 Å (for 1526 backbone atoms) and 0.95 Å (for 2068 backbone atoms) respectively, while sequence identities of 22%, 22%, 23% and 41%, respectively, are found. The bacterial oxidases Dbv29 and AknOx catalyze similar oxidations of alcohol groups and thus possess a very similar catalytic motif consisting of both tyrosine residues and the lysine residue also present in *AtBBE*-like 15 while the substrate recognition motif is clearly different as depicted in Figure 7 (panels C and D, respectively). In any case, these enzymes act on alcohol substrates that show no similarity to the substrates identified for *AtBBE*-like 15 and 13 and, moreover, are not related to lignin metabolism. Importantly, for Dbv29 and AknOx it was found that both tyrosine residues are crucial for catalysis thus supporting the proposed role of Y193 and Y479 in the mechanism shown in Figure 6 for *AtBBE*-like 15 (and *AtBBE*-like 13) (10,41). While Dbv29 and AknOx resemble *AtBBE*-like 15 and 13 concerning the composition of the active site on the *si*-side of the isoalloxazine ring, the residue that determines the reactivity towards dioxygen, i. e. L182 in the case of *AtBBE*-like 15, is a valine in both enzymes, defining them as oxidases (38). The active site of GOOX has the same substrate recognition motif but a distinct catalytic motif featuring a glutamate residue (shown in blue in Figure 7E) instead of the tyrosine and lysine seen in *AtBBE*-like 15 (compare panels B and E in Figure 7). In fact, this active site composition is similar to group one of the *AtBBE*-like family and thus it is conceivable that these BBE-homologs are also involved in the oxidation of carbohydrates as already reported for some plant BBE-like enzymes (8,9). Not surprisingly, the biggest difference in active site composition is seen with *EcBBE* as this enzyme catalyzes an unusual oxidative ring closure reaction in alkaloid biosynthesis: though the overall topology shows high similarity (Figure 7A) except for the tyrosine in the substrate recognition motif (Y106) all other residues vary (compare panel B and F in Figure 7). Moreover, E417 replacing the glutamine of the substrate recognition motif assumes a crucial role in the reaction mechanism of *EcBBE* and thus becomes part of the catalytic machinery of the enzyme (16). This comparison illustrates that this enzyme family can be tuned for new reactivities by strategic single or multiple exchanges of amino acids in the active site. In fact, even within a given active site different (oxidation) reactions are supported depending on the available substrates further demonstrating the plasticity of the active site (44).

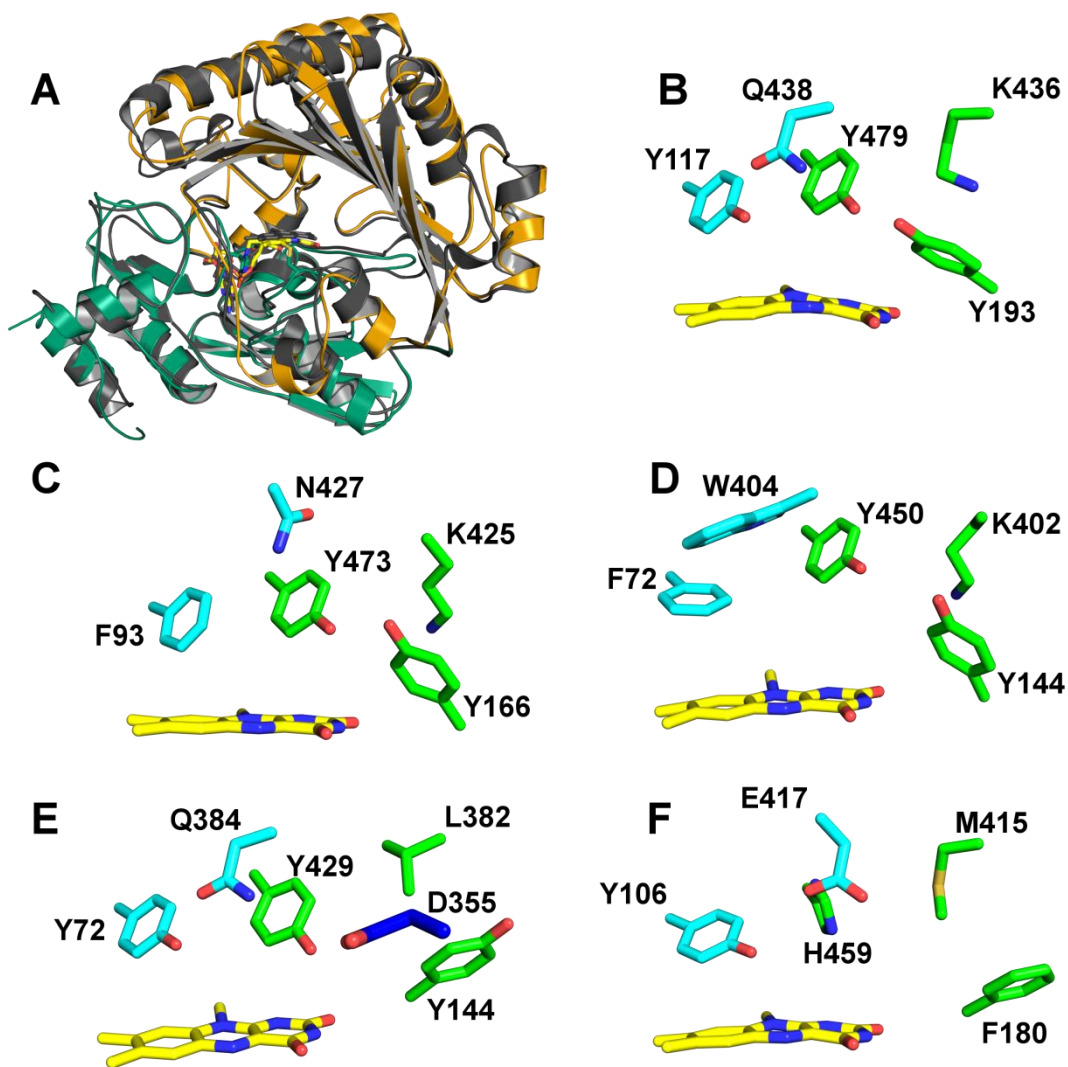


Figure 7: Comparison of overall topology and active site composition of various BBE-like enzymes and VAO superfamily members. Panel A: Overall topology of *AtBBE*-like 15 and superposition with *EcBBE*. Panels B to F show the substrate coordination and catalytic motif in green and cyan, respectively, for the following BBE-like proteins: B, *AtBBE*-like 15, the substrate coordination motif consists of Y117 and Q438 and the catalytic motif is formed by Y479, Y193 and K436; C, *Dbv29*, the catalytic motif is invariant, while the substrate coordination motif is different; D, *AknOx*, the catalytic motif is invariant, while the substrate coordination motif differs; E, *GOOX*, the catalytic motif is disrupted, and appears to be restored by the presence of another catalytic base, *i.e.* D355; F, *EcBBE*, both motifs are disrupted with E417 serving as a catalytic base.

Proposed role of AtBBE-like15/monolignol oxidoreductases in plants

Monolignols are secreted into the apoplast and polymerized to various cell wall components. Although monolignols are thought to be secreted in their alcohol forms, not all monolignol-derived cell wall components are coupling products of monolignols but also the aldehydes are incorporated into the cell wall (45). It has been shown by mass spectrometry that *AtBBE*-like 15 is located in the apoplastic fluid of *A. thaliana* and thus our findings that *AtBBE*-like 15 (and *AtBBE*-like 13) oxidizes monolignols to their corresponding aldehydes indicates that they are likely physiological substrates (46). In addition, the glycosylated form of coniferyl alcohol (coniferin) is also accepted as substrate. Additionally, oxidation of coniferin to its corresponding aldehyde has been postulated by Tsuji *et al.* for the plant *Gingko biloba* (47). According to their hypothesis, oxidation of the β -glycosylated monolignols precedes hydrolysis to the free monolignols and thus plays an important role for the mobilization of monolignols from their glycosidic storage forms. Hence the demonstrated activity of *AtBBE*-like 13 and *AtBBE*-like 15 *in vitro* suggests that the enzymes may participate in the mobilization and oxidation of monolignols required for polymerization processes in the plant cell wall (*e.g.* lignification). Interestingly, more than 20 different glycoside hydrolases were also identified during this proteome analysis, suggesting that *AtBBE*-like 15, and potentially also other members of the family work in concert with these hydrolases to mobilize building blocks from their storage forms. This concept receives further support by co-expression data retrieved from the ATTET II server (CoExSearch Version 4.1). Among the enzymes co-expressed with *AtBBE*-like 15 are phenylalanine ammonia-lyase 4 (PAL4), an important rate-determining entry point of the phenylpropanoid pathway, and β -glucosidase 41 clustering with the monolignol glucoside hydrolases At1g61810 (BGLU45), At1g61820 (BGLU46) (see supplementary Table S2) (48,49). Thus we suggest that *AtBBE*-like 13 and *AtBBE*-like 15 participate in the adaptation of the extracellular monolignol pool prior to polymerization and are thus involved in cell wall formation required during certain growth phases and in response to stressors. Since the active site motifs found in *AtBBE*-like 13 and *AtBBE*-like 15 are conserved in twelve other members of the BBE-like enzyme family in *A. thaliana* we predict that they play similar roles in the plant potentially with diverging substrate specificities or, alternatively, with different spatial (*i.e.* different tissues) or temporal (*i.e.* induced by different biotic or abiotic stressors) features. The presence of homologs of *AtBBE*-like 13 and *AtBBE*-like 15 in many other plants (see above) indicates a

general role of this enzyme family in the plant kingdom. In contrast, enzymes such as *EcBBE* and THCA-synthase serve in “secondary” pathways restricted to certain plant families or genera and hence these have evolved, *e.g.* by gene duplication and subsequent diversification by mutation, from the primordial monolignol oxidoreductases, a phenomenon well documented for the evolution of new plant defense compounds (50).

From the analysis of the active site signatures it is also evident that *AtBBE*-like enzymes in phylogenetic groups one, three and seven possess distinct catalytic machineries and probably act on as yet unidentified substrates. These BBE homologs are currently the target of further studies to reveal their biochemical properties and physiological function. In addition, we have initiated the generation, identification and characterization of gene knock-out plants with the aim to investigate the role of *AtBBE*-likes in cell wall metabolism during plant development and stress response.

References

1. Winkler, A., Hartner, F., Kutchan, T. M., Glieder, A., and Macheroux, P. (2006) Biochemical evidence that berberine bridge enzyme belongs to a novel family of flavoproteins containing a bi-covalently attached FAD cofactor *J. Biol. Chem.* **281**, 21276-21285
2. Facchini, P. J., Penzes, C., Johnson, A. G., and Bull, D. (1996) Molecular characterisation of berberine bridge enzyme genes from opium poppy *Plant Physiol.* **112**, 1669-1677
3. Kutchan, T. M., and Dittrich, H. (1995) Characterization and mechanism of the berberine bridge enzyme, a covalently flavinylated oxidase of benzophenanthridine alkaloid biosynthesis in plants *J. Biol. Chem.* **270**, 24475-24481
4. Wallner, S., Dully, C., Daniel, B., and Macheroux, P. (2012) Berberine bridge enzyme and the family of bicovalent flavoenzymes. in *Handbook of flavoproteins*, de Gruyter. pp 1-24
5. Winter, D., Vinegar, B., Nahal, H., Ammar, R., Wilson, G. V., and Provart, N. J. (2007) An "Electronic Fluorescent Pictograph" browser for exploring and analyzing large-scale biological data sets *PLoS One* **2**, e718
6. Gonzalez-Candelas, L., Alamar, S., Sanchez-Torres, P., Zacarias, L., and Marcos, J. F. (2010) A transcriptomic approach highlights induction of secondary metabolism in citrus fruit in response to *Penicillium digitatum* infection *BMC Plant Biol.* **10**, 194
7. Attila, C., Ueda, A., Cirillo, S. L., Cirillo, J. D., Chen, W., and Wood, T. K. (2008) *Pseudomonas aeruginosa* PAO1 virulence factors and poplar tree response in the rhizosphere *Microb. Biotechnol.* **1**, 17-29
8. Carter, C. J., and Thornburg, R. W. (2004) Tobacco nectarin V is a flavin-containing berberine bridge enzyme-like protein with glucose oxidase activity *Plant Physiol.* **134**, 460-469
9. Custers, J. H., Harrison, S. J., Sela-Buurlage, M. B., van Deventer, E., Lageweg, W., Howe, P. W., van der Meijs, P. J., Ponstein, A. S., Simons, B. H., Melchers, L. S., and Stuiver, M. H. (2004) Isolation and characterisation of a class of carbohydrate oxidases from higher plants, with a role in active defence *Plant J.* **39**, 147-160
10. Alexeev, I., Sultana, A., Mäntsälä, P., Niemi, J., and Schneider, G. (2007) Aclacinomycin oxidoreductase (AknOx) from the biosynthetic pathway of the antibiotic aclacinomycin is an unusual flavoenzyme with a dual active site *Proc. Natl. Acad. Sci. USA* **104**, 6170-6175
11. Carlson, J. C., Li, S., Gunatilleke, S. S., Anzai, Y., Burr, D. A., Podust, L. M., and Sherman, D. H. (2011) Tirandamycin biosynthesis is mediated by co-dependent oxidative enzymes *Nature Chem.* **3**, 628-633
12. Mo, X., Huang, H., Ma, J., Wang, Z., Wang, B., Zhang, S., Zhang, C., and Ju, J. (2011) Characterization of TrdL as a 10-hydroxy dehydrogenase and generation of new analogues from a tirandamycin biosynthetic pathway *Org. Lett.* **13**, 2212-2215
13. Pagnussat, G. C., Yu, H. J., Ngo, Q. A., Rajani, S., Mayalagu, S., Johnson, C. S., Capron, A., Xie, L. F., Ye, D., and Sundaresan, V. (2005) Genetic and molecular identification of genes

- required for female gametophyte development and function in *Arabidopsis* *Development* **132**, 603-614
14. Hooper, C. M., Tanz, S. K., Castleden, I. R., Vacher, M. A., Small, I. D., and Millar, A. H. (2014) SUBAcon: a consensus algorithm for unifying the subcellular localization data of the *Arabidopsis* proteome *Bioinformatics* **30**, 3356-3364
 15. Shoyama, Y., Tamada, T., Kurihara, K., Takeuchi, A., Taura, F., Arai, S., Blaber, M., Morimoto, S., and Kuroki, R. (2012) Structure and function of 1-tetrahydrocannabinolic acid (THCA) synthase, the enzyme controlling the psychoactivity of *Cannabis sativa* *J. Mol. Biol.* **423**, 96-105
 16. Winkler, A., Lyskowski, A., Riedl, S., Puhl, M., Kutchan, T. M., Macheroux, P., and Gruber, K. (2008) A concerted mechanism for berberine bridge enzyme *Nature Chem. Biol.* **4**, 739-741
 17. Petersen, T. N., Brunak, S., von Heijne, G., and Nielsen, H. (2011) SignalP 4.0: discriminating signal peptides from transmembrane regions *Nature Meth.* **8**, 785-786
 18. Weis, R., Luiten, R., Skranc, W., Schwab, H., Wubbolts, M., and Glieder, A. (2004) Reliable high-throughput screening with *Pichia pastoris* by limiting yeast cell death phenomena *FEMS Yeast Res.* **5**, 179-189
 19. Schrittwieser, J. H., Resch, V., Wallner, S., Lienhart, W. D., Sattler, J. H., Resch, J., Macheroux, P., and Kroutil, W. (2011) Biocatalytic organic synthesis of optically pure (S)-scoulerine and berbine and benzyloisoquinoline alkaloids *J. Org. Chem.* **76**, 6703-6714
 20. D'Arcy, A., Villard, F., and Marsh, M. (2007) An automated microseed matrix-screening method for protein crystallization *Acta Crystallogr.* **D63**, 550-554
 21. Kabsch, W. (2010) Integration, scaling, space-group assignment and post-refinement *Acta Crystallogr.* **D66**, 125-132
 22. Kantardjiev, K. A., and Rupp, B. (2003) Matthews coefficient probabilities: Improved estimates for unit cell contents of proteins, DNA, and protein-nucleic acid complex crystals *Protein Sci.* **12**, 1865-1871
 23. McCoy, A. J., Grosse-Kunstleve, R. W., Adams, P. D., Winn, M. D., Storoni, L. C., and Read, R. J. (2007) Phaser crystallographic software *J. Appl. Crystallogr.* **40**, 658-674
 24. Adams, P. D., Afonine, P. V., Bunkoczi, G., Chen, V. B., Davis, I. W., Echols, N., Headd, J. J., Hung, L.-W., Kapral, G. J., Grosse-Kunstleve, R. W., McCoy, A. J., Moriarty, N. W., Oeffner, R., Read, R. J., Richardson, D. C., Richardson, J. S., Terwilliger, T. C., and Zwart, P. H. (2010) PHENIX: a comprehensive Python-based system for macromolecular structure solution *Acta Crystallogr.* **D66**, 213-221
 25. Emsley, P., and Cowtan, K. (2004) Coot: Model-building tools for molecular graphics *Acta Crystallogr.* **D60**, 2126-2132

26. Painter, J., and Merritt, E. A. (2006) Optimal description of a protein structure in terms of multiple groups undergoing TLS motion *Acta Crystallogr.* **D62**, 439-450
27. Chen, V. B., Arendall, W. B., 3rd, Headd, J. J., Keedy, D. A., Immormino, R. M., Kapral, G. J., Murray, L. W., Richardson, J. S., and Richardson, D. C. (2010) MolProbity: all-atom structure validation for macromolecular crystallography *Acta Crystallogr.* **D66**, 12-21
28. Massey, V., and Hemmerich, P. (1978) Photoreduction of flavoproteins and other biological compounds catalyzed by deazaflavins *Biochemistry* **17**, 9-17
29. Gosch, C., Halbwirth, H., Schneider, B., Hölscher, D., and Stich, K. (2010) Cloning and heterologous expression of glycosyltransferases from *Malus x domestica* and *Pyrus communis*, which convert phloretin to phloretin 2'-O-glucoside (phloridzin) *Plant Sci.* **178**, 299-306
30. Wallace, I. M., O'Sullivan, O., Higgins, D.G., and Notredame, C. (2006) M-Coffee: combining multiple sequence alignment methods with T-Coffee *Nucleic Acids Res.* **34**, 1692-1699
31. Waterhouse, A. M., Procter, J. B., Martin, D. M., Clamp, M., and Barton, G. J. (2009) Jalview Version 2--a multiple sequence alignment editor and analysis workbench *Bioinformatics* **25**, 1189-1191
32. Felsenstein, J. (2005) PHYLIP - Phylogeny Inference Package v 3.6. *Department of Genome Sciences, University of Washington, Seattle*
33. Morris, G. M., Goodsell, D. S., Huey, R., and Olson, A. J. (1996) Distributed automated docking of flexible ligands to proteins: parallel applications of AutoDock 2.4 *J. Comput. Aided Mol. Des.* **10**, 293-304
34. Goodsell, D. S., Morris, G. M., and Olson, A. J. (1996) Automated docking of flexible ligands: applications of AutoDock *J. Mol. Recognit.* **9**, 1-5
35. Duan, Y., Wu, C., Chowdhury, S., Lee, M. C., Xiong, G., Zhang, W., Yang, R., Cieplak, P., Luo, R., Lee, T., Caldwell, J., Wang, J., and Kollman, P. (2003) A point-charge force field for molecular mechanics simulations of proteins based on condensed-phase quantum mechanical calculations *J. Comput. Chem.* **24**, 1999-2012
36. Krieger, E., Koraimann, G., and Vriend, G. (2002) Increasing the precision of comparative models with YASARA NOVA--a self-parameterizing force field *Proteins* **47**, 393-402.
37. Cummings, M. D., Farnum, M. A., and Nelen, M. I. (2006) Universal screening methods and applications of ThermoFluor *J. Biomol. Screen.* **11**, 854-863
38. Zafred, D., Steiner, B., Teufelberger, A. R., Hromic, A., Karplus, P. A., Schofield, C. J., Wallner, S., and Macheroux, P. (2015) Rationally engineered flavin-dependent oxidase reveals steric control of dioxygen reactivity *FEBS J.*, in press.
39. Winkler, A., Kutchan, T. M., and Macheroux, P. (2007) 6-S-cysteinylation of bi-covalently attached FAD in berberine bridge enzyme tunes the redox potential for optimal activity *J. Biol. Chem.* **282**, 24437-24443

40. Winkler, A., Motz, K., Riedl, S., Puhl, M., Macheroux, P., and Gruber, K. (2009) Structural and mechanistic studies reveal the functional role of bicovalent flavinylation in berberine bridge enzyme *J. Biol. Chem.* **284**, 19993-20001
41. Liu, Y. C., Li, Y. S., Lyu, S. Y., Hsu, L. J., Chen, Y. H., Huang, Y. T., Chan, H. C., Huang, C. J., Chen, G. H., Chou, C. C., Tsai, M. D., and Li, T. L. (2011) Interception of teicoplanin oxidation intermediates yields new antimicrobial scaffolds *Nature Chem. Biol.* **7**, 304-309
42. Huang, C.-H., Lai, W.-L., Lee, M.-H., Chen, C.-J., Vasella, A., Tsai, Y.-C., and Liaw, S.-H. (2005) Crystal structure of glucooligosaccharide oxidase from *Acremonium strictum*. A novel flavinylation of 6-S-cysteinyl, 8 α -N1-histidyl FAD *J. Biol. Chem.* **280**, 38831-38838
43. Noinaj, N., Bosserman, M. A., Schickli, M. A., Piszczek, G., Kharel, M. K., Pahari, P., Buchanan, S. K., and Rohr, J. (2011) The crystal structure and mechanism of an unusual oxidoreductase, GilR, involved in gilvocarcin V biosynthesis *J. Biol. Chem.* **286**, 23533-23543
44. Winkler, A., Puhl, M., Weber, H., Kutchan, T. M., Gruber, K., and Macheroux, P. (2009) Berberine bridge enzyme catalyzes the six electron oxidation of (S)-reticuline to dehydroscoulerine *Phytochemistry* **70**, 1092-1097
45. Morreel, K., Ralph, J., Kim, H., Lu, F., Goeminne, G., Ralph, S., Messens, E., and Boerjan, W. (2004) Profiling of oligolignols reveals monolignol coupling conditions in lignifying poplar xylem *Plant Physiol.* **136**, 3537-3549
46. Jamet, E., Canut, H., Boudart, G., and Pont-Lezica, R. F. (2006) Cell wall proteins: a new insight through proteomics *Trends Plant Sci.* **11**, 33-39
47. Tsuji, Y., Chen, F., Yasuda, S., and Fukushima, K. (2005) Unexpected behavior of coniferin in lignin biosynthesis of *Ginkgo biloba* L *Planta* **222**, 58-69
48. Escamilla-Trevino, L. L., Chen, W., Card, M. L., Shih, M. C., Cheng, C. L., and Poulton, J. E. (2006) *Arabidopsis thaliana* beta-Glucosidases BGLU45 and BGLU46 hydrolyse monolignol glucosides *Phytochemistry* **67**, 1651-1660
49. Xu, Z., Escamilla-Trevino, L., Zeng, L., Lalgondar, M., Bevan, D., Winkel, B., Mohamed, A., Cheng, C. L., Shih, M. C., Poulton, J., and Esen, A. (2004) Functional genomic analysis of *Arabidopsis thaliana* glycoside hydrolase family 1 *Plant Mol. Biol.* **55**, 343-367
50. Ober, D., and Kaltenecker, E. (2009) Pyrrolizidine alkaloid biosynthesis, evolution of a pathway in plant secondary metabolism *Phytochemistry* **70**, 1687-1695

Oxidation of Monolignols by Members of the Berberine Bridge Enzyme Family Suggests a Role in Plant Cell Wall Metabolism

Supplementary Information

Bastian Daniel,¹ Tea Pavkov-Keller^{2,3}, Barbara Steiner,¹ Anđela Dordic^{2,3}, Alexander Gutmann,⁴ Bernd Nidetzky,⁴ Christoph W. Sensen,⁵ Eric van der Graaff,⁶ Silvia Wallner,¹ Karl Gruber² and Peter Macheroux^{1*†}

¹Graz University of Technology, Institute of Biochemistry, Graz, Austria

²University of Graz, Institute of Molecular Biosciences, Graz, Austria

³Austrian Centre of Industrial Biotechnology, Graz, Austria

⁴Graz University of Technology, Institute of Biotechnology and Biochemical Engineering, Graz, Austria

⁵Graz University of Technology, Institute of Molecular Biotechnology, Graz, Austria

⁶Copenhagen University, Copenhagen, Denmark

Table S1: Thermofluor measurements with selected compounds

Substance	CAS-number	T _m [°C]	ΔT _m [°C]
2-Deoxyglucose	154-17-6	78	17
D,L-Proline	609-36-9	77.5	16.5
trans-Cinnamyl alcohol	104-54-1	76.5	15.5
D-Glucose	492-62-6	76	15
3-Aminobenzyl alcohol	1877-77-6	75	14
3,4-Dimethoxybenzyl alcohol	93-03-8	75	14
4-Isopropylbenzyl alcohol	536-60-7	74.5	13.5
(S)-(-)-Limonen	5989-54-8	74	13
Benzylalcohol	100-51-6	73	12
Geraniol	106-24-1	73	12
Lactose monohydrate	64044-51-5	72	11
D-Maltose		72	11
Anthranilic acid	118-92-3	71	10
Cellobiose	528-50-7	71	10
4-Chlorobenzyl alcohol	873-76-7	71	10
D-Galactose	59-23-4	71	10
D-Sorbitol	50-70-4	71	10
Furfuryl alcohol	98-00-0	70.5	9.5
2-Indanol	4254-29-9	70.5	9.5
Polygalacturonic acid	25990-10-7	70	9
(+)-Pulegone	89-82-7	70	9
Eugenol	97-53-0	65.5	4.5
Xylose	58-86-6	66.5	5.5
3-Methoxyphenol	150-19-6	64.5	3.5
D-Lyxose	1114-34-7	64	3
Acetylacetone	123-54-6	63.5	2.5
3-(3,4-Dihydroxyphenyl)-DL-alanine (L-DOPA)	63-84-3	63.5	2.5
3-Aminosalicylic acid	570-23-0	63	2
2-Aminothiophenol	137-07-5	63	2
p-Anisidine	104-94-9	63	2
(S)-(-)-β-Citronellol	7540-51-4	63	2
3,4-Dimethoxybenzotrile	2024-82-1	63	2
Flavone	525-82-6	63	2
Isopropyl salicylate	607-85-2	63	2
Vanillin	121-33-5	63	2
meso-Erythritol	149-32-6	62.5	1.5
2-Acetyl-5-bromothiophene	5370-25-2	62	1
1,1'-Bi-2-naphthol	602-09-5	62	1
3-Chlorocoumarin	92-45-5	62	1
Dihydrocarveol	619-01-2	62	1
3-Aminophenol	591-27-5	61.5	0.5
Coumarin	91-64-5	61.5	0.5
Diacetyldioxim	95-45-4	61.5	0.5
2,6-Lutidin	108-48-5	61.5	0.5

(+/-)-Mandelic acid	611-72-3	61.5	0.5
Acetone cyanohydrin	75-86-5	61	0
Acetonylacetone	110-13-4	61	0
Benzamide	55-21-0	61	0
(R)-(-)-3-Chloromandelic acid	61008-98-8	61	0
trans-Cinnamitrile	1885-38-7	61	0
o-Cresol	95-48-7	61	0
1,2-Dihydronaphtalen	446-53-0	61	0
4,4'-Dimethoxybenzoin	119-25-8	61	0
2,6-Dimethoxyphenol	91-10-1	61	0
2,6-Dimethylaniline	87-62-7	61	0
2,6-Dimethylanisol	1004-66-6	61	0
8-Hydroxyquinoline	148-24-3	61	0
Maltose	69-79-4	61	0
Mandelonitrile	532-28-5	61	0
D-Mannitol	69-65-8	61	0
exo-Norborneol	497-37-0	61	0
Norcamphor	497-38-1	61	0
Safrole	94-59-7	61	0
Sucrose	57-50-1	61	0
Tannin	1401-55-4	61	0
DL-Tryptophan	54-12-6	61	0
3-Acetylcoumarin	3949-36-8	60.5	-0.5
Adonitol	488-81-3	60.5	-0.5
Amylose	9005-82-7	60.5	-0.5
D-Arabinose	10323-20-3	60.5	-0.5
Benzylamine	100-46-9	60.5	-0.5
p-Bromo-DL-mandelic acid	6940-50-7	60.5	-0.5
rac-Camphor	76-22-2	60.5	-0.5
2-Chlorophenol	95-57-8	60.5	-0.5
Cholin acetate	14586-35-7	60.5	-0.5
4-Chromamone	491-37-2	60.5	-0.5
trans-Cinnamaldehyde	14371-10-9	60.5	-0.5
p-Cresol	106-44-5	60.5	-0.5
L-Fructose	2438-80-4	60.5	-0.5
Galactan	9037-55-2	60.5	-0.5
Hydroxyethylcellulose	9004-62-0	60.5	-0.5
Isobutyl cinnamate predominantly trans	122-67-8	60.5	-0.5
cis-Jasmone	488-10-8	60.5	-0.5
Lactulose	4618-18-2	60.5	-0.5
Methyl-D-mannopyranoside	617-04-9	60.5	-0.5
3-Acetylpyridine	350-03-8	60	-1
Adenine	73-24-5	60	-1
Aniline	62-53-3	60	-1
Anisole	100-66-3	60	-1
Anthranilic acid	118-92-3	60	-1
Arabuigalactan	9036-66-2	60	-1

Butyrophenone	495-40-9	60	-1
Carboxymethylcellulose	9004-32-4	60	-1
Carrageen		60	-1
Carvacrol	499-75-2	60	-1
4-Chloro-3-nitrocoumarin	38464-20-9	60	-1
rac-(-)-Citronellic acid	502-47-6	60	-1
Fructose	57-48-7	60	-1
D(+)-Galatosamine hydrochloride	1772-003-8	60	-1
Geranic acid	459-80-3	60	-1
Glucoseamine	3416-24-8	60	-1
Isobutyramide	563-83-7	60	-1
Isophorone	78-59-1	60	-1
4-Isopropyl aniline	99-88-7	60	-1
4-Isopropyl benzoic acid	536-66-3	60	-1
Maltodextrin	9050-36-6	60	-1
Methyl- β -D-glucoside	709-50-2	60	-1
Morpholine	110-91-8	60	-1
2-Naphtol	135-19-3	60	-1
Natriumalginat	9005-38-3	60	-1
D,L-Norvaline	760-78-1	60	-1
8-Quinolinol	148-24-3	60	-1
D-Ribose	50-69-1	60	-1
Trehalose Dihydrat	6138-23-4	60	-1
2,3,3-Trimethylindolenine	1640-39-7	60	-1
Xylitol	87-99-0	60	-1
L-Xylose	609-06-3	60	-1
m-Anisaldehyde	591-31-1	59.5	-1.5
m-Cresol	108-39-4	59.5	-1.5
Indole	120-72-9	59.5	-1.5
Methylnicotinate	93-60-7	59.5	-1.5
Methylvaleraldehyde	123-15-9	59.5	-1.5
L-Arabinose	5328-37-0	59	-2
Cellulose	9004-34-6	59	-2
Chitin	1398-61-4	59	-2
4-Chlorophenol	106-48-9	59	-2
D-Gluconic acid	526-95-4	59	-2
Pyrocatechol	120-80-9	59	-2
Quinoline	91-22-5	59	-2
Xylan	9014-63-5	59	-2
D,L-Phenylalanine	150-30-1	58.5	-2.5
Glucuronolactone	32449-92-6	58	-3
Mannan	9036-88-8	58	-3
D(+)-Glucuronic acid monohydrate	207300-70-7	56.5	-4.5
Valeraldehyde	110-62-3	56	-5
(+/-)-Menthol	89-78-1	55	-6
(-)-Ephedrine	299-42-3	54	-7
Gallic acid	149-91-7	54	-7

Benzoic acid	65-85-0	53.5	-7.5
4-Aminobenzoic acid	150-13-0	50	-11
3-Methylbutylaldehyde (Isovaleraldehyde)	590-86-3	48	-13
3,5-Dihydroxybenzoic acid	99-10-5	40.5	-20.5
D-Mandelic acid	611-71-2	37	-24
4-Acetylbenzoic acid	586-89-0	---	---
2-Acetyl-1-methylpyrrole	932-16-1	---	---
2-Aminophenol	95-55-6	---	---
4-Aminophenol	123-30-8	---	---
5-Aminosalicylic acid	89-57-6	---	---
trans-Anethole	4180-23-8	---	---
p-Anisaldehyde	123-11-5	---	---
p-Anisic acid	100-09-4	---	---
L-Arabinose	5328-37-0	---	---
Benzaldehyde	100-52-7	---	---
Caffeic acid	331-39-5	---	---
3-Chlorobenzylamine	4152-90-3	---	---
3-Chloro-2-norboranone	30860-22-1	---	---
trans-Cinnamic acid	140-10-3	---	---
Curcumin	458-37-7	---	---
2,4-Dihydroxybenzoic acid	89-86-1	---	---
2,5-Dihydroxybenzoic acid	490-79-9	---	---
4-Dimethylaminopyridine, DMAP	1122-58-3	---	---
4-Ethylaniline	589-16-2	---	---
Hydrocinnamaldehyde	104-53-0	---	---
4-Hydroxy-3-nitrocoumarin	20261-31-8	---	---
2-Iodobenzoic acid	88-67-5	---	---
cis/trans Isoeugenol	97-54-1	---	---
Kojic acid	501-30-4	---	---
Lignin		---	---
L-Mandelic acid	17199-29-0	---	---
1-Naphthol	90-15-3	---	---
Pectin	9000-69-5	---	---
Pyrogallol	87-66-1	---	---
Salicylaldehyde	90-02-8	---	---
Valeric acid	109-52-4	---	---

For details of the experimental set-up see “Materials & Methods”;

---, in the presence of these compounds no reproducible signal was obtained;

Table S2: Genes coexpressed with *AtBBE*-like 15 according to ATTET II server

Rank	Mutual rank	Correlation	Locus	Function
1	2.6	0.72	At1g26820	ribonuclease 3
2	3.5	0.68	At3g10340	phenylalanine ammonia-lyase 4
3	5.3	0.68	At1g62990	KNOTTED-like homeobox of Arabidopsis thaliana 7
4	6.5	0.64	At2g22560	Kinase interacting (KIP1-like) family protein
5	7.3	0.67	At2g14095	
6	7.5	0.67	At1g28470	NAC domain containing protein 10
7	8.1	0.69	At4g16620	nodulin MtN21 /EamA-like transporter family protein
8	8.7	0.68	At4g18425	Protein of unknown function (DUF679)
9	9.5	0.58	At4g24430	Rhamnogalacturonate lyase family protein
10	9.8	0.65	260208_s_at	At1g70670;At1g70680
11	10.9	0.66	At5g04200	metacaspase 9
12	12.4	0.66	At1g11190	bifunctional nuclease i
13	12.4	0.65	At4g04460	Saposin-like aspartyl protease family protein
14	13.0	0.62	At2g47670	Plant invertase/pectin methylesterase inhibitor superfamily protein
15	17.9	0.55	At2g18480	Major facilitator superfamily protein
16	22.4	0.66	267343_at	At2g44260
17	27.8	0.56	At1g23560	Domain of unknown function (DUF220)
18	28.0	0.58	At3g21550	DUF679 domain membrane protein 2
19	28.3	0.60	At5g65530	Protein kinase superfamily protein
20	30.5	0.54	At2g22800	Homeobox-leucine zipper protein family
21	32.2	0.59	At5g58730	pfkB-like carbohydrate kinase family protein
22	33.3	0.63	At4g34320	Protein of unknown function (DUF677)
23	33.6	0.58	At5g54570	beta glucosidase 41
24	34.3	0.62	At5g08480	VQ motif-containing protein
25	35.4	0.53	At3g27200	Cupredoxin superfamily protein

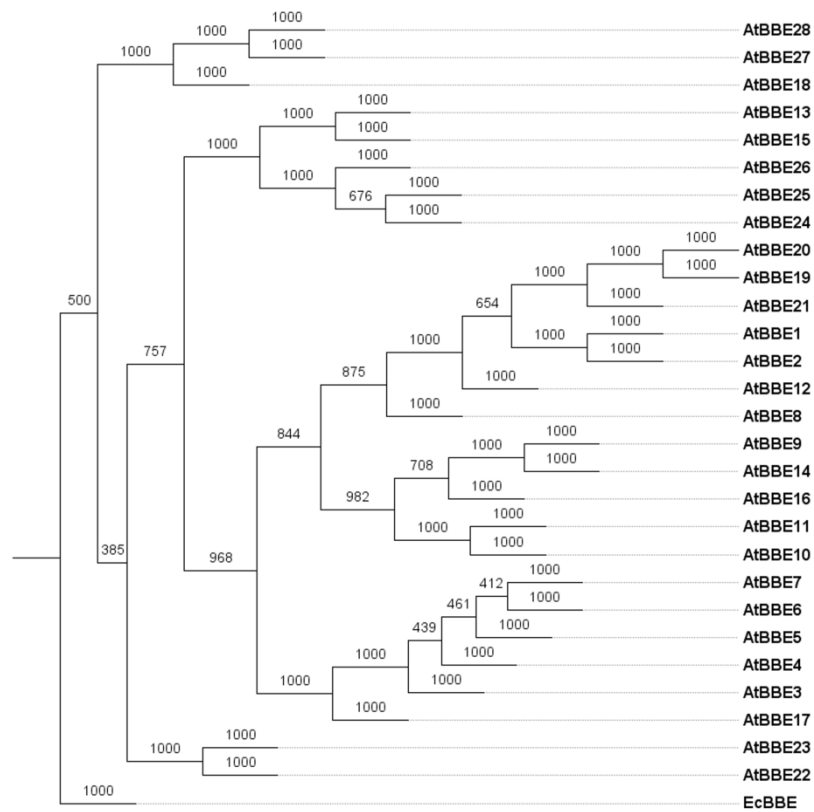


Figure S1: Bootstrapped phylogenetic tree including all *At*BBE-like proteins and *Ec*BBE. The following sequences were used for analysis (locus name/Accession number):

*At*BBE-like 1, AT1G01980.1/Q9LPC3; *At*BBE-like 2, AT1G11770.1/Q9SA99;
*At*BBE-like 3, AT1G26380.1/Q9FZC4; *At*BBE-like 4, AT1G26390.1/Q9FZC5;
*At*BBE-like 5, AT1G26400.1/Q9FZC6; *At*BBE-like 6, AT1G26410.1/Q9FZC7;
*At*BBE-like 7, AT1G26420.1/Q9FZC8; *At*BBE-like 8, AT1G30700.1/Q9SA85;
*At*BBE-like 9, AT1G30710.1/Q9SA86; *At*BBE-like 10, AT1G30720.1/Q9SA87;
*At*BBE-like 11, AT1G30730.1/Q9SA88; *At*BBE-like 12, AT1G30740.1/Q9SA89;
*At*BBE-like 13, AT1G30760.1/Q93ZA3; *At*BBE-like 14, AT1G34575.1/Q9LNL9;
*At*BBE-like 15, AT2G34790.1/O64743; *At*BBE-like 16, AT2G34810.1/O64745;
*At*BBE-like 17, AT4G20800.1/Q9SVG7; *At*BBE-like 18, AT4G20820.1/Q9SVG5;
*At*BBE-like 19, AT4G20830.1/Q9SVG4; *At*BBE-like 20, AT4G20830.2/Q9SVG4;
*At*BBE-like 21, AT4G20840.1/Q9SVG3; *At*BBE-like 22, AT4G20860.1/Q9SUC6;
*At*BBE-like 23, AT5G44360.1/Q9FKV2; *At*BBE-like 24, AT5G44380.1/Q9FKV0;
*At*BBE-like 25, AT5G44390.1/Q9FKU9; *At*BBE-like 26, AT5G44400.1/Q9FKU8;
*At*BBE-like 27, AT5G44410.1/Q9FI25; *At*BBE-like 28, AT5G44440.1/Q9FI21; *Ec*BBE, AAC39358.

Chapter 3: Form follows function: structure based reaction mechanism of monolignol oxidoreductases

Bastian Daniel¹, Silvia Wallner¹, Barbara Steiner¹, Karl Gruber², and Peter Macheroux^{1*}

¹Graz University of Technology, Institute of Biochemistry, Graz, Austria

²University of Graz, Institute of Molecular Biosciences, Graz, Austria

To whom correspondence should be addressed:

Prof. Dr. Peter Macheroux, Graz University of Technology, Institute of Biochemistry, Petersgasse 12/II, A-8010 Graz, Austria, Tel.: +43-316-873 6450; Fax: +43-316-873 6952; Email: peter.macheroux@tugraz.at

Author contributions:

B.D chose the residues for site directed mutagenesis. B.D., S.W. and B.S. performed the protein expression and biochemical assays. B.D., K.G. and P.M. wrote the manuscript.

Abstract

Monolignol oxidoreductases are members of the berberine bridge enzyme-like (BBE-like) protein family (pfam 08031), they are flavin dependent enzymes that follow the VAO-topology. Recently, we have published the structural and biochemical characterization of two monolignol oxidoreductases from *Arabidopsis thaliana*. We have now conducted a site directed mutagenesis study for one of the enzyme, *AtBBE*-like 15, to extent our understanding of the catalytic mechanism of this enzyme class. In this report, we propose a reaction mechanism based on kinetic properties of active site variants in regard to the crystal structure of the wild type enzyme. Monolignol oxidoreductases were found to oxidize monolignols to the corresponding aldehydes. We propose that this reaction is facilitated by the concerted deprotonation of the allylic alcohol and a hydride transfer from the C α -atom of the alcohol to the flavin. We analyzed the active site and propose Tyr479 and Tyr193 to act concertedly as active catalytic base to facilitate the proton abstraction. Lys436 is indirectly involved in the deprotonation this residue determines the position of Tyr193 via a cation- π interaction. Additionally Tyr117 and Asn438 were found to have an impact on the kinetic properties of the enzyme. Asn438 is proposed to stabilize the transition state, while Tyr117 determines the position of Asn438. Sequence alignments reveal that 14 out of 28 *AtBBE*-likes feature exactly the same active site composition as *AtBBE*-like 15, therefore we anticipate these enzymes to function in an analog manner.

Introduction

Flavoproteins are a diverse protein class utilizing the isoalloxazine ring in form of the flavin mononucleotide (FMN) or the flavine adenine dinucleotide (FAD) for catalysis^{1,2}. Among them is the BBE-like protein family, that was named after the berberine bridge enzyme (*EcBBE*) from *Eschscholzia californica* (*California poppy*) that catalyzes the conversion of (*S*)-reticuline to (*S*)-scoulerine^{3,4}. BBE-likes occur in fungi, bacteria, archaea and plants. In the latter they form a multigene family, the number of members varies from one in the moss *Physcomitrella patens* to 64 in western poplar (*Populus trichocarpa*)⁵. *Arabidopsis thaliana* has 28 genes for BBE-likes (*AtBBE*-likes) and recently we could identify two of them (*AtBBE*-like 13 and 15) as monolignol oxidoreductases⁶. In the course of this study we have solved the crystal structure of *AtBBE*-like 15 and proposed a catalytic mechanism for the enzyme. In this paper we present a site directed mutagenesis study to prove and refine the postulated mechanism by the analysis of the kinetic of

active site variants of *At*BBE-like 15 in respect to the structure of the enzyme. The *At*BBE-like 15 overall topology is shown in Figure 1A with the FAD-binding domain in green, the substrate-binding domain in orange and the FAD cofactor in yellow. In Figure 1B a surface representation of *At*BBE-like 15 is shown.

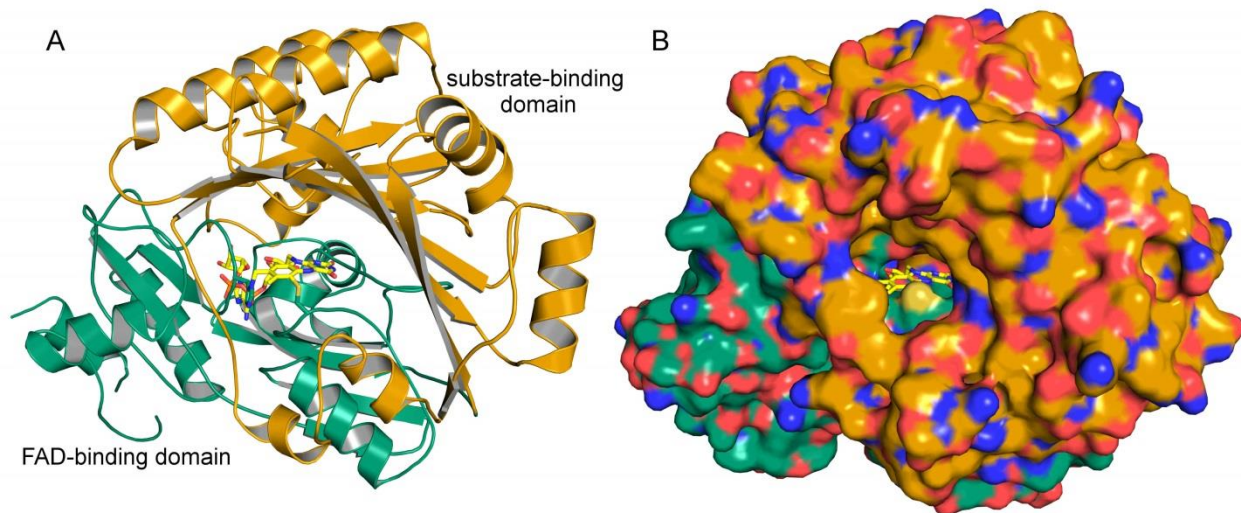


Figure 1: A: Overall topology of *At*BBE-like 15; Sustrate-binding domain is shown in organe, the FAD-binding domain in green. B: Surface representation of *At*BBE-like 15. A cavity harboring the substrate-binding site and the active site is visible that grants access to the flavin (yellow).

As shown in Figure 1A at the interface of the FAD-binding domain (green) and the substrate-binding domain (orange) the isoalloxazine ring is located. A cavity is visible the surface of the protein in Figure 1B which is predominantly formed by the substrate-binding domain. The cavity grants access to the cofactor shown in yellow. Functionally, the cavity can be divided in a substrate binding site that is predominantly formed by hydrophobic or aromatic residues and the active site that is located at the N5 of the isoalloxazine ring and is predominantly formed by polar residues. The cavity was visualized and analyzed using the CASoX tool, in Figure 2 an imprint of the cavity is shown with the surrounding residues ^{7, 8}. In Figure 2A the active site forming residues are shown and in Figure 2B the residues that predominantly contribute to the hydrophobic nature of the substrate binding site. The surrounding of the isoalloxazine ring can be divided in a *re*- and a *si*-side. The *re*- and *si*-side of *At*BBE-like 15 are shown in Figure 2C and B, respectively. Visualized are the secondary structural elements and the residues that establish the major protein-isoalloxazine ring and putatively protein-substrate interactions.

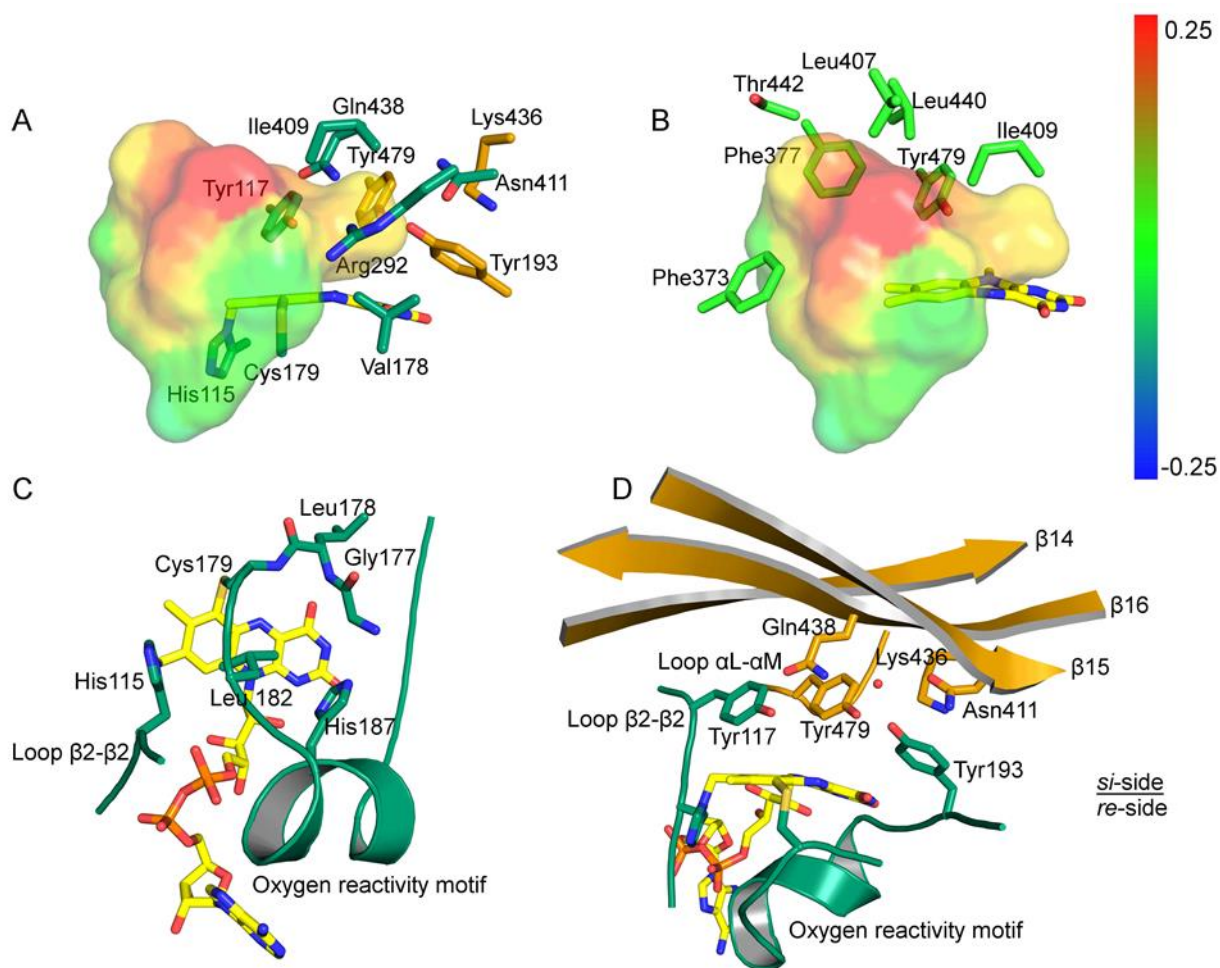


Figure 2: In panel A and B an imprint of the cavity that harbors the substrate-binding site and the active site is shown. Hydrophobic regions are shown in red and hydrophilic in blue. In panel A polar residues are shown that are putatively involved in the catalytic mechanism and residues that determine the shape of the active site. In panel B hydrophobic residues are highlighted that contribute to the lipophilic character of the substrate-binding. In panel C the *re*-side of the isoalloxazine ring is shown. Visualized is the oxygen reactivity motif and the loop β 2- β 3. The bicovalent attachment is established by His115 and Cys179, the reactivity towards oxygen is modulated by the backbone of Cys179, Leu178 and the he gatekeeper residue Leu182 that sterically controls the access to the oxygen hole. In panel D the secondary structural elements that harbor residues that are anticipated to be involved in the catalytic mechanism are shown. All residues that are labelled in this panel were varied to probe their role in the catalytic mechanism.

In Figure 2A and B an imprint of the cavity at the *si*-side is shown, hydrophobic regions are colored red and hydrophilic regions in blue. A set of hydrophobic and aromatic residues is shown in Figure 2A that determines the protein surface of the part of the cavity that is anticipated to facilitate substrate binding. Next to the binding site the diameter of the cavity is reduced by

Tyr117, Ile409, Arg292, Val178, and Cys179, beyond this contraction the protein surface is predominantly formed by polar residues that are anticipated to contribute to the catalytic mechanism (compare Figure 2A). The aromatic ring of the monolignols is anticipated to bind to the hydrophobic binding site while the allylic alcohol enters the active site. In Figure 2C and D the secondary structural elements determining the *re*- and *si*-side of the isoalloxazine ring are shown. In Figure 2C “oxygen reactivity motif” (ORM) and the bivalent cofactor attachment of *AtBBE*-like 15 are shown, the latter is established by His115 and Cys179. Additionally His187 is shown in Figure 2C, Wallner *et al.* have shown for the His174 in *EcBBE* (corresponding to His187 in *AtBBE*-like 15) that the stabilization of the negative charge of the reduced isoalloxazine ring is realized by this residue⁹. The same conformation as described for *EcBBE* can be observed in *AtBBE*-like 15 formed by His187, Gly177 and the hydroxyl group at C2' of the ribityl side chain of the cofactor. As the ORM regulates the reactivity of BBE-likes towards oxygen, all residues involved in the regulation are visualized in Figure 2C. The “oxygen hole” proposed by Zafred *et al.* is formed by the amid backbone of Leu178 and Cys179, as *AtBBE*-like 15 is a dehydrogenase the cavity occupied by the gatekeeper residue Leu182 to prevent the oxidation of the cofactor by molecular oxygen⁶. While interactions between the protein and the isoalloxazine ring are highly conserved and well understood, composition of the *si*-side of BBE-likes is more flexible. Though the active site type present in *AtBBE*-like 15 was shown to be widely distributed in plant kingdom, to the best of our knowledge this is the first characterization of a representative of this enzyme class. In Figure 2D the residues that form the environment of the N5 on the *si*-side are shown. As the hydride transfer takes place at this atom, the surrounding amino acids are bound to be involved in the catalytic mechanism. To probe their function, we have created variants for every residue labeled in Figure 2D.

Experimental and Procedures

Mutagenesis, Protein Expression and Purification

Mutagenesis was conducted as described in Daniel *et al.*, expression and purification has been done as reported before ⁶.

Determination of the extinction coefficient

The extinction coefficient (ϵ_{450}) of AtBBE-like 15 was determined according to Kasprzak *et al.*¹⁰. First a spectrum of the enzyme in the native state was recorded, the enzyme was denatured by the addition of SDS to a final concentration of 0.4% (w/v). Prior to recording the spectrum of the denatured enzyme, the sample was heated to 96 °C for 5 min.

Rapid Reaction Kinetics Using Stopped Flow

Kinetic measurements were conducted as previously reported for the wild type enzyme ⁶. Prior to kinetic measurements the activity of the variants was verified employing coniferyl alcohol. Spectra of the oxidized and reduced variants were recorded employing a specord 205 spectrometer (Analytik Jena AG, Jena, Germany) at a protein concentration of 30 μ M in 50 mM TRIS/HCl buffer pH 8.0. The spectrum of the substrate reduced species was recorded after the addition of coniferyl alcohol to a final concentration of 40 μ M.

Results

Expression and Purification

AtBBE-like 15 variants were expressed using *Komagataella pastoris* as expression host as described before ⁶. The yields of purified protein are summarized in Table 1, enzyme concentration was determined by measuring the absorption at 450 nm. No spectral changes of the variants in comparison with the wild type enzyme were observed with exception of the Y479F variant. Spectra of the oxidized and substrate reduced species of the wild type enzyme and the Y479F variant are shown in Figure 3

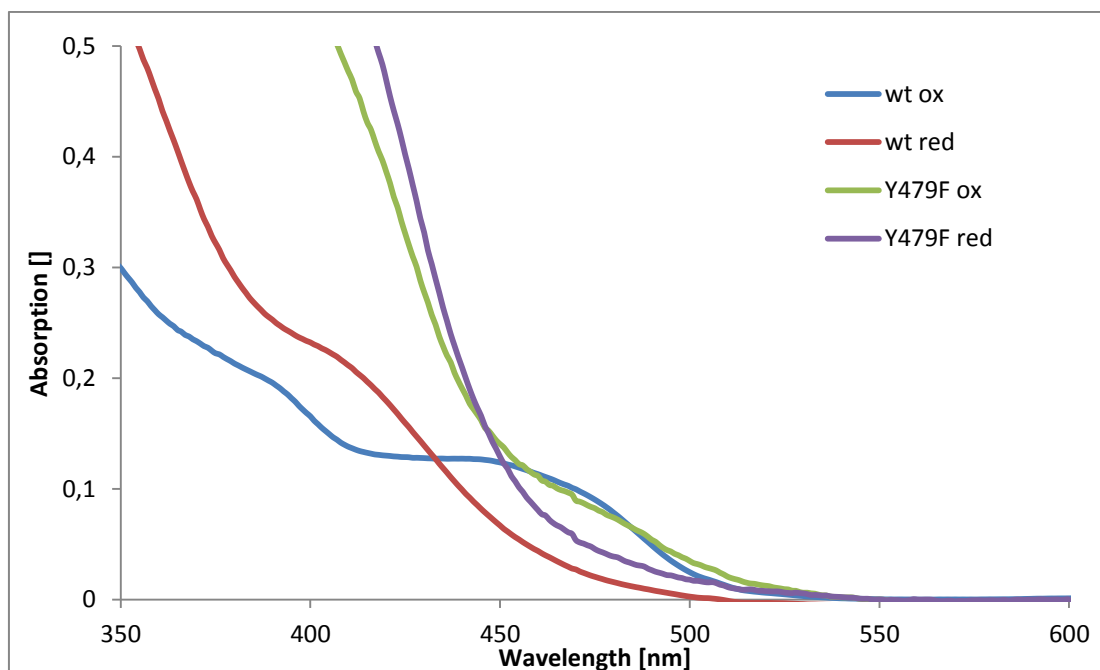


Figure 3: UV-Vis Absorption spectra of the oxidized and substrate reduced species of the wild type enzyme and the Y479F variant.

Table 1: Yield of purified protein of *AtBBE*-like 15 variants per liter fermentation culture, *taken from ⁶, **not determined due to unknown extinction coefficient.

Variant	Yield [mg L ⁻¹]
wild type	150*
K436L	12
Q438V	54
N411V	65
Y117F	28
Y479F	nd**
Y193F	nd**

Determination of the extinction coefficient

The absorption spectrum of *AtBBE*-like 15 was found to differ markedly from the spectrum of free FAD. As reported by Winkler *et al.* the absorption of the 6-S-cytenyl FMN as reported by Kasprzak *et al.* was used to determine the extinction coefficient of *AtBBE*-like 15 ^{11,10}. The spectrum of the native and denatured *AtBBE*-like 15 species are shown in Figure 4.

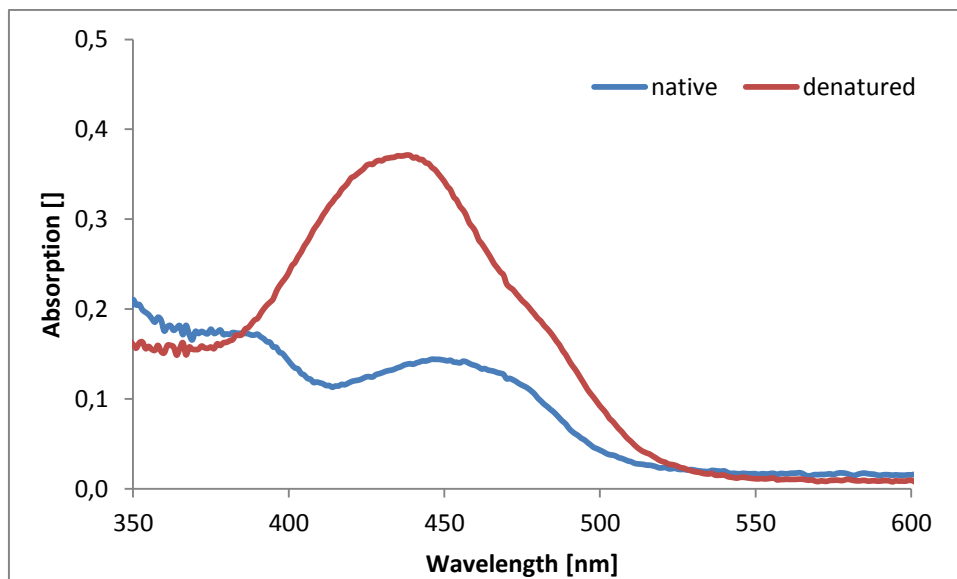


Figure 4: UV-Vis absorption spectra of the native (blue line) and denatured (red line) species of *AtBBE*-like 15

Rapid Reaction Kinetics Using Stopped Flow

The reductive half reaction was determined for all variants employing *p*-coumaryl alcohol and cinnamyl alcohol as substrates. The observed rate constants are summarized in Figure 3 (panel A: cinnamyl alcohol, panel B *p*-coumaryl alcohol). As the reaction follows pseudo first order kinetics, the observed rates were calculated by a monoexponential fit.

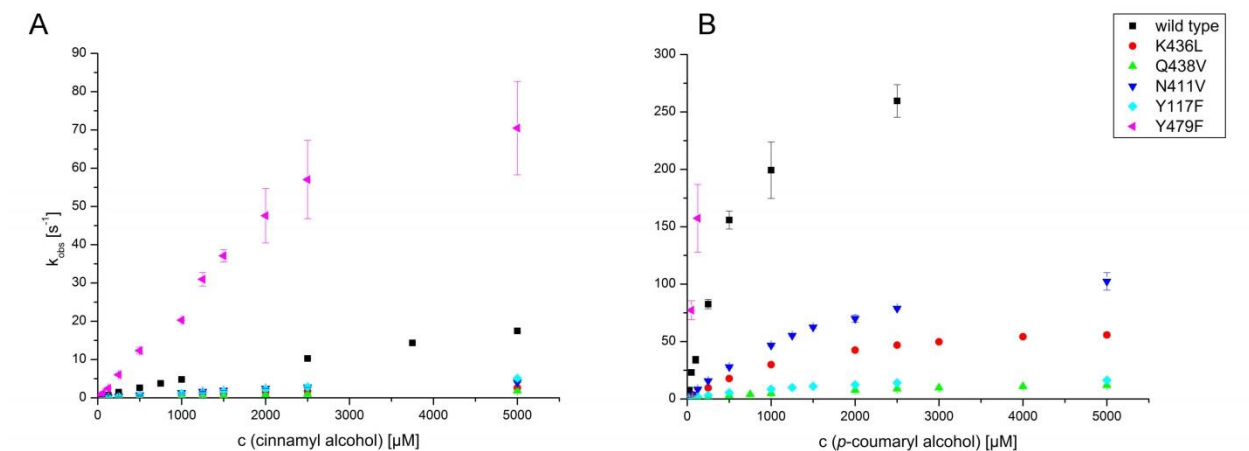


Figure 3: Rates observed for the reductive half-reaction of *AtBBE*-like variants determined with cinnamyl alcohol (panel A) and *p*-coumaryl alcohol (panel B) by stopped flow kinetics.

In Figure 3 the observed rates determined by pre steady state kinetics employing cinnamyl alcohol and *p*-coumaryl alcohol as reducing agents for all active site variants with exception of *AtBBE*-like 15 Y193F are shown. As the Y193F variant does not exhibit any absorption at 450 nm and this property is crucial for this measurement, it was excluded from this experiment.

The reductive rate k_{red} and the dissociation constant K_d were calculated from the observed rates determined with *p*-coumaryl alcohol. Due to solubility limitation the saturation phase cannot be reached with cinnamyl alcohol, the observed rates at a substrate concentration of 500 μM were used to evaluate the impact of the variations in the active site. The kinetic data is summarized in Table 2. k_{red} and k_{obs} determined at 500 μM cinnamyl alcohol of the wild type enzyme were set to 100% to compare the impact of the active site variations.

Table 2: Kinetic parameters and dissociation constants of the *AtBBE*-like 15 variants

variant	cinnamyl alcohol		<i>p</i> -coumaryl alcohol		
	$k_{\text{obs}} [\text{s}^{-1}]^{**}$	$k_{\text{obs}} [\%]$	$k_{\text{red}} [\text{s}^{-1}]$	$k_{\text{red}} [\%]$	$K_d [\mu\text{M}]$
wild type	2.6 ± 0.1	100	332 ± 17	100	665 ± 85
K436L	0.42 ± 0.01	16	74 ± 1	22	1505 ± 70
Q438V	0.20 ± 0.02	8	19 ± 0.3	6	2890 ± 87
N411V	0.70 ± 0.01	26	143 ± 2	43	2024 ± 61
Y117F	0.56 ± 0.01	21	21 ± 2	6	1408 ± 202
Y479F	12 ± 0.9	462	nd***	336*	nd***

With all variants a comparable effects on k_{red} or k_{obs} were determined. For the K436L variant a reduction of k_{red} to 16% and k_{obs} to 22% was found, respectively. A more pronounced effect is determined for the Q438V variant exhibiting a residual k_{red} of 6% and k_{obs} of 8%. While the velocity of the reductive half reaction is lowered, the K_d is increased to $2890 \pm 87 \mu\text{M}$ indicating that also substrate binding is affected by this replacement. The N411V variant shows a reduction of reaction velocity with a k_{red} of 43% and k_{obs} of 26%, again also the substrate binding is affected leading to an increase of K_d to $2024 \pm 61 \mu\text{M}$. For the Y117F variant a decrease of the reaction velocity was determined leading to a residual k_{red} of 6% and k_{obs} of 21%, the K_d is increased to $1408 \pm 202 \mu\text{M}$. Interestingly the Y479F variant shows an increase of the reaction velocity. Due to dead time limitation k_{red} for *p*-coumaryl alcohol was not determined for this variant. k_{obs} determined at 500 μM with cinnamyl alcohol is increased to 436% and k_{obs} determined at 50 μM

p-coumaryl alcohol increased to 336%. Although for all other variants a monoexponential decay of the absorption at 450 nm was observed in the stopped flow experiments, for the Y479F variant a biexponential decay was found. The impact of the variation of Tyr479 on the structure and the kinetic behavior is currently under investigation.

Discussion

Expression and purification

Expression of the variants was conducted as described for the wild type enzyme before ⁶. For the Q438V, N411V and Y117F variants yields are in the same range as for the wild type enzyme. For the K436V variant a yield of 12 mg L⁻¹ was achieved. The Y476F variant shows a distinct change in the spectral properties. The reason for this could be a change in the environment of the isoalloxazine ring that is directly leading to a spectral change or an enhanced susceptibility to cofactor degeneration. The exact properties despite of the kinetic behavior of this variant will be elaborated in future works. The Y193F variant was expressed but does not show the typical flavin spectrum. Therefore the flavin cofactor is considered to be absent in this variant, suggesting a crucial role of Tyr193 in the formation of the covalent attachment. In future works the role of this residue in the cofactor attachment will to be addressed more closely.

Determination of the extinction coefficient

An extinction coefficient at 450 nm of 4800 M⁻¹ cm⁻¹ was calculated while the extinction coefficient of the free FAD is 10300 M⁻¹ cm⁻¹ ¹². The reason for perturbation of the spectral properties of the FAD in *AtBBE*-like 15 is currently under investigation. The cofactor was not found to be planar, it exhibits a butterfly like bending at the N5-N10 axis, the angle found between both sides of the isoalloxazin ring is 161.5°. This might reduce the aromatic properties of the isoalloxazine ring and thereby have an impact on its spectral properties.

Stopped flow kinetics and crystal structure: Structure function relationships in the AtBBE-like 15 active site

The impact on the kinetic parameters by the variation of specific active site residues gives an insight in their role in catalysis especially if this data is combined with the enzyme structure. The active site was analysed with respect to the results of the stopped flow experiments and the crystal structure of the wild type enzyme. Fraaije *et al.* have reported some frequently reoccurring features of flavoproteins¹³. Among them is the position of the oxidized carbon atom that is referred to as “side of oxidative attack” (SAO)¹³. The SAO was placed according to the findings of Fraaije *et al.*, a substrate activating group was defined and transition state stabilizing residues are proposed in the course of this analysis.

In Figure 4 the residues involved in catalysis in *AtBBE*-like 15 are shown, the SOA is indicated as a blue sphere, the residues forming the substrate activating group are colored in magenta. In Figure 4A polar contacts of the substrate activating group are shown, in Figure 4B contacts of the remaining polar amino acids (cyan) in the active site are highlighted. The mechanism we propose based on the structural and kinetic data we have obtained is shown in Figure 4C.

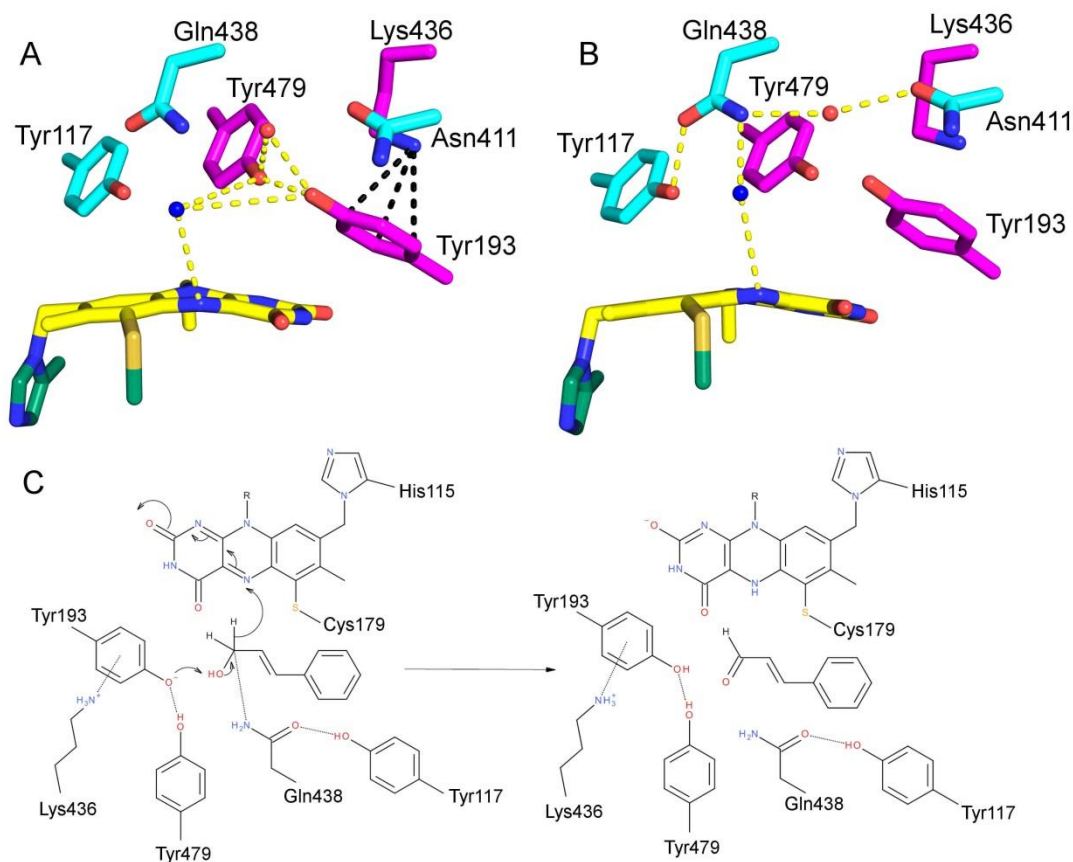


Figure 4: In panel A and B the active site of *AtBBE*-like 15 is shown, the catalytic base motif is colored in magenta, the isoalloxazine ring in yellow and the residual polar active site residues in cyan. The SAO is indicated by a blue sphere. In panel A the polar contacts of the catalytic base motif are shown. In panel B the contacts of the residual polar active residues are shown. In panel C the proposed catalytic mechanism for *AtBBE*-like 15 is shown.

In Figure 4A and B the proposed position of the SOA is indicated by a blue sphere. It was placed in a distance of 3.5 Å to the N5 position of the flavin with an angle of 109° (N10, N5, SOA). Tyr479 and Tyr193 are anticipated to act concertedly as substrate activation group, *i.e.*, they deprotonate the hydroxyl group of the substrate in the course of the reaction. The SAO is placed in a distance of 3.7 Å and 4.4 Å to the hydroxyl groups of Tyr479 and Tyr193, respectively. This position is in good agreement with the docking results we have presented before⁶. In Figure 4A the interactions within the substrate activation group are shown which is formed by Lys436, Tyr479 and Tyr193. These three residues were found to be conserved in 17 out of 28 BBE-likes in *A. thaliana*⁶. Lys436 is in a cation- π interaction with Tyr193. The K436L variant was found to exhibit an increased K_d and a decreased k_{red} (compare Table 2). Cation- π interactions can

contribute to the stability of a protein in a similar manner as hydrogen bonds, a typical binding energy of a cation- π interaction is 2-4 kcal mol⁻¹ ^{14,15}. In this setting the electrostatic attraction between the methylammonium cation of Lys436 and the negative partial charge of the π -system of Tyr193 is important for the optimal positioning of Tyr193. Lys436 pulls Tyr193 towards Tyr479 and thereby contributes to the remarkably low distance between the hydroxyl groups of these residues of 2.4 Å. This distance indicates that both residues share one single proton, *i.e.* a negative charge is delocalized and thereby stabilized over both residues. The close contact of two hydroxyl groups putatively lowers their pKa and enables the enzyme to rest in a triggered ground state with a negative charge captured in the active site. One single tyrosine is not capable to provide this feature as the pKa of approximately 10 is too high. A water molecule that is complexed by Gln438 and Asn411 is found in a distance of 2.8 Å and 3.3 Å to the hydroxyl groups of Tyr193 and Tyr479, respectively. This water is highly coordinated and might also contribute to the stabilization of the negative charge that is required to abstract a proton in the course of the oxidation. For the wild Y479F variant a biexponential decay was found in the stopped flow experiments, *i.e.* the reaction can be divided into two phases. During the first phase k_{obs} of variant is higher than determined for the wild type, in the second phase k_{obs} is significantly lower. An explanation for this behavior could be, that in Y479F variant the stabilization of the negative charge is disturbed, leading to a loss of the negative charge in a certain contingent of the overall enzymes. For the enzyme fraction without negative charge in the active site at the beginning of the stopped flow experiment, the deprotonation of Tyr193 is putatively the rate determining step.

The Y193F variant was not found to harbor a flavin cofactor. A similar effect was found for the BBE-like Dbv29 ¹⁶. This enzyme harbors a substrate activating group consisting from Lys425, Tyr165 and Tyr473 corresponding to Lys436, Tyr193 and Tyr479 in *At*BBE-like 15. Both tyrosines were shown to act as catalytic base by mutagenesis, the Dbv29Y165F/Y473F variant was not found to harbor a FAD-cofactor ¹⁶. Therefore we anticipate that Y193 does not only act as catalytic base in the course of the alcohol oxidation but does also play in role in the establishment of the covalent attachment to the cofactor. Work on the reconstitution of a FAD-loaded Y193F variant from the apo-protein are currently going on.

As the catalytic base motif, the residual polar residues in the active site are likewise conserved in the BBE-like family in *Arabidopsis*, the combination of a glutamine and tyrosine

corresponding to Gln438 and Tyr117 is found in 21 out of 28 *AtBBE*-likes, an asparagine corresponding to N411 is found in 21 *AtBBE*-likes. The exact active site composition as shown for *AtBBE*-like 15 in Figure 4 is found in 14 *AtBBE*-likes⁶. In Figure 4B the polar contacts of Tyr117, Gln438 and Asn411 are shown. Gln438 and Tyr117 are in contact via a 2.6 Å hydrogen bond the Q438V variant shows a residual k_{red} of 6% if compared to the wild type enzyme, also the K_d is increased from $665 \pm 85 \mu\text{M}$ to $2890 \pm 87 \mu\text{M}$. The SOA has been placed in a distance of 2.7 Å to Gln438, a positive partial charge at the SAO during the course of the hydride transfer can therefore be stabilized by Gln438. The hydroxyl group of Tyr117 is in a distance of 3.9 Å to the SOA, therefore a direct interaction in the stabilization of the transition state is less likely but cannot be ruled out completely. Still a reduction of k_{red} to 6% for the Y117F variant has been determined, therefore Tyr117 is anticipated to determine the position of Gln438.

The position of Asn411 does not suggest direct role in the substrate activation nor in the stabilization of the transition state, what is in good agreement with the moderate effect on the reductive rate. Still the replacement of this residue leads to a significant increase of K_d , therefore it might be involved in substrate binding prior to the oxidation as it represents a putative polar contact partner for the allyl alcohol.

Finally the following mechanism can be postulated taking into account the above mentioned effects (compare Figure 4C). In the ground state a negative charge is located at Tyr193 that is stabilized by Tyr479. The substrate is deprotonated by Tyr193, concertedly a hydride is transferred from the alcohol α -carbon to the N5 position of the flavin. The transition state between the alcohol and the aldehyde species of the substrate is stabilized by Asn438 that is positioned by Tyr117. Asn411 and Asn438 are involved in the coordination of a water molecule near the substrate activating group that is possibly involved in the stabilization of a negative charge needed for proton abstraction.

Conclusion

In this report we have presented a site directed mutagenesis study to elucidate the enzymatic mechanism of the enzyme class of monolignol oxidoreductases. We postulate a mechanism that includes the concerted deprotonation of the substrate by Tyr193 and a hydride transfer to the FAD. The transition state is stabilized by Gln438. In prior works we have shown that the active site residues of *AtBBE*-like 15 are conserved 14 out of 28 *AtBBE*-likes, we anticipate them to fulfill the same function in these enzymes⁶.

References

1. Fagan, R. L. & Palfey, B. A. in *Compr. Nat. Prod. II* (2010). doi:10.1016/B978-008045382-8.00135-0
2. Macheroux, P., Kappes, B. & Ealick, S. E. Flavogenomics - A genomic and structural view of flavin-dependent proteins. *FEBS J.* **278**, 2625–2634 (2011).
3. Winkler, A. *et al.* A concerted mechanism for berberine bridge enzyme. *Nat. Chem. Biol.* **4**, 739–741 (2008).
4. Steffens, P., Nagakura, N. & Zenk, M. H. The berberine bridge forming enzyme in tetrahydroprotoberberine biosynthesis. *Tetrahedron Lett.* **25**, 951–952 (1984).
5. Handbook of Flavoproteins, Volume 1 Oxidases, Dehydrogenases and related systems . (2012). doi:10.1515/9783110268911
6. Daniel, B. *et al.* Oxidation of monolignols by members of the berberine bridge enzyme family suggests a role in cell wall metabolism. *J. Biol. Chem.* **290**, 18770–18781 (2015).
7. Steinkellner, G., Rader, R., Thallinger, G. G., Kratky, C. & Gruber, K. VASCo: computation and visualization of annotated protein surface contacts. *BMC Bioinformatics* **10**, 32 (2009).
8. Hendlich, M., Rippmann, F. & Barnickel, G. LIGSITE: Automatic and efficient detection of potential small molecule-binding sites in proteins. *J. Mol. Graph. Model.* **15**, 359–363 (1997).
9. Wallner, S. *et al.* Catalytic and structural role of a conserved active site histidine in berberine bridge enzyme. *Biochemistry* **51**, 6139–6147 (2012).
10. Kasprzak, a a, Papas, E. J. & Steenkamp, D. J. Identity of the subunits and the stoichiometry of prosthetic groups in trimethylamine dehydrogenase and dimethylamine dehydrogenase. *Biochem. J.* **211**, 535–541 (1983).

11. Winkler, A., Hartner, F., Kutchan, T. M., Glieder, A. & Macheroux, P. Biochemical evidence that berberine bridge enzyme belongs to a novel family of flavoproteins containing a bi-covalently attached FAD cofactor. *J. Biol. Chem.* **281**, 21276–21285 (2006).
12. Macheroux, P. in *Flavoprotein Protoc. SE - 1* (Chapman, S. & Reid, G.) **131**, 1–7 (Humana Press, 1999).
13. Fraaije, M. W. & Mattevi, A. Flavoenzymes: Diverse catalysts with recurrent features. *Trends Biochem. Sci.* **25**, 126–132 (2000).
14. Zacharias, N. & Dougherty, D. a. Cation- π interactions in ligand recognition and catalysis. *Trends Pharmacol. Sci.* **23**, 281–287 (2002).
15. Zhong, W. *et al.* From ab initio quantum mechanics to molecular neurobiology: a cation- π binding site in the nicotinic receptor. *Proc. Natl. Acad. Sci. U. S. A.* **95**, 12088–12093 (1998).
16. Liu, Y.-C. *et al.* Interception of teicoplanin oxidation intermediates yields new antimicrobial scaffolds. *Nat. Chem. Biol.* **7**, 304–309 (2011).

Chapter 4: Characterization of a monolignol oxidoreductase from *Arabidopsis thaliana* for biocatalytic applications

Sabine Pils¹, Silvia Wallner¹, Marko Kljajic², Rolf Breinbauer², Jörg Schrittwieser³, Wolfgang Kroutil³, Peter Macheroux¹ and Bastian Daniel¹

¹Graz University of Technology, Institute of Biochemistry, Graz, Austria

²Graz University of Technology, Institute of Organic Chemistry, Graz, Austria

³University of Graz, Department of Chemistry, Organic and Bioorganic Chemistry, NAWI Graz, Graz, Austria

To whom correspondence should be addressed: Bastian Daniel, Graz University of Technology, Institute of Biochemistry, Petersgasse 12/II, A-8010 Graz, Austria, Tel.: +43-316-873 4528, Fax: +43-316-873 6952; Email: bastian.daniel@tugraz.at

Author contributions:

S.P., S.W., and B.D., performed the enzyme expression and biochemical assays. M.K., J.S. and R.B. synthesized compounds. J.S., B.D, S.P. and W.K. analyzed the products of the enzymatic conversions. S.P., B.D. and P.M wrote the manuscript.

Abstract

Monolignol oxidoreductases from the berberine bridge enzyme-like (BBE-like) protein family (pfam 08031) catalyze the oxidation of monolignols to the corresponding aldehydes. In this report, we elucidate the potential of a monolignol oxidoreductase from *Arabidopsis thaliana* (*At*BBE-like 15) as biocatalyst for oxidative reactions. For this study we employed a variant with enhanced reactivity towards oxygen, which could be achieved by a single amino acid exchange (L182V). The performance of purified *At*BBE-like 15 L182V was tested under various reaction conditions: The pH and temperature optima were determined, the tolerance towards organic co-solvents was investigated and the substrate scope was elucidated. The enzyme has a temperature optimum at 50°C and retains more than 50% activity between pH 5 and pH 10, it shows increased activity in the presence of various co-solvents, including acetonitrile, 2-propanol, 1,4-dioxan and dimethyl sulfoxide. Primary benzylic and primary or secondary allylic alcohols were accepted as substrates. The enantioselectivity in the oxidation of secondary alcohols was good to excellent ($E >34$ to >200).

Introduction

Flavoproteins are a diverse protein class employing either the flavin mononucleotide (FMN) or the flavin adenine dinucleotide (FAD) cofactor for catalysis [1]. Among them, the BBE-likes (pfam 08031) can be distinguished due to their bicovalent cofactor tethering [2], [3]. Namesake of this protein family is the berberine bridge enzyme (BBE) from California poppy (*Eschscholzia californica*), which catalysis the oxidative ring closure from (*S*)-reticulín to (*S*)-scoulerine in isoquinoline alkaloid biosynthesis [4], [5].

The majority of flavoproteins, including the BBE-likes, catalyze redox reactions, and they are involved in a plethora of biological processes [6]. The catalytically active structure of the flavin cofactor is the isoalloxazine ring, whose properties are modulated by the protein environment in which it is embedded. The isoalloxazine ring is capable of one or two electron exchange reactions: Next to its fully reduced (hydroquinone) or oxidized (quinone) state, also stable radical species (semiquinone) can be formed. A comprehensive overview of the function and mechanism of different flavoproteins has been provided by Fagan *et al.* [6].

The catalytic cycle of a flavoprotein can be divided into two half reactions: In the resting state the flavin cofactor is in its oxidized. In the reductive half reaction, the flavin is reduced by a given substrate. In the oxidative half reaction, the flavin reacts with an appropriate electron acceptor, thus becomes reoxidized and is then able to enter another catalytic cycle. The nature of the final electron acceptor is a crucial attribute of flavoproteins. Enzymes that promote the reaction of the flavin cofactor with oxygen are considered as oxidases, while enzymes that inhibit the reaction of the reduced flavin with oxygen are defined as dehydrogenases. For BBE-likes it has been shown that a single gatekeeper residue controls the enzymes' reactivity towards oxygen [8].

We have recently identified two BBE-likes from *Arabidopsis thaliana* as monolignol oxidoreductases (*At*BBE-like 13 and *At*BBE-like 15) [9]. The enzymes were heterologously expressed in *Komagatella pastoris* (formerly *Pichia pastoris*), and a biochemical and structural characterization has been conducted in our laboratory. Both enzymes were found to oxidize monolignols (coniferyl, sinapyl and *p*-coumaryl alcohol) to the corresponding aldehydes while reacting only sluggishly with molecular oxygen, and were hence considered as monolignol dehydrogenases. The physiological electron acceptor for *At*BBE-like 15 and 13 is not known yet; therefore, the sluggish oxidative rate hampers the potential application of *At*BBE-likes as biocatalysts. Moreover, while *At*BBE-like 15 was found to be stable and expressed in good yields, expression of *At*BBE-like 13 was very cumbersome and the enzyme was found to be unstable. To overcome these limitations, the oxygen gatekeeper residue in *At*BBE-like 15 was changed from leucine to valine to turn the enzyme into an oxidase. The resulting enzyme variant *At*BBE-like 15 L182V reacts more than 400 times faster with oxygen compared to the wild type enzyme [9]. This enables the usage of this enzyme for steady state kinetics and the putative application of the enzyme as biocatalyst in oxidative reactions.

The proposed reaction mechanism of *At*BBE-like 15 is shown in Figure 1 B. Tyr193 is stabilized in the deprotonated form by Tyr479 and is positioned Lys436 via a cation- π interaction. Tyr193 deprotonates the allylic alcohol to facilitate the hydride transfer to the flavin. We have solved the crystal structure of *At*BBE-like 15, which revealed a broad cavity harboring the substrate binding site and the active site that is readily accessible from the protein surface [9]. This cavity was visualized and analyzed using the CASoX tool (Figure 1 C and D) [10] ,[11]. The broad hydrophobic part is anticipated to act as substrate binding site. Residues with a major contribution to the hydrophobicity of the binding site are shown in green in Figure 1 D, also the

flavin cofactor shown in yellow contributes to the binding site. Attached to the binding site is the active site. In Figure 1 C in dark green the residues that contribute to the active site are shown. Tyr117, Gln438, Ile409, Arg292, Val178 and Cys179 are contracting the cavity and thereby form the entrance to the active site. The catalytic base motif, formed by Tyr193, Lys436 and Tyr479, is located opposite to this entrance [9]. Asn411 also contributes to the properties of the active site. On the one hand it is involved in the complexation of a water molecule together with Gln438, on the other hand it is a putative binding partner to anchor the monolignols prior to oxidation. His115 and Cys179 are responsible for the bicovalent attachment of the FAD which confers a very tight steric control of the position of the cofactor to the enzyme (Figure 1 C) [2].

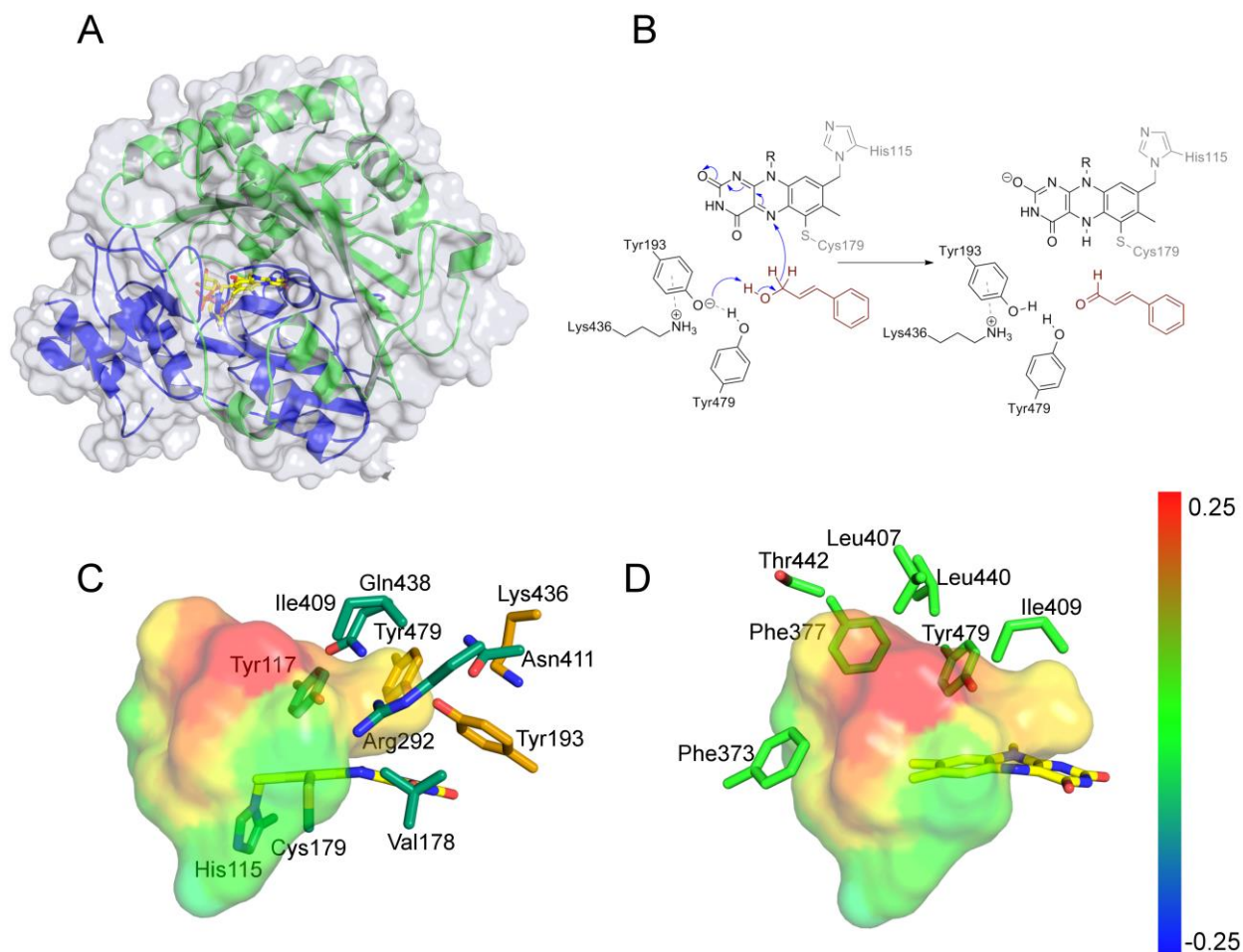


Figure 1: A: overall structure of *AtBBE*-like 15, blue: cofactor binding domain, green: Substrate binding domain, yellow: FAD; B: Reaction mechanism; C: active site and substrate binding pocket colored by hydrophobicity (red: hydrophobic, blue: hydrophilic).

Green residues determine the shape of the active site, orange residues also act as a catalytic base. D: Active site and substrate binding pocket: The green residues are responsible for the hydrophobic properties of the substrate binding pocket.

The application of flavin-containing enzymes as oxidative catalysts is highly desirable as they combine the advantage of using molecular oxygen as the most environmental benign oxidant with the substrate-, regio-, and enantioselectivity of an enzyme [12]. Therefore we initiated a feasibility study to determine the potential of *At*BBE-like 15 L182V as a biocatalyst. In particular, the substrate scope, the pH and temperature optima, solvent tolerance and enantioselectivity were in the focus of our attention.

2 Experimental

2.1 pH optimum

The pH optimum was determined with an optical oxygen meter FireSting O2 (Pyro Science GmbH, Aachen, Germany) equipped with a retractable needle-type oxygen sensor (Pyro Science GmbH, Aachen, Germany). The reaction was performed in a measuring cell with an integrated magnetic stirrer in triplicate at 25°C and 500 rpm. 575 μL 50 mM MES buffer pH 7 containing 1.05 μM *At*BBE-like 15 L182V was stirred until a stable oxygen level was reached. The reaction was started by the addition of 25 μL sinapyl alcohol solution to reach a final substrate concentration of 0.2 mM. The reaction was recorded for at least 300 seconds. The consumption of oxygen reflects the conversion of the substrate during the reaction.

2.2 Temperature optimum

The temperature optimum of *At*BBE-like 15 L182V was determined spectrophotometrically by measuring the formation of coniferyl aldehyde from coniferyl alcohol. The reaction was performed in 1.5 mL plastic reaction tubes in a thermomixer (Eppendorf, Hamburg, Germany) at various temperatures. 500 μL 50 mM MES buffer pH 7 containing 0.2 μM *At*BBE-like 15 L182V was preheated for 10 min at 500 rpm. The reaction was started by the addition of 100 μL coniferyl alcohol solution to reach a final concentration of 3.33 mM. The reaction was followed over 10 minutes, whereby every 60 s a sample was taken. To this end, 20 μL of the reaction solution was mixed with 10 μL 1M TRIS-buffer pH 11. 2 μL of this solution was used to determine the product formation with a NanoDrop 2000 spectrometer (Thermo Fisher Scientific, Waltham, USA). The coniferyl aldehyde concentration was measured at 402 nm, the extinction coefficient of 3712 $\text{M}^{-1} \text{cm}^{-1}$ was determined with an authentic standard under the given conditions.

2.3 Activity in the presence of 10% (v/v) of organic co-solvents

The measurements were conducted as described in section 2.2 in the presence of 10 % (v/v) of the respective co-solvents. Methanol, ethanol, 2-propanol, 1-butanol, acetone, acetonitrile, tetrahydrofuran (THF), dimethylformamide (DMF), dimethyl sulfoxide (DMSO) and 1,4-

dioxane were investigated. The activity found in pure buffer was set to 100%. The presence of co-solvents was found not to influence the extinction coefficient of the coniferyl aldehyde.

2.4 Activity in the presence of 10–50% (v/v) of organic co-solvents

The measurements were conducted as described in section 2.2 in the presence of 10–50% (v/v) cosolvent. Chosen for this experiment were solvents that were found to increase the activity of the enzyme according to the experiments described in section 2.3 (ethanol, 2-propanol, 1-butanol, acetonitrile, tetrahydrofuran, dimethyl sulfoxide and 1,4-dioxane).

2.5 Long-term stability in the presence of 30% (v/v) of organic co-solvents

The measurements were conducted as described in section 2.2. For every solvent, six identical preparations were made. Three reactions were started immediately by the addition of substrate and three preparations were incubated for 24 h at 25°C and 500 rpm in a thermomixer (Eppendorf, Hamburg, Germany) before the reaction was started.

2.6 Substrate Screening

The activity of *At*BBE-like 15 L182V was tested with different substrates. Reactions were carried out in 50 mM MES buffer pH 7.0 in the presence of 20% (v/v) DMSO. 200 µL of 50 mM substrate stock solution (DMSO) was mixed with 800 µL buffer and incubated for 3 h at 25 °C in a thermomixer (Eppendorf, Hamburg, Germany) at 500 rpm to achieve a constant oxygen concentration. The reaction was started by the addition of 5 µL enzyme to achieve a final enzyme concentration of 0.6 µM. The course of the reaction was determined by measuring the oxygen partial pressure employing an optical oxygen meter FireSting O2 (Pyro Science GmbH, Aachen, Germany) equipped with a solvent resistant oxygen probe (OXSOLOV, Pyro Science GmbH, Aachen, Germany). The reaction was followed for at least 300 s. Representatives of different substance classes were screened: cinnamyl alcohol (**1**), *p*-coumaryl alcohol (**2**), 4-phenyl-3-buten-2-ol (**3**), benzyl alcohol (**4**), piperonyl alcohol (**5**), 2-cyclohexen-1-ol (**6**), 3-octen-2-ol (**7**), 3-penten-2-ol (**8**), *trans*-2-hexen-1-ol (**9**), *cis*-2-hexen-1-ol (**10**) and *cis/trans*-crotyl alcohol (**11**).

2.7 Product identification

The reaction products of *AtBBE*-like 15 L182V with the substrates mentioned in section 2.6 were determined by GC–MS employing authentic standards. Next to the aforementioned substrates, 3-phenylprop-2-yn-1-ol (**12**) and (*Z*)-2-fluoro-3-phenyl-prop-2-en-1-ol (**13**) were identified as substrates for *AtBBE*-like 15 L182V by GC–MS measurements.

2.8.1 GC–MS

GC–MS analyses were carried out on an Agilent 7890A GC system equipped with an Agilent J&W HP-5ms capillary column (30 m × 0.25 mm × 0.25 μm; stationary phase: bonded & cross-linked 5%-phenyl-methylpolysiloxane) (Agilent Technologies, Santa Clara, USA) and coupled to an Agilent 5975C mass-selective detector (electron impact ionisation, 70 eV; quadrupole mass selection) using helium as carrier gas.

Method **M1**: Inlet temperature: 250 °C; split ratio: 90:1; injection volume: 1 μL; column flow rate: 0.7 mL/min; oven program: 100 °C for 0.5 min, 10 °C/min to 300 °C; MS transfer line temperature: 300 °C, MS source temperature: 230 °C, MS quadrupole temperature: 150 °C; MS scan range: $m/z = 33\text{--}400$.

Method **M2**: Inlet temperature: 250 °C; split ratio: 90:1; injection volume: 1 μL; column flow rate: 0.7 mL/min; oven program: 40 °C for 2 min, 10 °C/min to 180 °C, 180 °C for 1 min; MS transfer line temperature: 300 °C, MS source temperature: 230 °C, MS quadrupole temperature: 150 °C; MS scan range: $m/z = 33\text{--}400$.

Method **M3**: Inlet temperature: 250 °C; split ratio: 90:1; injection volume: 1 μL; column flow rate: 0.7 mL/min; oven program: 40 °C for 5 min, 5 °C/min to 100 °C, 25 °C/min to 200 °C, 200 °C for 1 min; MS transfer line temperature: 300 °C, MS source temperature: 230 °C, MS quadrupole temperature: 150 °C; MS scan range: $m/z = 33\text{--}400$.

2.8.2 GC–FID (achiral stationary phase)

Achiral GC–FID analyses were carried out on an Agilent 7890A GC system equipped with an Agilent J&W DB-1701 capillary column (30 m × 0.25 mm × 0.25 µm; stationary phase: bonded & cross-linked 14%-cyanopropylphenyl-methylpolysiloxane) using helium as carrier gas.

Method **M4**: Inlet temperature: 220 °C; split ratio: 50:1; injection volume: 1 µL; column flow rate: 1 mL/min; oven program: 60 °C for 1 min, 10 °C/min to 280 °C, 280 °C for 2 min; detector temperature: 300 °C.

The products were identified by their retention times, which are summarized in Table 1.

Table 1: GS-MS analytics: Retention times employing a non-chiral stationary phase

Substance	Method	Retention time starting material [min]	Retention time product [min]	Retention time aldehyde
1 Cinnamyl alcohol	M2	13.4	12.9	12.9
4 Benzyl alcohol	M1	3.4	7.55	8.0
5 Piperonyl alcohol	M2	14.4	13.8	13.9
9 trans-2-Hexen-1-ol	M2	6.3	3.0	6.0
10 cis-2-Hexen-1-ol	M2	6.3	6.0	
11 Crotyl alcohol	M3	3.2	3.0	3.0
12 3-Phenyl-2-propyn-1-ol	M1	6.2	5.1	5.1
13 (Z)-2-fluoro-3-phenyl-prop-2-en-1-ol	M1	6.2	5.7	

2.8 Kinetic resolutions

Kinetic resolutions were carried out with substrates **3**, **6**, **7** and **8** as described in section 2.6. The product identification was conducted by GC–FID.

2.9.1 GC–FID (chiral stationary phase)

Chiral GC–FID analyses of 3-penten-2-ol (**8**), 3-octen-2-ol (**7**), and cyclohex-2-en-1-ol (**6**) were carried out on an Agilent 7890A GC system equipped with a Varian CP-Chirasil Dex-CB capillary column (25 m × 0.32 mm × 0.25 μm; stationary phase: β-cyclodextrin bonded to dimethylpolysiloxane) (Agilent Technologies, Santa Clara, USA) using hydrogen as carrier gas.

Method **M5** (used for **8**): Inlet temperature: 220 °C; split ratio: 90:1; injection volume: 1 μL; column flow rate: 1 mL/min; oven program: 60 °C for 1 min, 20 °C/min to 70 °C, 70 °C for 5 min, 20 °C/min to 180 °C, 180 °C for 1 min; detector temperature: 250 °C.

Method **M6** (used for **7** and **6**): Inlet temperature: 220 °C; split ratio: 90:1; injection volume: 1 μL; column flow rate: 1 mL/min; oven program: 60 °C for 1 min, 20 °C/min to 95 °C, 95 °C for 9 min, 20 °C/min to 180 °C, 180 °C for 1 min; detector temperature: 250 °C.

4-Phenyl-3-buten-2-ol (**3**) was converted into the corresponding acetate derivative prior to chiral-phase GC analysis by reaction with acetic anhydride (20 μL/mL sample) and 4-dimethylaminopyridine (DMAP; 1 mg/mL sample) at room temperature for 3 h.

Chiral GC–FID analyses of the resulting 4-phenyl-3-buten-2-yl acetate (**3b**) were carried out on an Agilent 7890A GC system equipped with a Restek Rt@-βDEXse capillary column (25 m × 0.32 mm × 0.25 μm; stationary phase: 2,3-di-O-ethyl-6-O-tert-butyltrimethylsilyl-β-cyclodextrin added into 14%-cyanopropylphenyl/86%-dimethylpolysiloxane) using hydrogen as carrier gas.

Method **M7**: Inlet temperature: 220 °C; split ratio: 50:1; injection volume: 1 μL; column flow rate: 2 mL/min; oven program: 60 °C for 1 min, 5 °C/min to 180 °C; detector temperature: 250 °C.

The retention times of the observed in these measurements are summarized in Table 2.

Table 2: GC-FID analytics: Retention times employed a chiral stationary phase

Substance	Method	Retention time alc. 1 [min]	Retention time alc. 2 [min]	Retention time ketone [min]
3b 4-Phenylbut-3-en-2-ol (acetyl derivative)	M7	21.7	22.0	19.3
6 3-Octen-2-ol	M6	10.2	10.5	9.0
8 3-Penten-2-ol	M5	5.4	5.6	4.1
9 Cyclohex-2-en-1-ol	M6	9.8	10.2	7.6

3 Results and discussion

3.1 pH optimum

The pH optimum was determined employing 1 μM *At*BBE-like L182V and 0.2 mM sinapylalcohol. The consumption of oxygen was recorded during the course of the reaction to estimate the reaction velocity. One mol consumed oxygen equals one mol formed product, the given values equal the initial rate in mol product / mol enzyme per second.

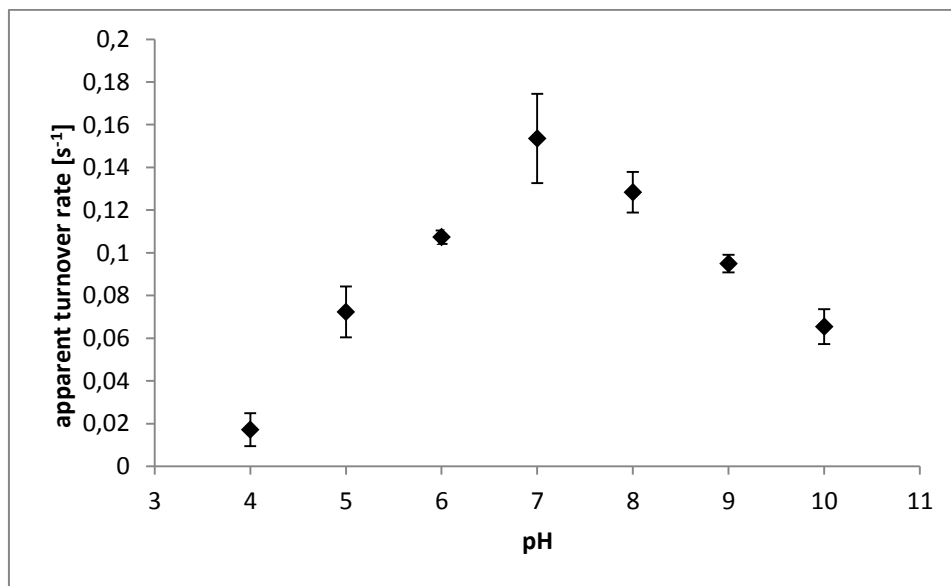


Figure 2: pH optimum of *At*BBE-like 15 L182V. Plotted is the observed consumption of mol oxygen per mol enzyme per second.

The enzyme is active over a broad pH range. The highest activity is found at pH 7, and between pH 5 and pH 10 the enzyme retains more than 50% activity.

3.2 Temperature optimum

The temperature optimum was determined employing 0.2 μM enzyme and 3.33 mM coniferyl alcohol. The course of the reaction was followed spectrophotometrically. The given values equal one mol product/mol enzyme per second of the initial rate of the reaction.

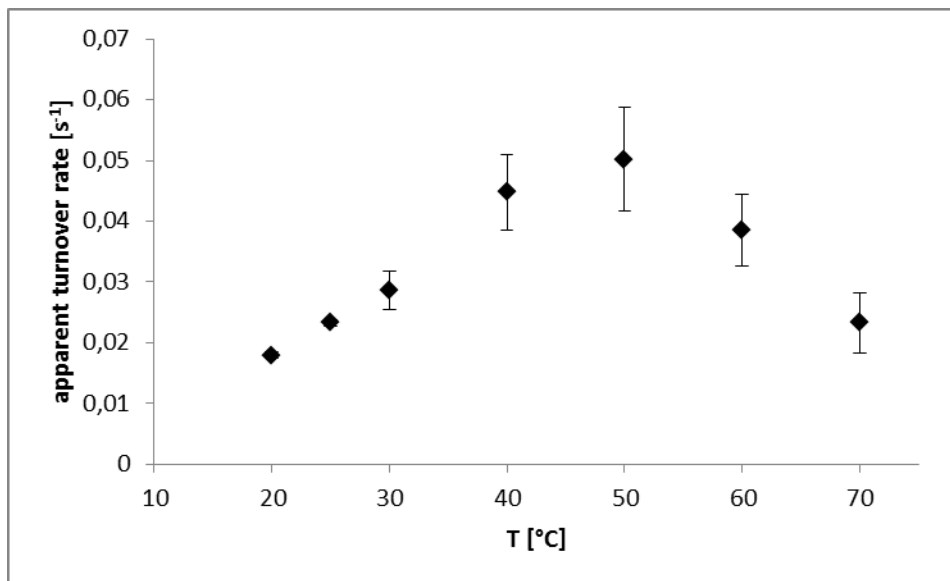


Figure 3: Temperature optimum of *AtBBE*-like 15 L182V. Plotted is the formation of coniferyl aldehyde per second per mol enzyme at different temperatures.

The highest activity was found at 50°C. The findings are in good agreement with the melting point of the wild type enzyme of 56°C [9].

3.3 Activity in presence of 10% (v/v) of organic co-solvents

While an aqueous system is the natural environment of enzymes the solubility of nonpolar substrates is limited under purely aqueous conditions. This limitation can be overcome by the addition of co-solvents. A high tolerance of the enzyme towards organic solvents is also required if a thermomorphic solvent system is supposed to be applied for enzyme recycling [13]. As oxygen is the final electron acceptor of *AtBBE*-like L182V, also the oxygen solubility is an important factor for the overall performance of the catalyst. The addition of co-solvent is not only beneficial for substrate solubility but can also enhance the oxygen solubility [14]. To determine the effect of organic solvents on the enzyme stability, measurements in the presence of 10% (v/v) were conducted. The course of the reaction was followed spectrophotometrically. The enzyme activity in buffer was set to 100%. In Figure 4 the activities found in the presence of various organic solvents are shown.

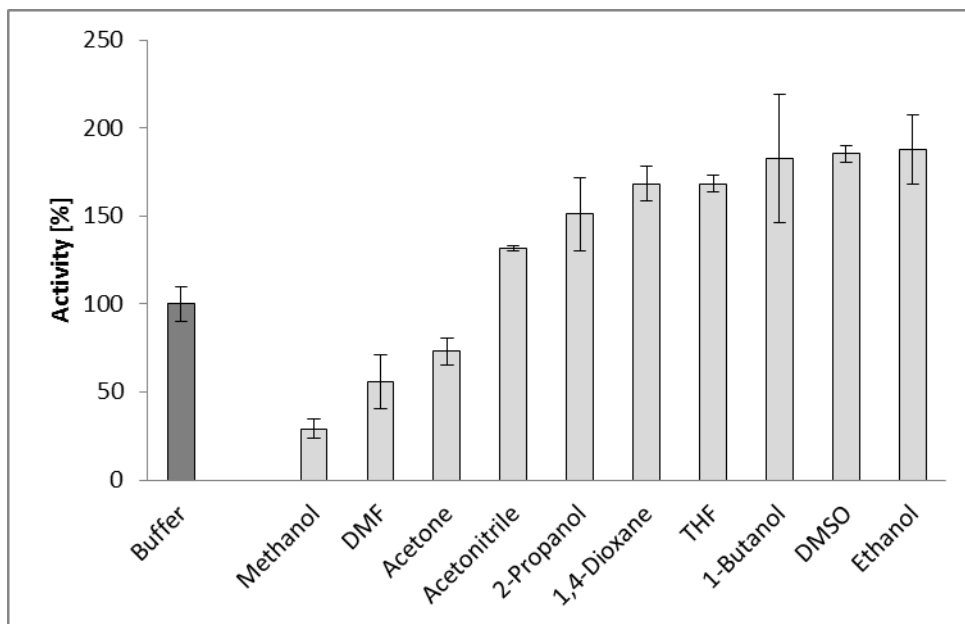


Figure 4: Activity of *AtBBE*-like 15 L182V with 10% (v/v) of organic co-solvents.

An increased activity of the enzyme was found in acetonitrile, 2-propanol, 1,4-dioxane, tetrahydrofuran, 1-butanol, dimethyl sulfoxide and ethanol. The highest degree of activation was found for ethanol with 188% of the activity observed in buffer. A decreased activity was determined in the presence of methanol, dimethyl formamide and acetone, with the lowest activity of found in the presence of methanol (29%).

3.4 Activity in the presence of 10–50% (v/v) of organic co-solvents

The high solvent tolerance of the enzyme encouraged us to further increase the co-solvent concentration to probe the enzyme stability. To this end, experiments were conducted with all solvents that were found to increase the enzyme activity. The enzyme activity was determined with acetonitrile, 2-propanol, 1,4-dioxane, tetrahydrofuran, 1-butanol, dimethyl sulfoxide, and ethanol at concentrations of 10%, 20%, 30%, 40% and 50% (v/v). The measured activities are shown in Figure 5.

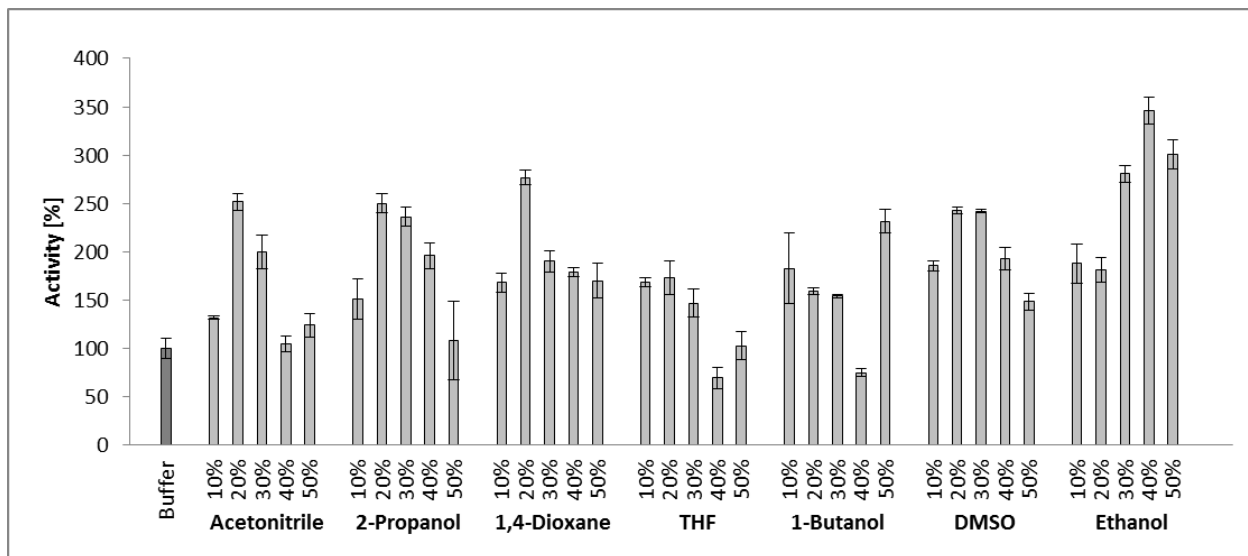


Figure 5: Effect on the enzyme activity of different solvents at concentrations between 10% and 50% (v/v).

An increasing solvent concentration led to an increased enzyme activity in all cases except for tetrahydrofuran, which was not tolerated well at higher concentrations. The highest degree of activation was found in 40% ethanol with 346% of the activity measured in buffer. The enzyme was shown not only to tolerate high solvent concentrations, also the activity can be enhanced. Still, high solvent concentrations can lead to the denaturation and thereby deactivation of the enzyme. A good long-term stability of the enzyme under the given reaction conditions is essential to achieve a high space/time yield.

3.5 Long-term stability in the presence of 30% (v/v) of organic co-solvents

The presence of various organic solvents was found to enhance the activity of the enzyme. To test the long-term stability of the enzyme, it was incubated with 30% (v/v) of the respective solvents for 24 h (t₂) before the reaction was started. The activity in buffer was set to 100%.

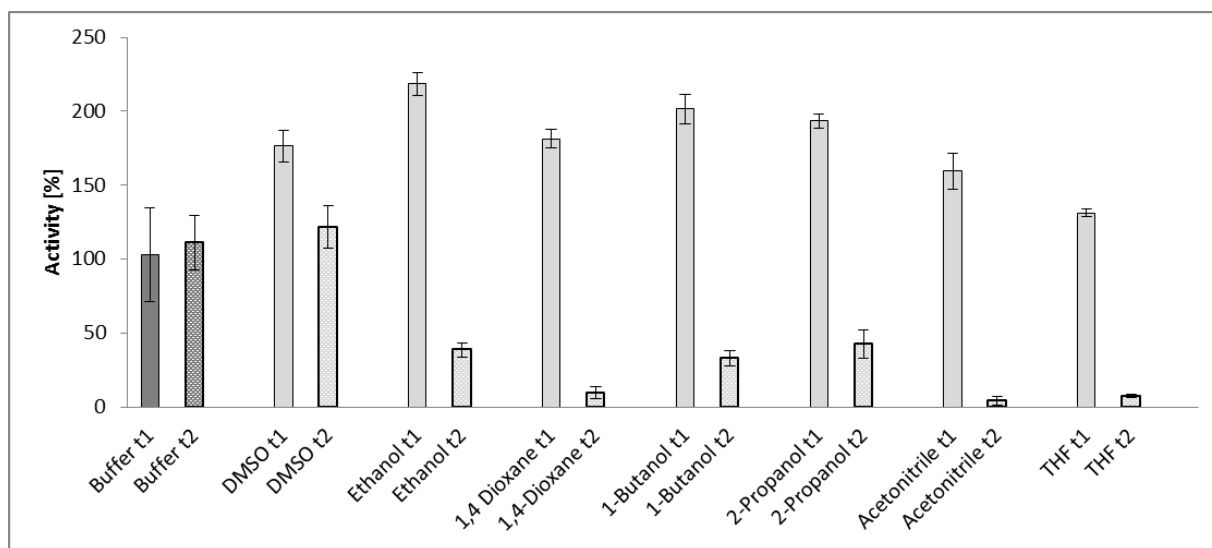


Figure 6: Long-term activity of *AtBBE*-like 15 L182V with 30% (v/v) of organic co-solvents with t1 = 0 h, t2 = 24 h.

While no deactivation of the enzyme in buffer was detectable, the presence of organic solvents led to enhanced activity but also a decreased life-time of the enzyme. The highest activity after 24 h incubation was determined in 30% DMSO. The enzyme activity in DMSO was 177% initially and dropped to 122% within 24 h. Also for other solvents a lower but still acceptable retention of the initial activity was determined. The initial activity dropped in ethanol from 218% to 38%, in 2-propanol from 194% to 47% and in 1-butanol from 201% to 33%. Especially the long-term stability in 2-propanol makes interesting options feasible with regard to coupled reactions with NADH dependent alcohol dehydrogenases [15]. 2-Propanol is frequently used to regenerate NADH from NAD⁺. In a one-pot process, *AtBBE*-like 15 L182V could be employed for kinetic resolutions of secondary allylic alcohols, while an alcohol dehydrogenase with NADH regeneration by 2-propanol could be employed to reduce the allylic ketone formed *in situ* to reach a theoretical yield of 100% of the desired enantiopure alcohol.

3.6 Substrate Screening

In order to elucidate the substrate scope of *AtBBE*-like 15 L182V the enzyme was screened for activity with various alcohols. To ensure the solubility of all substrates, experiments were conducted in 20% DMSO and a substrate concentration of 10 mM was used. The course of the

reaction was followed by measurement of the oxygen partial pressure. The values obtained in these experiments are summarized in Figure 7.

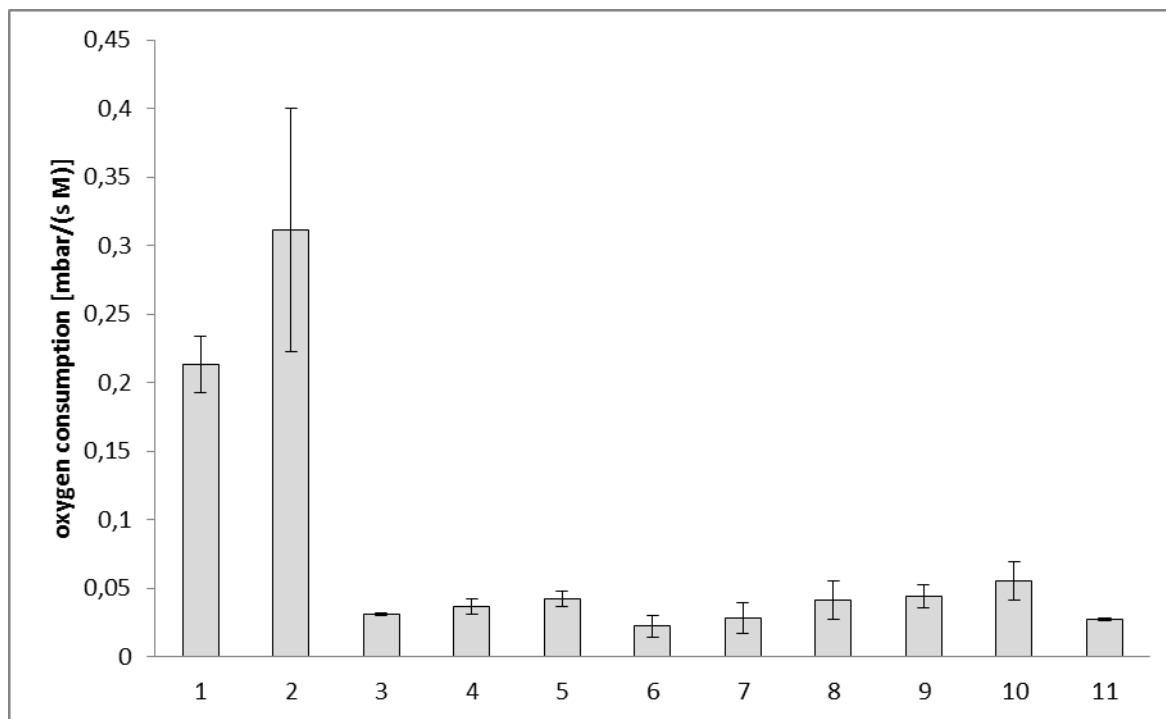


Figure 7: Substrate screening of *At*BBE-like 15 L182V with cinnamyl alcohol (**1**) and *p*-coumaryl alcohol (**2**), 4-phenyl-3-buten-2-ol (**3**), benzyl alcohol (**4**), piperonyl alcohol (**5**), 2-cyclohexen-1-ol (**6**), 3-octen-2-ol (**7**), 3-penten-2-ol (**8**), *trans*-2-hexen-1-ol (**9**), *cis*-2-hexen-1-ol (**10**) and *cis/trans*-crotyl alcohol (**11**).

For the cinnamyl alcohol derivatives **1** and **2**, oxygen consumption was found to be 0.21 ± 0.02 mbar/(s M) and 0.31 ± 0.09 , respectively. In **3** a methyl group is placed at the alcohol carbon atom transforming cinnamyl alcohol into a secondary alcohol. This structural change leads to a drop of the oxygen consumption rate by a factor of 7 to 0.031 mbar/(s M). As the active site was shown to be well defined and tightly packed, the additional steric demand of the methyl group seems to hamper the oxidation of **3** compared to **1** (compare also Figure 1 C and D). The oxygen consumption rates of benzylic alcohols **4** and **5** were found to be 0.036 mbar/(s M) and 0.042 mbar/(s M). **5** is electronically activated but also sterically more demanding due to the decoration of the benzene ring. As the methoxy bridge of **5** does not interfere with the catalytic machinery but is probably located in the hydrophobic pocket, it does not seem to influence the oxidation of **5** by the enzyme. The oxygen consumption rate determined for the secondary and primary allylic alcohols **6**, **7**, **8**, **9**, **10**, and **11** is in the same range as seen for benzylic alcohols **4**

and **5**. All substances listed in Figure 7 were converted to the corresponding aldehydes, which was confirmed by GC–MS analysis of small-scale biotransformations and comparison of the obtained chromatograms with those of authentic standards. The formation of carboxylic acids, which has been reported as a follow-up reaction in the oxidation of primary alcohols by other flavin-dependent oxidases, has never been observed in our experiments. The conversions observed by GC-MS are summarized in Table 3.

Table 3: Substrate conversion determined by GC

Substance	Conversion [%]
1 Cinnamyl alcohol	96.7
4 Benzyl alcohol	99.9
5 Piperonyl alcohol	49.4
9 trans-2-Hexen-1-ol	47.4
10 cis-2-Hexen-1-ol	28.3
11 Crotyl alcohol	15.4
12 3-Phenyl-2-propyn-1-ol	19.2
13 (Z)-2-fluoro-3-phenyl-prop-2-en-1-ol	99.9

With cinnamyl alcohol derivatives **1** and **13** high conversions are achieved. With benzylic alcohol derivatives **4** and **5**, 99.9% and 49.4% conversion is achieved, while with allylic alcohols between 15.4% and 47.4% conversion can be determined.

No conversion was determined for 1-phenylethanol, 2-phenylethanol 3-phenyl-1-propanol and geranylamin.

3.9 Kinetic resolutions

As secondary allylic alcohols were found to be converted by the enzyme, this substance class was chosen for testing the enantioselectivity of the enzyme. Kinetic resolutions were conducted starting from racemic alcohols. Enantiomeric excess (*e.e.*) of the remaining substrate as well as conversion were determined by chiral-phase and achiral-phase GC analysis, and the enantioselectivity (*E*) was calculated according to Rakels *et al.* [16]. The results are summarized in Table 2

Table 2: Kinetic resolutions with *AtBBE*-like 15 L182V

Substance	Alcohol 1 [%]	Alcohol 2 [%]	Ketone [%]	Sum alcohols [%]	<i>e.e.</i>	<i>E</i>
3b 4-Phenylbut-3-en-2-ol (acetyl derivative)	41,7	0,0	58,3	41,7	99,9	>34
6 3-Octen-2-ol	44,8	0,0	55,2	44,8	99,9	>47
8 3-Penten-2-ol	52,5	35,1	12,4	87,6	19,9	>200
9 Cyclohex-2-en-1-ol	15,0	49,8	35,2	64,8	53,0	>200

The results indicate that the enzyme shows a high enantioselectivity in the oxidation of secondary allylic alcohols. The absolute configuration of the remaining alcohol, and hence the stereopreference of the enzyme, is currently under investigation. The selectivity might even be higher than indicated by the results as the starting material and product of the reaction are extracted with a different efficiency.

Conclusions

In the present study we have probed the applicability of a monoglignol oxidoreductase for biocatalytic applications. We employed the *AtBBE*-like 15 L182V variant that previously was engineered towards higher oxygen reactivity. We elucidated the pH and temperature optima of the enzyme, the substrate scope and tolerance towards organic co-solvents. *AtBBE*-like 15 L182V retained more than 50% of activity in a broad pH range between 5 and 10. The highest activity was reached at 50°C. The enzyme exhibits an enhanced activity in the presence of organic co-solvents. Various organic co-solvents are tolerated by the enzyme at concentrations up to 50% (v/v) and for a time span of up to 24 h. Various allylic and benzylic alcohols were accepted as substrates and converted to the corresponding aldehydes. Aliphatic alcohols were not converted by the enzyme. Therefore *AtBBE*-like L182V can be anticipated as a good candidate for future biocatalytic applications.

References

1. Macheroux, P., Kappes, B. & Ealick, S. E. Flavogenomics - A genomic and structural view of flavin-dependent proteins. *FEBS J.* **278**, 2625–2634 (2011).
2. Winkler, A., Hartner, F., Kutchan, T. M., Glieder, A. & Macheroux, P. Biochemical evidence that berberine bridge enzyme belongs to a novel family of flavoproteins containing a bi-covalently attached FAD cofactor. *J. Biol. Chem.* **281**, 21276–21285 (2006).
3. Winkler, A. *et al.* Structural and mechanistic studies reveal the functional role of bicovalent flavinylation in berberine bridge enzyme. *J. Biol. Chem.* **284**, 19993–20001 (2009).
4. Facchini, P. J., Penzes, C., Johnson, A. G. & Bull, D. Molecular characterization of berberine bridge enzyme genes from opium poppy. *Plant Physiol.* **112**, 1669–1677 (1996).
5. Winkler, A. *et al.* A concerted mechanism for berberine bridge enzyme. *Nat. Chem. Biol.* **4**, 739–741 (2008).
6. Fagan, R. L. & Palfey, B. A. in *Compr. Nat. Prod. II* (2010). doi:10.1016/B978-008045382-8.00135-0
7. Zafred, D. *et al.* Rationally engineered flavin-dependent oxidase reveals steric control of dioxygen reduction. *FEBS J.* **282**, 3060–3074 (2015).
8. Daniel, B. *et al.* oxidation of monolignols by members of the berberine bridge enzyme family suggests a role in cell wall metabolism. *J. Biol. Chem.* **290**, 18770–18781 (2015).
9. Steinkellner, G., Rader, R., Thallinger, G. G., Kratky, C. & Gruber, K. VASCo: computation and visualization of annotated protein surface contacts. *BMC Bioinformatics* **10**, 32 (2009).
10. Hendlich, M., Rippmann, F. & Barnickel, G. LIGSITE: Automatic and efficient detection of potential small molecule-binding sites in proteins. *J. Mol. Graph. Model.* **15**, 359–363 (1997).
11. Lenoir, D. Selective oxidation of organic compounds—sustainable catalytic reactions with oxygen and without transition metals? *Angew. Chemie Int. Ed.* **45**, 3206–3210 (2006).
12. Behr, A., Johnen, L. & Daniel, B. A liquid immobilisation concept for enzymes by thermomorphic solvent systems. *Green Chem.* **13**, 3168–3172 (2011).
13. Battino, R., Rettich, T. R. & Tominaga, T. The solubility of oxygen and ozone in liquids. *J. Phys. Chem. Ref. Data* **12**, 163–177 (1983).
14. Tauber, K. *et al.* A highly efficient ADH-coupled NADH-recycling system for the asymmetric bioreduction of carbon-carbon double bonds using enoate reductases. *Biotechnol. Bioeng.* **108**, 1462–7 (2011).
15. Rakels, J. L. L., Straathof, A. J. J. & Heijnen, J. J. A simple method to determine the enantiomeric ratio in enantioselective biocatalysis. *Enzyme Microb. Technol.* **15**, 1051–1056 (1993).

Chapter 5: Structure of a berberine bridge enzyme-like enzyme with an active site specific to the plant family of *Brassicaceae*

Bastian Daniel,¹ Silvia Wallner,¹ Barbara Steiner,¹ Gustav Oberdorfer,² Prashant Kumar,²
Christioph W. Sensen,³ Karl Gruber,² and Peter Macheroux^{1*}

¹Graz University of Technology, Institute of Biochemistry, Graz, Austria

²University of Graz, Institute of Molecular Biosciences, Graz, Austria

³Graz University of Technology, Institute of Molecular Biotechnology

To whom correspondence should be addressed:

Prof. Dr. Peter Macheroux, Graz University of Technology, Institute of Biochemistry,
Petersgasse 12/II, A-8010 Graz, Austria, Tel.: +43-316-873 6450; Fax: +43-316-873 6952;
Email: peter.macheroux@tugraz.at

Author contributions:

B. D., S. W. and B. S., performed the protein expression and biochemical assays. B. D., G. O, P. K. and K. G. determined the crystal structure. B. D. and C. W. S. elaborated the phylogenetics. B. D., and P.M wrote the manuscript.

Abstract

Berberine bridge enzyme-like (BBE-like) proteins (pfam 08031) form a multigene family present in plants, fungi and bacteria. They adopt the vanillyl alcohol oxidase fold and predominantly show bicovalent tethering of the FAD cofactor to a cysteine and histidine residue. *Arabidopsis thaliana* was recently shown to possess 28 BBE-like proteins featuring four distinct active site compositions. Here we present the structure of a member of the *At*BBE-like protein family (termed *At*BBE-like 28), which has an active site composition that was not structurally and biochemically characterized so far. The most salient and distinguishing features of the active site found in *At*BBE-like 28 are a mono-covalent linkage of a histidine to the 8 α -position of the flavin isoalloxazine ring and the lack of a second covalent linkage to the 6-position owing to the replacement of cysteine to histidine. In addition, the structure reveals the interaction of a glutamic acid (Glu426) with an aspartic acid (Asp369), which appear to share a proton. This arrangement leads to the delocalization of a negative charge in the active site that may be exploited for catalysis. The structure also indicates a shift of the position of the isoalloxazine ring in comparison to other members of the BBE-like family. The dioxygen surrogate chloride was found near the C(4a) position of the isoalloxazine ring in the oxygen pocket rationalizing a rapid reoxidation of reduced enzyme by dioxygen. Multiple sequence analysis showed that this particular active site composition in BBE-like enzymes is confined to the *Brassicaceae* suggesting that they play a specific role in the metabolism of this plant family.

Introduction

Flavoproteins are a large and diverse family that requires either FMN or FAD as cofactor. The majority of flavoproteins (ca. 90%) act as oxidoreductases in a plethora of biochemical redox processes¹. Among these flavin-dependent oxidoreductases berberine bridge, enzyme-like enzymes stand out because of the bicovalent attachment of the cofactor to the protein via a histidine and a cysteine^{2,3}. The namesake of this protein family is the berberine bridge enzyme from *Eschscholzia californica* (California poppy), which catalyzes the oxidative ring-closure reaction from (*S*)-reticuline to (*S*)-scoulerine. The C-C-bond formed in this reaction is the so called “berberine bridge”. This reaction marks a branch point in the biosynthesis of isoquinoline alkaloids⁴. As the number of sequenced plant genomes increases constantly, more and more genes encoding BBE-like enzymes have been identified in diverse plant families. Interestingly, most of these plant families are not known to biosynthesize any alkaloids and thus the role of BBE-like enzymes in these plants remains elusive. Despite this lack of knowledge on the biochemical properties of BBE-like enzymes, they have caught the attention of scientists due to the exceptionally high up-regulation observed during pathogen responses in plants^{5,6,7}. The BBE-like enzymes are predominantly secreted and have been found to contribute a significant part of the plant cell wall proteome (up to 2.5%)^{8,9}. Moreover, BBE-like enzymes contribute to the expressed secretome during infection by various plant pathogens, suggesting a role in plant-pathogen interactions^{10,11,12}.

Recently, we have shown that two BBE-like enzymes from *Arabidopsis thaliana* oxidize monolignols to the corresponding aldehydes, *i.e.* function as monolignol oxidoreductases⁹. This activity suggests that these enzymes are involved in the manipulation of the extracellular monolignol pool and thereby influence plant cell wall metabolism with as yet unknown implications for lignin formation. A detailed study to reveal the physiological role of the oxidoreductases using knock-out plants is currently under way. Monolignol oxidoreductase activity appears to be associated with a defined composition of the active site, as shown in Figure 1 (panel A). Characteristic features of this active site, designated type I, are Tyr117 and Gln438 engaging in a hydrogen bond as well as Tyr479, Tyr193 and Lys436 forming the catalytic base motif. In this motif, the hydroxyl groups of Tyr479 and Tyr193 point toward each other (oxygen-oxygen distance = 2.4 Å) and Lys436 apparently engages in a cation- π interaction with Tyr193. This arrangement presumably adjusts the pK_a value of Tyr193 to facilitate its role as a catalytic

base. The type I composition clearly dominates the BBE-like enzyme family in *A. thaliana* with 18 out of 28 possessing identical or very similar active sites.

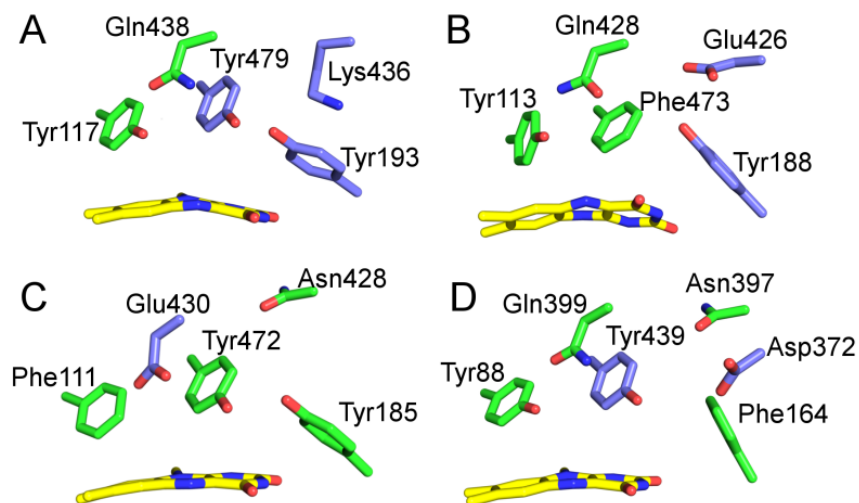


Figure 1: Active site composition of types I-IV (panel A to D) of BBE-like enzymes. The isoalloxazine ring is shown in yellow. Residues forming the active site are shown in green and residues involved in the abstraction of a proton during catalysis are shown in violet. A: Type I: Tyr117 and Gln438 are engaged in a hydrogen bond. Tyr193 acts as catalytic base, it is stabilized in the deprotonated state by Tyr479 and Lys436 (PDB entry 4UD8). B: Type II. Tyr113 and Gln428 are engaged in a hydrogen bond. Tyr188 putatively acts as catalytic base after deprotonation by Glu426 (PDB entry 5D79). C: Type III: Glu430 putatively acts as catalytic base in the active site. The involvement of Tyr472 and Tyr185 is conceivable. A homology model of Q9SA88 based on 4UD8 and prepared with YASARA was used for visualization⁴³. D: Type IV: Tyr88 and Gln399 are engaged in a hydrogen bond, Tyr439 acts as catalytic base after deprotonation by Asp372 via a water molecule (PDB entry 4PWC).

Further inspection of multiple sequence alignments and homology models of BBE-like enzymes revealed the presence of three additional and distinct active site compositions in the remainder of BBE-like enzymes, as shown in Figure 1 (panels B-D, designated type II-IV). In the active site of type II, shown in Figure 1B, the hydrogen bond interaction between Tyr113 and Gln428 is retained, however, the catalytic base motif has substantially changed by exchange of a tyrosine to a phenylalanine and a lysine to a glutamic acid (compare panels A and B). Yet other changes are apparent in the composition of the active sites found in type III and IV (Figure 1). The characteristic active site composition described by type II, III and IV are found in 3, 3 and 2 *At*BBE-like enzymes, respectively. Although it appears likely that these BBE-like enzymes also

serve as oxidoreductases neither their substrate spectrum nor the catalyzed reactions were identified thus far.

Due to the high sequence identity within the BBE-like family sequence alignments and homology models can be valuable tools to predict the active site composition of structurally uncharacterized members. However, side chain orientations cannot be predicted with the same confidence and thus homology models are not sufficient to determine how residues are oriented in the active site. Therefore, we set out to crystallize a representative of the type II BBE-like enzymes in order to pave the way for further studies into their function. Here we report the crystallographic structure of *AtBBE*-like 28, a member of the type II BBE-like enzyme sub-family. In addition, we have partially characterized the enzyme with regard to the oxidative half-reaction and its redox potential.

Results

Structural characterization of AtBBE-like 28

AtBBE-like 28 was expressed in *Komagataella pastoris* and purified as reported previously⁹. Crystallization was conducted using the sitting-drop method, yielding crystals diffracting to a resolution of 1.8 Å. The structure was solved using molecular replacement employing the structure of BBE from *Eschscholzia californica* (*EcBBE*, PDB code 3D2H) as the search template. Like *EcBBE*, *AtBBE*-like 28 adopts the VAO topology, as shown in Figure 2A. The protein consists of two domains: a substrate and an FAD binding domain shown in orange and green, respectively (Figure 2). The structural elements directly interacting with the isoalloxazine ring are shown in Figure 2B. Typically, the covalent linkage between the thiol group of a cysteine and the C6-position of the isoalloxazine ring, reported for BBE from *E. californica* and *AtBBE*-like 15, originate from the oxygen binding motif. In the case of *AtBBE*-like 28, the cysteine is replaced by His174, which does not form a covalent bond to the C6-position (Figure 3A and B). However, the covalent linkage established by the conserved GGHD motif was clearly seen in the crystal structure (His111 in Figure 3).

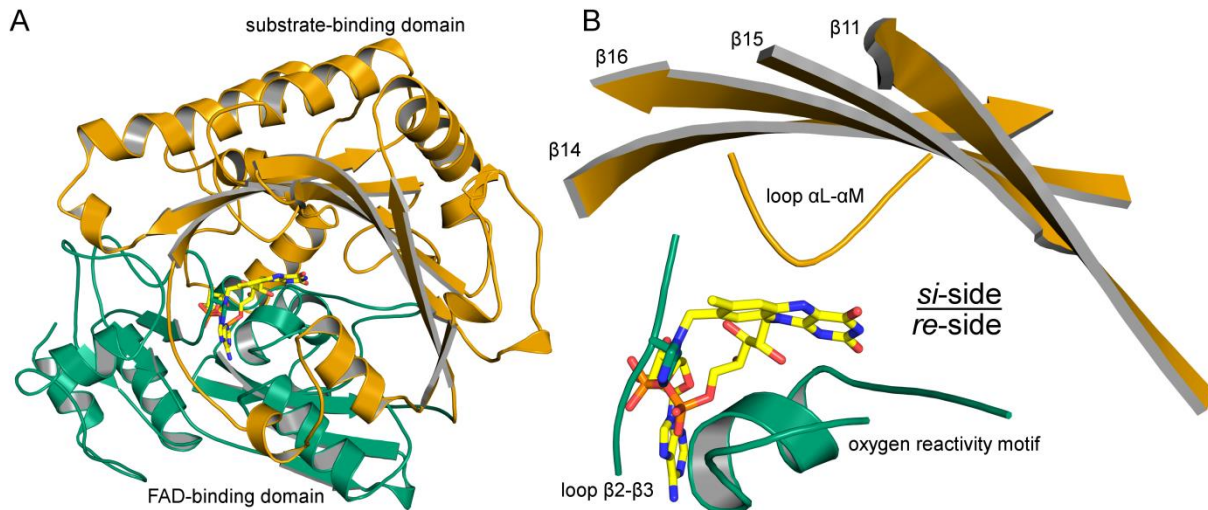


Figure 2: A: Overall topology of *AtBBE*-like 28; green: FAD-binding domain, orange: substrate-binding domain. The active site is formed between the FAD-binding site and a substrate binding domain. B: structural elements interacting directly with the isoalloxazine ring of the FAD-cofactor and structural elements harboring residues involved in the formation of the active site.

As indicated in Figure 2B, the space “above” and “below” the plane of the isoalloxazine ring, *i.e.* the *si*- and *re*-side, play different catalytic roles. One catalytic cycle of a flavoprotein can be split into two half reactions. In the resting state the flavin is oxidized. In the reductive half reaction a putative substrate is oxidized by the flavin, subsequently dissociates from the active site and leaving the flavin in the reduced state. In BBE-like enzymes this reaction takes place at the *si*-side. In the oxidative half reaction the reduced flavin reacts with an appropriate electron acceptor, *e.g.* dioxygen. Enzymes that promote the oxidation of the flavin with dioxygen are classified as oxidases, enzymes that inhibit this reaction are classified as dehydrogenases. In the BBE-like family the oxidation of the flavin by dioxygen is catalyzed at the *re*-side.

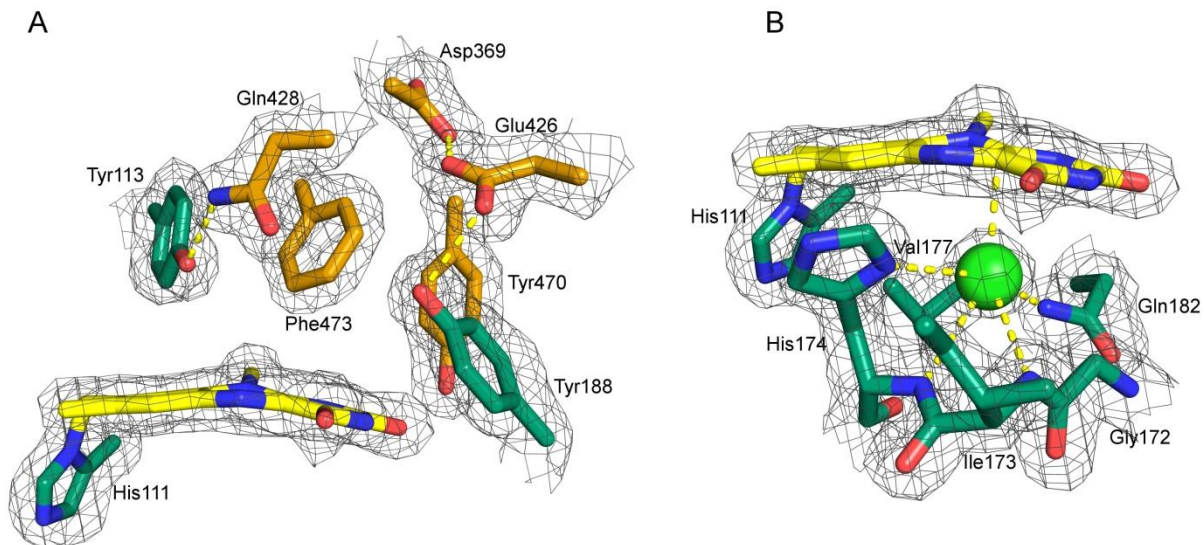


Figure 3: A: Amino acid residues present on the *si*-side of the isoalloxazine ring. Residues originating from the FAD- and substrate binding site are shown in green and orange, respectively. The 2Fo-Fc is shown at 1.5 σ . The carboxylate groups of Asp369 and Glu426 are found at a distance of 2.4 Å. The proximity of these residues suggests a shared proton and a negative charge delocalized over both carboxylic acids. Glu426 interacts with Tyr188 that putatively acts as catalytic base after deprotonation by Glu426. B: Residues defining the *re*-side of the isoalloxazine ring. An oxygen pocket is formed by the oxygen reactivity motif (compare Figure 2B). The electron density was interpreted as a chloride ion (light green), which is complexed by the backbone amides of His174 and Ile173 as well as N π of His174 and the side chain amide of Gln182.

The residues defining the composition of the protein on the *si*-side of *AtBBE*-like 28 and thereby putatively responsible for the catalysis of the first half reaction are shown in Figure 3A. The flavin adopts a butterfly-bent shape, with an angle at the N5-N10 axis of 6°. A hydrogen bond of 2.6 Å is formed between Tyr113 and Gln428. Tyr470 forms a hydrogen bond to the C(2)=O locus of the isoalloxazine ring. Asp369 and Glu426 are found in a distance of 2.4 Å, indicating that they are sharing a proton. Thus this conformation may stabilize a negative charge, which is delocalized between Asp369 and Glu426 and may be exploited for catalysis.

Direct interactions on the *re*-side of the protein matrix and the isoalloxazine ring are established by the oxygen reactivity motif (Figure 2B). It originates from the FAD binding domain and regulates the reactivity of the enzyme towards dioxygen by sterically controlling access to an oxygen binding pocket near the C(4a)-position of the isoalloxazine ring¹³. Recently, Zafred *et al.* have identified a single residue as the gatekeeper of the oxygen binding pocket: a

valine in this position allows the formation of an oxygen binding pocket whereas the presence of a leucine occupies the pocket and thus denies access to this site. In *AtBBE*-like 28, this position is occupied by Val177 and thus we assume that the pocket is available for oxygen binding. In agreement with this assumption, an electron density in this pocket was clearly detectable and we propose that a chloride ion, acting as an oxygen surrogate, is bound to the pocket (Figure 3B, green sphere). It is complexed by $N\pi$ and the nitrogen involved in the amide bond of the backbone of His174, with a distance of 3.6 Å and 3.7 Å, respectively. In addition, the chloride ion is complexed by the nitrogen from the backbone amide of Ile173 and side chain amide of Gln182 with a distance of 3.7 Å and 3.3 Å, respectively. The distance between the chloride and the C(4a) of the isoalloxazine ring is 3.1 Å. Dioxygen is thought to attack the reduced flavin to form a C(4a)-peroxy species in the course of the oxidative half reaction.

Biochemical characterization

Recently, we have reported a successful strategy to identify substrates for *AtBBE*-like 13 and 15 that involved screening of a chemical compound library based on observed effects on protein thermal stability ⁹. In the case of *AtBBE*-like 28, this approach was not successful. Similarly, molecular docking of a compound library using our crystallographic structure did not lead to the identification of the nature of the cognate substrate of *AtBBE*-like 28. In the absence of a substrate, we thus employed photoreduction according to the method described by Massey *et al.* to gain information on the spectral properties of *AtBBE*-28 in its reduced state ¹⁴. Initially, stepwise photoreduction of *AtBBE*-like 28 results in an increase of absorption at 370 nm that is characteristic for the anionic (red) flavin semiquinone ¹⁵. Further photoreduction yields the fully reduced dihydroquinone species with a rather featureless absorption spectrum in the visible range. Selected spectra observed during photoreduction are shown in Figure 4A.

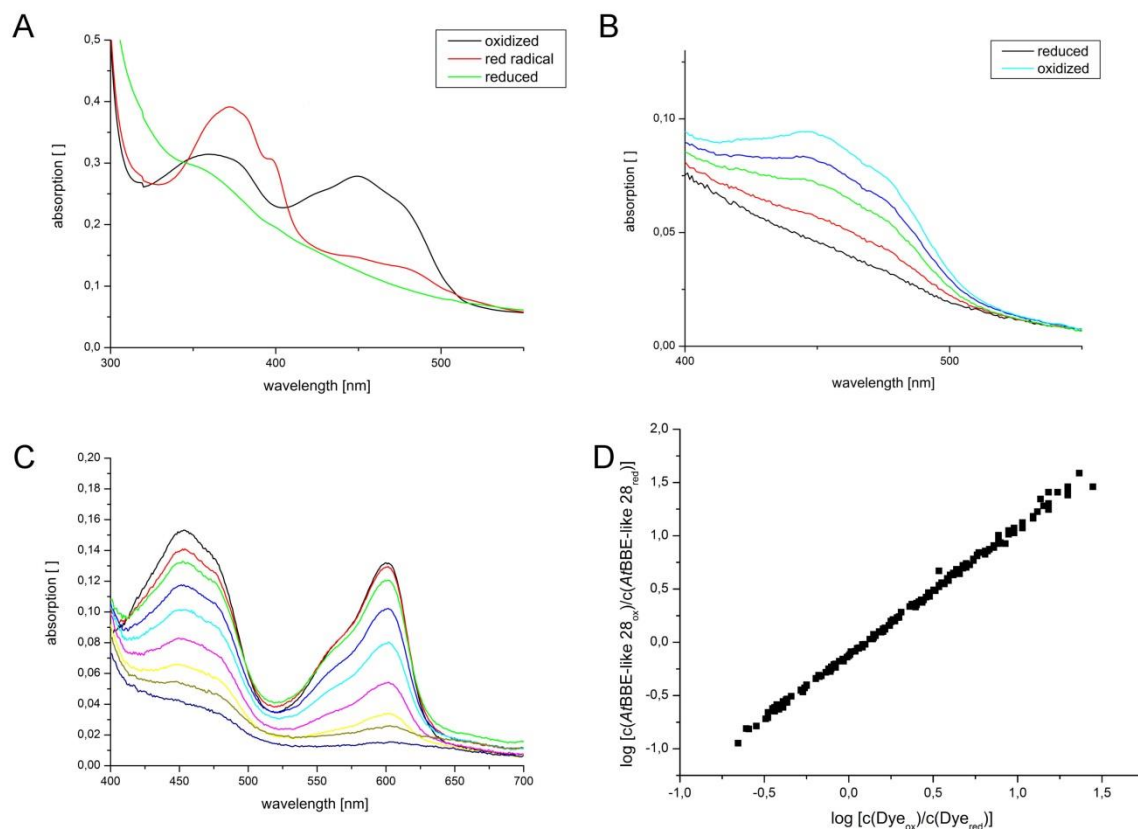


Figure 4: A: Photoreduction of *AtBBE*-like 28: The formation of an anionic radical semiquinone species is indicated by the increase of absorbance at 370 nm in the course of the reduction B: Selected spectra recorded during the reoxidation of photoreduced *AtBBE*-like 28 by oxygen to determine the oxidative rate. C: Selected spectra of the simultaneous reduction of *AtBBE*-like 28 and thionine acetate using the xanthine/xanthine oxidase system as an electron source. D: Double logarithmic plot of the concentration of *AtBBE*-like 28 (ox/red) and thionine acetate (ox/red) used for the determination of the redox potential of *AtBBE*-like 28.

The pronounced spectral difference at 450 nm was exploited in further experiments to investigate the rate of reoxidation of reduced *AtBBE*-like 28 by molecular oxygen in a stopped-flow device. Photoreduced enzyme was mixed with air-saturated buffer and the course of re-oxidation of the flavin was followed at 450 nm. Selected spectra recorded during the experiment are shown in Figure 4B. Kinetic analysis of reoxidation yields a bimolecular rate constant of $3040 \pm 50 \text{ M}^{-1} \text{ s}^{-1}$ and is thus 12 times faster than the reaction of free FAD with molecular oxygen ($250 \text{ M}^{-1} \text{ s}^{-1}$)¹⁵. Therefore, *AtBBE*-like 28 accelerates the rate of reaction with molecular oxygen and can be

classified as an oxidase, in agreement with the presence of an oxygen binding pocket near the C(4a)-atom of the isoalloxazine ring, as described in the previous section.

The redox potential is an important parameter to characterize a redox system. In the case of BBE-like enzymes the bicovalent cofactor attachment results in a large shift to ca. +130 mV for BBE or +211 mV for the pollen allergen Phl p 4, to give two examples^{16,13}. For the latter this means that the redox potential is shifted by 411 mV compared to that of free FAD (-210mV)¹⁷. The redox potential of *At*BBE-like 28 was determined with thionine acetate as reference dye, according to Minnaert *et al.*¹⁸. Using the xanthine/xanthine oxidase electron delivery system, *At*BBE-like 28 and the dye were simultaneously reduced indicating that the redox systems are in equilibrium during the time course of the experiment. Selected spectra and the double logarithmic plot used for data evaluation are shown in Figure 4 C and D. A redox potential E° of $+60.5 \pm 1.1$ mV was determined for *At*BBE-like 28 at 25 °C and pH 7.0.

Sequence comparison and phylogenetic inference

As mentioned in the introduction, *A. thaliana* harbors 3 BBE-like enzymes with the active site composition of type II. To investigate how common this particular active site composition is in other plant families we used the sequence of *At*BBE-like 28 to search the genomes of a variety of plants for BBE-like enzymes. Our analysis revealed that BBE-like enzymes featuring a type II active site composition can be sub-classified according to their mode of covalent attachment with type IIa and IIb showing monocovalent and bicovalent cofactor attachment, respectively.

Surprisingly, type IIa BBE-like enzymes, such as *At*BBE-like 28, were found exclusively in plant species of the *Brassicaceae* family¹⁹. Therefore, sequences coding for BBE-like enzymes out of the genomes of seven species of this family (*Arabidopsis lyrata*, *Arabidopsis thaliana*, *Boechera stricta*, *Brassica rapa*, *Capsella grandiflora*, *Capsella rubella*, and *Eutrema salsugineum*) were retrieved from the Phytozome website and aligned with Clustal Omega²⁰. A phylogenetic tree was prepared using the PHYLIP package 3.69 as shown in Figure 5²¹. In six of these species we found at least one enzyme that belongs to the type IIa BBE-like enzymes indicating a widespread occurrence in *Brassicaceae*. On the other hand, our analysis revealed that type IIa BBE-like enzymes are absent in all other plant families investigated. In our view this may turn out to be an important finding in light of the yet unsuccessful search for a cognate substrate of *At*BBE-like 28.

The *Brassicaceae* family is known to have several specific metabolites, such as the glucosinolates or camalexin, and thus it appears likely that type IIa BBE-like enzymes are involved in metabolic (oxidation) processes confined to this plant family ^{22,23}. Currently, characterization of *At*BBE-like 28 knock out plants is under way to identify possible substrates of *At*BBE-like enzyme 28.

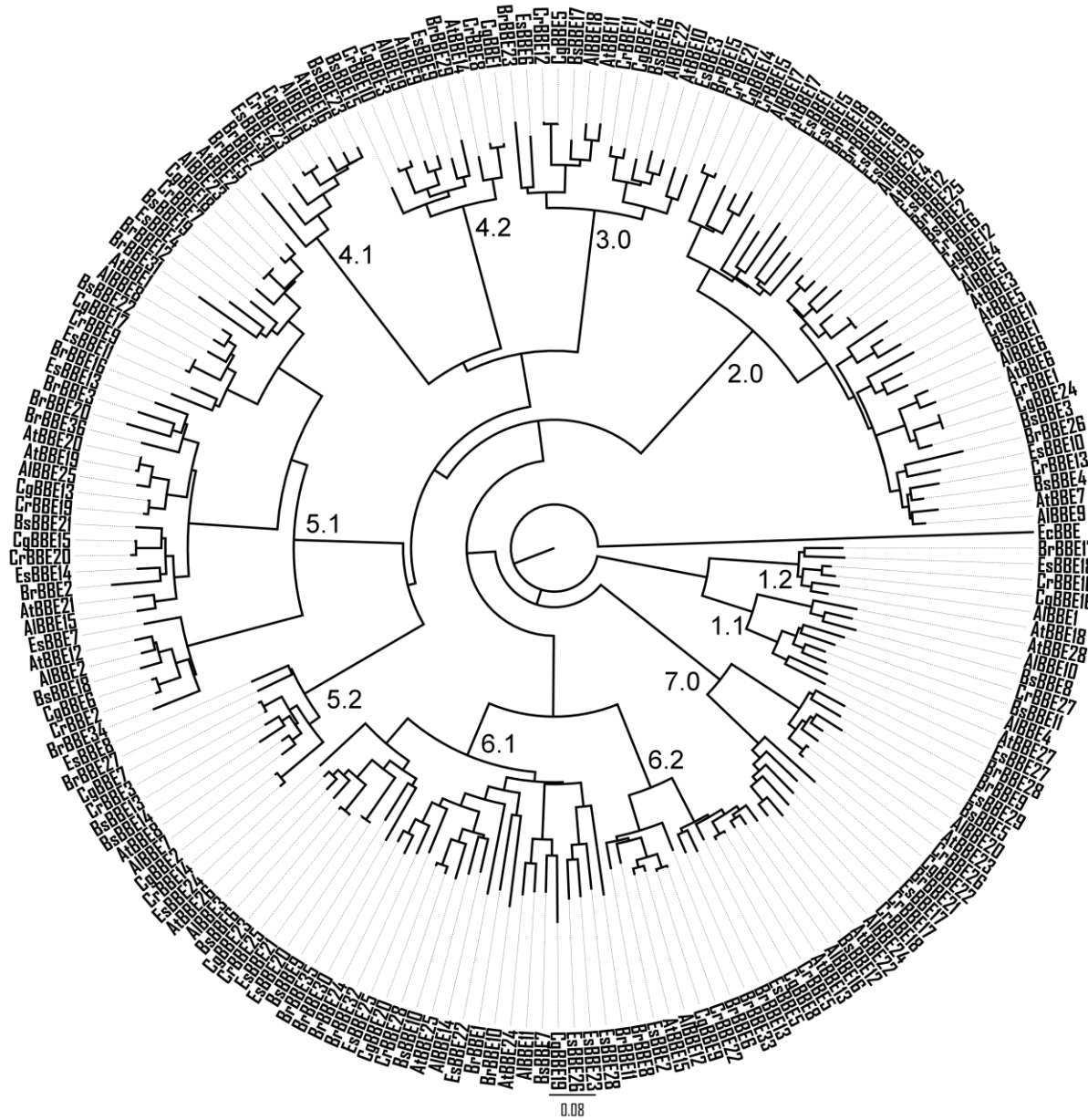


Figure 5: Phylogenetic tree of the BBE-like enzymes within the *Brassicaceae*. Sequences from *Arabidopsis lyrata* (Al), *Arabidopsis thaliana* (At), *Boechera stricta* (Bs), *Brassica rapa* (Br), *Capsella grandiflora* (Cg), *Capsella rubella* (Cr), and *Eutrema salsugineum* (Es) were used. The composition of the phylogenetic groups is summarized in Table 1.

Table 1: Composition of the phylogenetic groups of the BBE-like enzymes from *Brassicaceae* as defined in Figure 5 sorted by species.

Group	<i>At</i> BBE	<i>A/B</i> BBE	<i>Br</i> BBE	<i>Bs</i> BBE	<i>Cg</i> BBE	<i>Cr</i> BBE	<i>Es</i> BBE
1.1	27, 28	4, 10	28	8, 11		27	27
1.2	18	1	17		16	16	18
2.0	17, 4, 3, 6, 7, 5	5, 6, 9, 17, 26	18, 19, 25, 26	1, 2, 3, 4	11, 12, 14, 24,	1, 4, 6, 13, 15, 21	1, 10, 12, 15, 16, 19,
3.0	10, 11	18, 22	15, 23	16, 17	4, 5	11, 12	3, 6
4.1	16	13	5, 7	23	10	23	30
4.2	9, 14	19	29	15	1, 3	8, 10	9
5.1	1, 2, 12, 19, 20, 21	2, 8, 15, 23, 25	2, 3, 12, 16, 20, 31, 36, 34	18, 19, 22, 21	6, 13, 15, 17, 18,	2, 9, 19, 20,	4, 7, 11, 13, 14
5.2	8	7	27	13, 14	7, 2	3, 14	8
6.1	24, 25, 26	3, 11, 14	1, 10, 11, 24, 30, 32, 35,	6, 7, 9, 10	19, 20, 23	25, 28	20, 21, 22, 23, 24, 25, 26, 28
6.2	13, 15	12, 16	6, 8, 13, 33	12	8, 9	5, 22	2, 5
7.0	22, 23	20, 24	9, 21	5	22	17, 18, 26	17, 29

Overall, the same phylogenetic groups as described before in the analysis of the *At*BBE-like enzymes can be found in *Brassicaceae*⁹, if reasonable sub groups were defined according to sequence distances. To visualize and compare the active sites of different groups we generated sequence logos for the amino acids in pertinent motifs (Figure 2B). As shown in Figure 6, amino acids originating in the β -sheets and pointing towards the isoalloxazine ring contribute to the decoration of the active site (downward arrows in Figure 6). The sequence logos of the active site

forming residues allow the identification of features that are conserved in the overall family or that are specific for a certain subgroup. In general, the active site of BBE-like enzymes possess a remarkable plasticity that is mainly achieved by the variation of polar contacts at positions 401, 426, and 428 (black boxes in Figure 6) and aromatic residues 113, 188 and 473 (red boxes Figure 6). The mode of covalent cofactor tethering is indicated by amino acid positions 111 and 174 (labeled with * in Figure 6) whereas the reactivity toward oxygen is revealed by consulting position 177 (labeled with ▼). The active site composition found in *At*BBE-like enzyme 28 is found only in group 1 and can be differentiated in type a and b as noted above. Type IIa is present in group 1.1 and the cofactor is attached strictly mono-covalently via His111 (loop β 2- β 3). In position 174, corresponding to the predominant cysteine responsible for cofactor tethering in other BBE-like enzymes, a histidine or a tyrosine is found (compare Figure 6, group 1.1, Figure 3B). Furthermore, a unique and conserved arrangement is found in type II with Asp369 (β 14) replacing a highly conserved serine in the rest of the family. This residue is in close contact to Glu426 (β 16), which is also invariant in group 1.1. In combination, Asp369 and Glu426 presumably facilitate deprotonation of Tyr188 (oxygen reactivity motif, compare also Figure 3A), which presumably acts as active site base. In group 1.2 a similar arrangement of amino acids is found with the notable exception of Asp369, hence the catalytic triad appears to be replaced by a diad. On the other hand, the cofactor in group 1.2 is bi-covalently linked to the protein backbone and Gln182 is replaced by histidine, as is typical for BBE-like enzymes with bicovalent cofactor linkage.

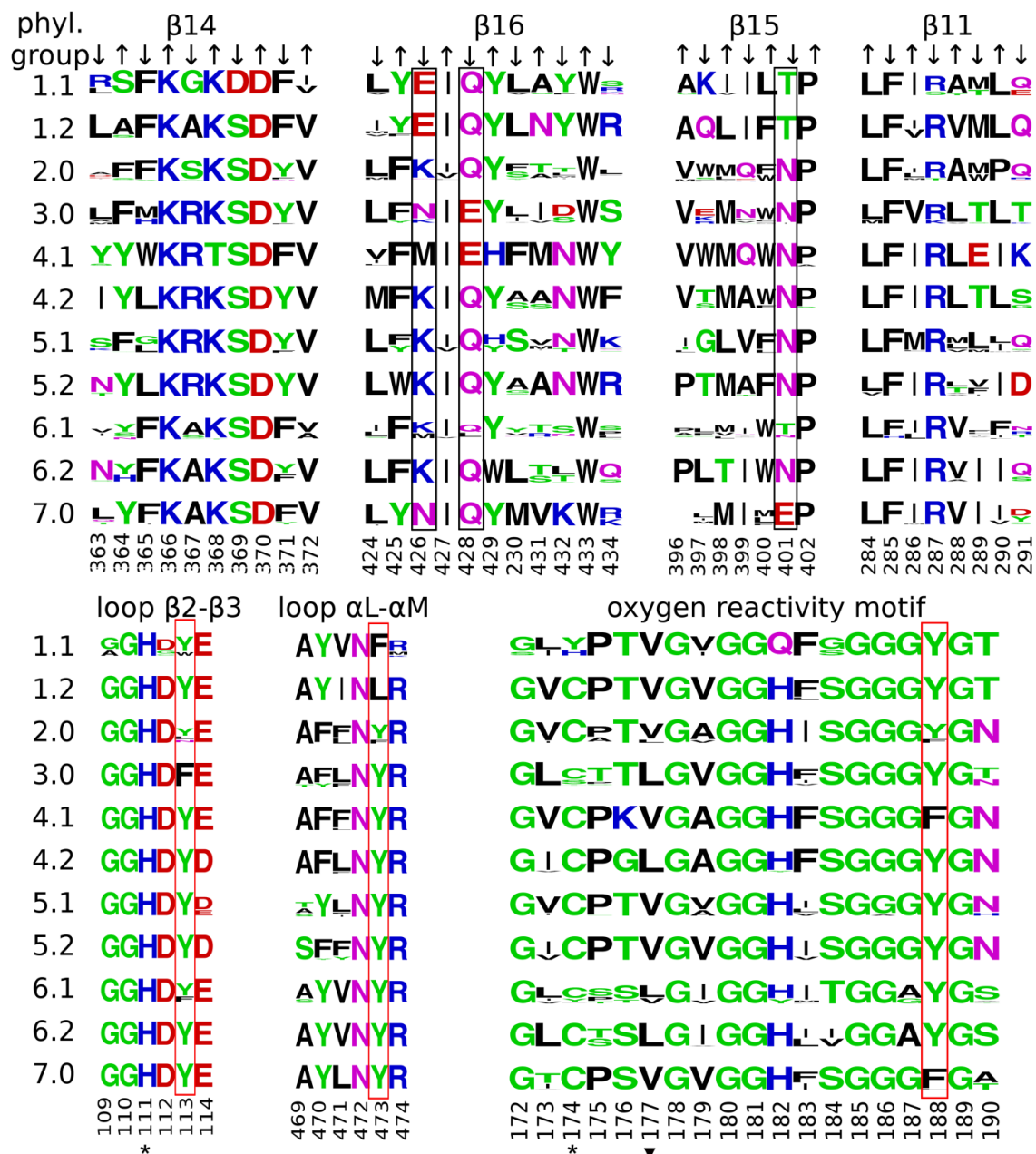


Figure 6: Sequence logos representing the secondary elements directly interacting with the isoalloxazine ring for all phylogenetic groups defined in Figure 5. The numbering is according to the sequence of *AtBBE*-like 28. *: site of covalent cofactor attachment, ▼: Gatekeeper residue controlling access to the oxygen pocket; Valine is found in oxidases, leucine in dehydrogenases. Black boxes: Variable polar residues putatively involved in catalysis. Red boxes: Variable aromatic residues putatively involved in catalysis. β 14, 16, 15 and 11 cover the *si*-side of the isoalloxazine ring. Arrows indicate the orientation of the residues in the β -strands. An upward arrow indicates the residue points towards the α -

helices covering the 7-stranded antiparallel β -sheet (compare Figure 2B). These residues are found to be structurally relevant and predominantly conserved in the overall family (compare β 14 positions 366, 368, 370 and β 16 position 433). A downward arrow indicates the residue points towards the active site. Residues contributing to the decoration of the active site are conserved within the phylogenetic groups but are variable within the overall family (compare β 16 positions 426, 428 and β 15 position 401).

Discussion

BBE-like enzymes are versatile biocatalysts catalyzing a broad range of reactions such as two-electron oxidations as reported for *At*BBE-like 15 or four-electron oxidations as catalyzed by Dbv29^{9,24}. In the case of BBE from *E. californica* substrate oxidation is coupled to a ring closure reaction leading to benzoisoquinoline alkaloids²⁵. A similar reaction that couples substrate oxidation with ring formation was reported for Δ 1-tetrahydrocannabinolic acid synthase²⁶. More recently BBE-like enzymes were discovered in the biosynthesis of the ergot alkaloid intermediate chanoclavine I and the indole alkaloid communesin^{27,28}. Although the exact mechanism of the reactions catalyzed by the latter two BBE-like enzymes has not been analyzed in detail yet, the structures of the generated products suggest that a similar coupling of substrate oxidation and ring formation may occur. Despite the observed structural differences of the cognate substrates all BBE-like enzymes share a common structural topology and adopt the vanillyl oxidase (VAO) fold. The ability to accept different substrates and catalyze regio- and stereospecific cyclization reactions is controlled by the specific composition of amino acid residues in the active sites. In the case of *At*BBE-like 28, we confirmed that the protein adopts the canonical BBE-like topology. However, *At*BBE-like 28 has a unique composition of the active site that has not been characterized so far. As the substrate of *At*BBE-like 28 is still unknown, it is difficult to assign distinct roles to the residues in the active site. Fraaije *et al.* (2000) have reported some recurrent features present in flavoenzymes that are carrying out an oxidation reaction²⁹. According to their analysis the position of the oxidized atom relative to the flavin ring is conserved (“site of oxidative attack”, see Figure 7). Furthermore, flavin dependent oxidoreductases have a hydrogen bond donor to N(5), a catalytic base to activate the substrate and possess a redox potential above +25 mV. As shown in Figure 7, *At*BBE-like 28 features a hydrogen bond donor to N(5) (N π of His174) and a catalytic base to initiate substrate oxidation (Tyr188) and hence shares the

hallmarks of a flavoprotein oxidase as proposed by Fraaije and coworkers²⁹. An additional interesting feature of the active site is the proton-relay established between the putative catalytic base, Tyr188, and the neighboring acidic side chains of Glu426 and Asp369, which presumably activate Tyr188 to facilitate proton abstraction. The experimentally determined redox potential of *At*BBE-like 28 of $+60.5 \pm 1.1$ mV is also in accordance with a potential function as an oxidase.

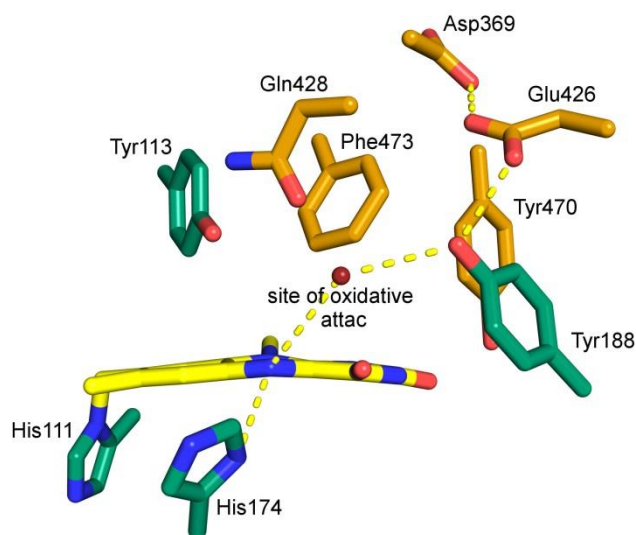


Figure 7: Model of the active site of *At*BBE-like 28 indicating the putative site of oxidative attack (red sphere). Hydrogen bond interactions are represented by dashed yellow lines.

On the other hand, the oxidative half reaction of BBE-like enzymes was recently analyzed in more detail demonstrating that a single gatekeeper residue plays a major role in controlling oxygen reactivity¹³. Accordingly, the presence of an “oxygen pocket” on the *re*-side of the isoalloxazine ring in direct vicinity of the reactive C(4a)-atom promotes the reaction between dioxygen and reduced flavin in a similar manner as the “oxyanion hole” stabilizes the transition state in hydrolases¹³. This oxygen pocket is created by the oxygen reactivity motif (see Figure 2B and 3B) where either a valine or a leucine is found in a central position. The presence of valine creates enough space for oxygen to bind in the oxygen pocket whereas the presence of leucine occupies the oxygen pocket and hence oxygen cannot react with the C(4a)-atom to oxidize the reduced isoalloxazine ring. Crystallographic studies also demonstrated that dioxygen surrogates, such as halide anions, bind to the oxygen pocket¹³. In the case of *At*BBE-like enzyme 28 we observed an electron density in the oxygen binding pocket that was interpreted as a bound

chloride (Figure 3B). An overlay of the previously reported structure of Phl p 4, a pollen allergen from timothy grass with glucose dehydrogenase activity³⁰, and the structure of *At*BBE-like enzyme 28 is shown in Figure 8. The location of the halide binding site relative to the isoalloxazine ring of the flavin is structurally conserved. Previous studies have also shown that a single amino acid replacement at this position reverses reactivity towards oxygen^{13,9}. In this sense, the sequence logos shown in Figure 6 are useful to predict the reactivity towards oxygen in *At*BBE-like enzymes, *i.e.* enzymes with valine in position 177 will behave more like oxidases while those with leucine in position 177 will act like dehydrogenases.

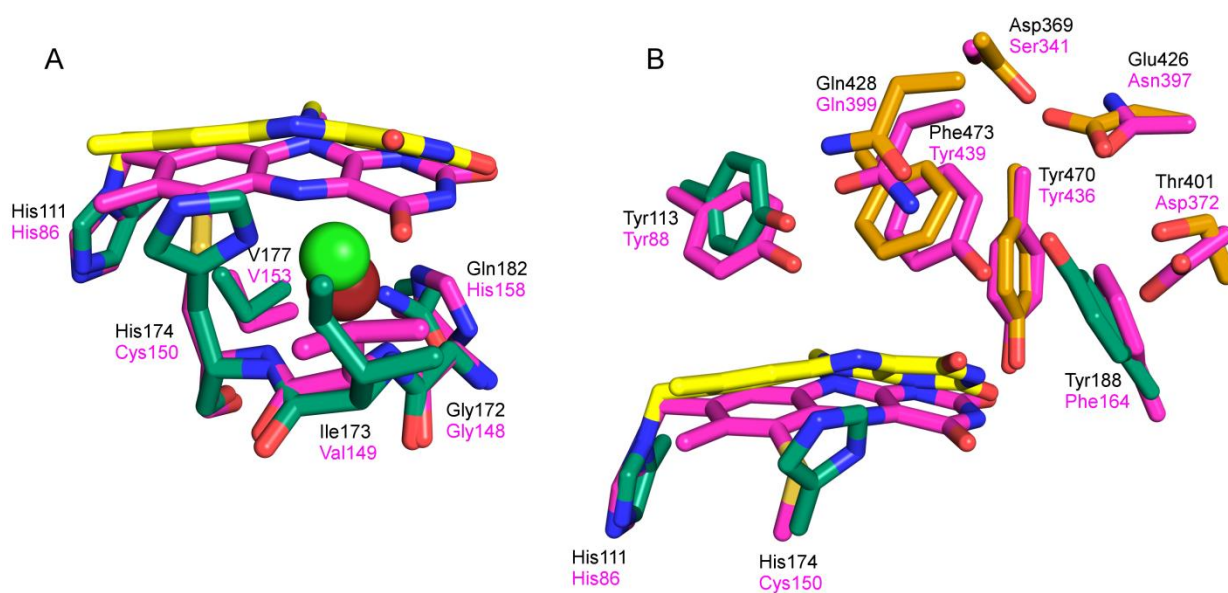


Figure 8: Overlay of *At*BBE-like 28 and Phl p 4 I153V N158H (magenta, PDB: 4PWC). A: *re*-side: *At*BBE-like 28 is shown in green and yellow, Phl p4 is shown in magenta. The chloride ion embedded in *At*BBE-like 28 is shown in green, bromide from Phl p 4 is shown in red. The oxygen pocket is highly conserved and in both structures occupied by oxygen surrogating halide ions. In Phl p4 the halide ion is complexed by the nitrogen of the peptide bond between Cys150 and Val149 and the nitrogen of the peptide bond between Val149 and Gly148. In *At*BBE-like 28 the halide ion is complexed by the corresponding residues, additionally His174 and Gln182 are involved in hydrogen bonds towards the chloride ion. B: *si*-side: The positions of the active site forming residues are conserved. Their nature has been changed leading to two different active sites embedded in a very similar proteins scaffold. Though the position of the isoalloxazine ring is highly conserved in the BBE-like family the C4 C6 axis of the plane N10 C4 C6 has been shifted 32° resulting in a displacement of N5 of 1.6 Å.

Conclusions

Four different active site types have been described for BBE-like enzymes from the plant kingdom thus far. In this report, we have elucidated the structure and appearance of the active site type II found in *At*BBE-like enzyme 28. This enzyme was expressed heterologously and the structure was solved by X-ray crystallography. The structure reveals the unique spatial arrangement of this active site type. A crucial aspect of the active site is the nature and position of the catalytic base: In *At*BBE-like enzyme 28, Asp369, Glu426 and Tyr188 are arranged as a catalytic triad that stabilizes the deprotonated form of the tyrosine by delocalization of a negative charge. Thus Tyr188 is activated to act as a catalytic base in the active site of *At*BBE-like 28. *At*BBE-like 28 was found to catalyze the reoxidation of the reduced FAD-cofactor by dioxygen in keeping with the accessibility of the oxygen binding pocket created by the oxygen binding motif of the BBE-like enzyme family. Currently, studies using *At*BBE-like 28 knock out plants are conducted to support the search for potential substrates accepted by this BBE-like enzyme family.

Experimental Procedures

All chemicals were purchased at Sigma Aldrich (St. Louis, USA) and were of the highest grade commercially available. Restriction enzymes were obtained from Thermo Fisher Scientific (Waltham, Massachusetts, USA). Ni Sepharose 6 Fast Flow column material was purchased from GE Healthcare (Chalfont St Giles, UK). A synthetic gene coding for *At*BBE28 was from VBC Biotech (Vienna, Austria).

Cloning and transformation

The protein was expressed using *Komagataella pastoris* as expression host according the EasySelect™ *Pichia* Expression Kit provided by Invitrogen (Carlsbad, USA). The gene was adapted to *K. pastoris* codon usage and a C-terminal His-tag was added. SignalP was used to identify the native signal sequence of 27 amino acids³¹. The gene lacking the signal sequence was cloned into the pPICZα vector® (Invitrogen), using standard techniques. *K. pastoris* strain KM71H was transformed with pPICK-PDI vector harboring the gene for the protein disulfide isomerase from *Saccharomyces cerevisiae*. The modified KM71H strain was transformed with

the linearized pPICZ α -AtBBE-like 28 construct. All transformations were done by electroporation. Applicable expression strains were identified using the method proposed by Weis *et al.*³².

Expression and purification

Expression was carried out using BBI CT-2 fermenter (Sartorius AG, Goettingen, Germany) in basal minimal medium as described by Schrittwieser *et al.*³³. After 96 h of induction pH was set to 8.0 and the cells were removed by centrifugation at 4000 rpm at 4 °C for 30 min. The supernatant was subsequently filtered through membranes with pore diameter of 0.8 μ m, 0.45 μ m and 0.22 μ m. The volume was reduced from 3 to 0.5 L using a cross flow apparatus (Centramate 500S, Pall Corporation, Dreieich, Germany), equipped with a membrane with a cut off at 22 kDa (Omega Centramate membrane cassettes, Pall Corporation, Dreieich, Germany). The buffer was changed to 50 mM potassium phosphate buffer pH 7.0 containing 150 mM NaCl and 10 mM imidazole. The supernatant was loaded to a Ni SepharoseTM 6 Fast Flow column. The column was washed with 10 CV loading buffer, the protein was eluted using 50 mM phosphate buffer containing 150 mM NaCl and 150 mM imidazole. After elution, the column was stripped using 20 mM potassium phosphate buffer pH 7.4 containing 0.5 M NaCl and 50 mM EDTA. A second yellow flavoprotein containing fraction was collected. The purity of the different fractions was checked by SDS-PAGE. Fractions eluted with 50 mM phosphate buffer containing 150 mM NaCl and 150 mM imidazole were concentrated using Amicon Ultra centrifugal filter units and loaded on a Superdex 200 gel filtration column using an Äkta system. Separation was achieved using 50 mM TRIS/HCl buffer pH 8 containing 150 mM NaCl. Fractions containing AtBBE-like 28 were concentrated and the buffer was changed to 20 mM TRIS/HCl (buffer A). The protein was loaded to a MonoQ column and eluted applying a stepwise gradient to 100 % of a 20 mM TRIS/HCl buffer pH 8 containing 1 M NaCl (buffer B). The flow rate was 1 mL/min, buffer A was kept at 100% for 5 min, then a gradient to 20% buffer B in 30 min was set. 20% buffer B was kept for 10 min, then a gradient to 100% B was set in 20 min.

Crystallization and data collection

The *A*tBBE-like fraction collected during column stripping was used for crystallization without further purification steps. After purification *A*tBBE-like 28 was stored over night at 4 °C in 20 mM potassium phosphate buffer pH 7.4 containing 0.5 M NaCl and 50 mM EDTA. The buffer was changed to 20 mM TRIS/HCl pH 9.0 using a PD-10 Desalting Column (GE Healthcare) and the protein concentration was set to 20 mg/mL. Crystallization in the optimized condition was performed using microbatch, mixing 1 μ L of protein and 0.5 μ L of 0.1 M HEPES buffer pH 7.0 containing 30 % v/v Jeffamine ED 2001 pH 7.0 at 277 K. Tetragonal bipyramidal crystals appeared after streak seeding and grew to a dimension of approximately 300 μ m within 14 days. Surplus crystallization buffer was removed by streaking the crystals over the micropatch plate's surface under oil before flash freezing the crystals in liquid nitrogen without any additional cryo protection. A data set was collected at 100 K at beam line BM14 (ESRF, Grenoble, France). The diffraction data were processed using XDS³⁴. The structure was solved by molecular replacement using the program Phaser with the structure of BBE (PDB ID 3D2H)³⁵ as search template. Structure refinement was done by repetitive runs the programs COOT³⁶ and Phenix³⁷. A TLS restrained refinement was included using four TLS groups obtained from the TLSMD webserver for each chain^{38,39}. R_{free} values were calculated from 5 % randomly chosen reflections excluded from refinement. A summary of data collection, processing and refinement statistics is given in Table 2. Two protein chains were present in the asymmetric unit. Clear electron density was observed for the most residues in both chains with the exception of gaps between Tyr37 and Thr43 in chain A and between Cys34 and Val48 in chain B.

Table 2: Data collection and refinement statistics

Wavelength (Å)	
Beamline	ESRF BM14
Resolution range (Å)	15.89 - 1.849 (1.915 - 1.849)
Space group	$C222_1$
Unit cell	127.02 133.13 139.00 90 90 90
Total reflections	376130 (35085)
Unique reflections	93337 (9111)

Multiplicity	4.0 (3.9)
Completeness (%)	93.16 (91.72)
Mean I/sigma(I)	7.22 (2.00)
Wilson B-factor	23.30
R-merge	0.1224 (0.5576)
R-meas	0.1406
CC1/2	0.987 (0.767)
CC*	0.997 (0.932)
R-work	0.1781 (0.2913)
R-free	0.2205 (0.3205)
Number of non-hydrogen atoms	9336
Macromolecules	7927
Ligands	118
Water	1291
Protein residues	994
RMS(bonds)	0.007
RMS(angles)	1.10
Ramachandran favored (%)	95
Ramachandran outliers (%)	0.2
Clashscore	9.98
Average B-factor	33.70
Macromolecules	32.80
Ligands	25.70
Solvent	39.70
PDB code	5D79

Redox potential determination

The redox potential was determined using the dye-equilibrium method employing the xanthine/xanthine oxidase system as electron source and thionine acetate ($E^\circ = 64$ mV) as described by Massey *et al.*⁴⁰ Experiments were performed in 50 mM potassium phosphate buffer pH 7.0 at 25 °C. The reaction mixture contained 5 μ M methyl viologen as mediator, 15 μ M enzyme and xanthine oxidase in catalytic amounts (approximately 2 nM). Solutions with methylviologen, *AtBBE*-like 28 and xanthine were mixed under anoxic conditions with solutions of xanthine oxidase and thionine acetate. Reactions were carried out using a stopped flow device SF-61DX2 (TgK Scientific, Bradford-On-Avon, UK) positioned in a glove box (Belle Technology, Weymouth, UK). Spectra were recorded with a KinetaScanT diode array detector MG-6560 (TgK Scientific). One experiment lasted for 50 min, 300 scans were recorded during that time. The potential of *AtBBE*-like 28 was calculated from the plot of $\log([ox]/[red])$ of the protein *versus* $\log([ox]/[red])$ of thionine acetate according to Minnaert *et al.*(1965)¹⁸.

Photoreduction

Photoreduction was carried out according to Massey *et al.*(1978), Reactions were carried out in 50 mM potassium phosphate buffer pH 7.0 at ambient temperature¹⁴. Solutions were flushed with nitrogen and stored 1 h in an anaerobic glove box to remove all oxygen. Reaction mixtures containing 20 μ M *AtBBE*-like 28 and 10 mM EDTA were tightly closed in the glove box and irradiated with a projector (Luminea™ 10 W, Pearl GmbH, Buggingen, Germany). Spectra were recorded with a photometer (Specord 205, Analytik Jena, Jena, Germany).

Determination of the oxidative rate

Photoreduced enzyme was mixed with air saturated buffer in the above described stopped flow device. Reoxidation of the enzyme was followed at a wavelength of 450 nm. Oxidative rate was determined via the Kinetic Studio software (TgK Scientific, Bradford-on-Avon, UK).

Phylogenetic analysis

Sequences were retrieved from Phytosome 10.2 website ¹⁹. Clustal omega was used to create a multiple sequence alignment including all *AtBBE*-like family members using the default parameters ²⁰. The alignment was manually edited by hand using Jalview ⁴¹. The PHYLIP package (PHYLIP 3.69) was used to create a bootstrapped phylogenetic tree using the programs SEQBOOT, PROTDIST, NEIGHBOR and CONSENSE ²¹. We created 1000 Jackknife sub-alignments with SEQBOOT, which were subsequently subjected to a bootstrapped protein-distance analysis. We chose *EcBBE* (AC39358) as the outgroup sequence. The tree shown in Figure 5 was visualized using Figtree (Tree Figure Drawing Tool, version 1.4.0 by Andrew Rambaut) ⁴². The tree including the bootstrap values is shown in the supplement (Figure S1). The accession codes for the sequences used for the analysis are given in Table S1.

References

1. Macheroux, P., Kappes, B. & Ealick, S. E. Flavogenomics - A genomic and structural view of flavin-dependent proteins. *FEBS J.* **278**, 2625–2634 (2011).
2. Winkler, A., Hartner, F., Kutchan, T. M., Glieder, A. & Macheroux, P. Biochemical evidence that berberine bridge enzyme belongs to a novel family of flavoproteins containing a bi-covalently attached FAD cofactor. *J. Biol. Chem.* **281**, 21276–21285 (2006).
3. Winkler, A. *et al.* Structural and mechanistic studies reveal the functional role of bicovalent flavinylation in berberine bridge enzyme. *J. Biol. Chem.* **284**, 19993–20001 (2009).
4. Facchini, P. J., Penzes, C., Johnson, A. G. & Bull, D. Molecular characterization of berberine bridge enzyme genes from opium poppy. *Plant Physiol.* **112**, 1669–1677 (1996).
5. Attila, C. *et al.* *Pseudomonas aeruginosa* PAO1 virulence factors and poplar tree response in the rhizosphere. *Microb. Biotechnol.* **1**, 17–29 (2008).
6. González-Candelas, L., Alamar, S., Sánchez-Torres, P., Zacarías, L. & Marcos, J. F. A transcriptomic approach highlights induction of secondary metabolism in citrus fruit in response to *Penicillium digitatum* infection. *BMC Plant Biol.* **10**, 194 (2010).
7. Coram, T., Huang, X., Zhan, G., Settles, M. & Chen, X. Meta-analysis of transcripts associated with race-specific resistance to stripe rust in wheat demonstrates common induction of blue copper-binding protein, heat-stress transcription factor, pathogen-induced WIR1A protein, and entkaurene synthase transcri. *Funct. Integr. Genomics* **10**, 383–392 (2010).
8. Jamet, E., Canut, H., Boudart, G. & Pont-Lezica, R. F. Cell wall proteins: A new insight through proteomics. *Trends Plant Sci.* **11**, 33–39 (2006).
9. Daniel, B. *et al.* oxidation of monolignols by members of the berberine bridge enzyme family suggests a role in cell wall metabolism. *J. Biol. Chem.* **290**, 18770–18781 (2015).
10. Seidl, M. F., Van den Ackerveken, G., Govers, F. & Snel, B. A domain-centric analysis of oomycete plant pathogen genomes reveals unique protein organization. *Plant Physiol.* **155**, 628–644 (2011).

11. Raffaele, S., Win, J., Cano, L. M. & Kamoun, S. Analyses of genome architecture and gene expression reveal novel candidate virulence factors in the secretome of *Phytophthora infestans*. *BMC Genomics* **11**, 637 (2010).
12. Morais do Amaral, A., Antoniwi, J., Rudd, J. J. & Hammond-Kosack, K. E. Defining the predicted protein secretome of the fungal wheat leaf pathogen *mycosphaerella graminicola*. *PLoS One* **7**, (2012).
13. Zafred, D. *et al.* Rationally engineered flavin-dependent oxidase reveals steric control of dioxygen reduction. *FEBS J.* **282**, 3060–3074 (2015).
14. Massey, V. & Hemmerich, P. Photoreduction of flavoproteins and other biological compounds catalyzed by deazaflavins. *Biochemistry* **17**, 9–16 (1978).
15. Mayhew, S. G. The effects of pH and semiquinone formation on the oxidation-reduction potentials of flavin mononucleotide. A reappraisal. *Eur. J. Biochem.* **265**, 698–702 (1999).
16. Winkler, A., Kutchan, T. M. & Macheroux, P. 6-S-cysteinylation of bi-covalently attached FAD in berberine bridge enzyme tunes the redox potential for optimal activity. *J. Biol. Chem.* **282**, 24437–24443 (2007).
17. Massey, V. Activation of molecular oxygen by flavins and flavoproteins. *J. Biol. Chem.* **269**, 22459–22462 (1994).
18. Minnaert, K. Measurement of the equilibrium constant of the reaction between cytochrome c and cytochrome a. *Biochim. Biophys. Acta - Enzymol. Biol. Oxid.* **110**, 42–56 (1965).
19. Goodstein, D. M. *et al.* Phytozome: A comparative platform for green plant genomics. *Nucleic Acids Res.* **40**, (2012).
20. Sievers, F. *et al.* Fast, scalable generation of high-quality protein multiple sequence alignments using Clustal Omega. *Mol. Syst. Biol.* **7**, (2011).
21. Felsenstein, J. Phylip: phylogeny inference package (version 3.2). *Cladistics* **5**, 164–166 (1989).
22. Ishida, M., Hara, M., Fukino, N., Kakizaki, T. & Morimitsu, Y. Glucosinolate metabolism, functionality and breeding for the improvement of *Brassicaceae* vegetables. *Breed. Sci.* **64**, 48–59 (2014).

23. Glawischnig, E. Camalexin. *Phytochemistry* **68**, 401–406 (2007).
24. Liu, Y.-C. *et al.* Interception of teicoplanin oxidation intermediates yields new antimicrobial scaffolds. *Nat. Chem. Biol.* **7**, 304–309 (2011).
25. Winkler, A. *et al.* A concerted mechanism for berberine bridge enzyme. *Nat. Chem. Biol.* **4**, 739–741 (2008).
26. Sirikantaramas, S. *et al.* The gene controlling marijuana psychoactivity: molecular cloning and heterologous expression of Delta1-tetrahydrocannabinolic acid synthase from *Cannabis sativa* L. *J. Biol. Chem.* **279**, 39767–39774 (2004).
27. Lorenz, N., Olšovská, J., Šulc, M. & Tudzynski, P. Alkaloid cluster gene *ccsA* of the ergot fungus *Claviceps purpurea* encodes chanoclavine I synthase, a flavin adenine dinucleotide-containing oxidoreductase mediating the transformation of N-methyl-dimethylallyltryptophan to chanoclavine I. *Appl. Environ. Microbiol.* **76**, 1822–1830 (2010).
28. Lin, H.-C. *et al.* Elucidation of the Concise Biosynthetic Pathway of the Communesin Indole Alkaloids. *Angew. Chemie Int. Ed.* **54**, 3004–3007 (2015).
29. Fraaije, M. W. & Mattevi, A. Flavoenzymes: Diverse catalysts with recurrent features. *Trends Biochem. Sci.* **25**, 126–132 (2000).
30. Zafred, D., Nandy, A., Pump, L., Kahlert, H. & Keller, W. Crystal structure and immunologic characterization of the major grass pollen allergen Phl p 4. *J. Allergy Clin. Immunol.* **132**, (2013).
31. Petersen, T. N., Brunak, S., von Heijne, G. & Nielsen, H. SignalP 4.0: discriminating signal peptides from transmembrane regions. *Nat. Methods* **8**, 785–786 (2011).
32. Weis, R. *et al.* Reliable high-throughput screening with *Pichia pastoris* by limiting yeast cell death phenomena. *FEMS Yeast Res.* **5**, 179–189 (2004).
33. Schrittwieser, J. H. *et al.* Biocatalytic organic synthesis of optically pure (s)-scoulerine and berbine and benzyloquinoline alkaloids. *J. Org. Chem.* **76**, 6703–6714 (2011).
34. Kabsch, W. Automatic processing of rotation diffraction data from crystals of initially unknown symmetry and cell constants. *J. Appl. Crystallogr.* **26**, 795–800 (1993).

35. McCoy, A. J. *et al.* Phaser crystallographic software. *J. Appl. Crystallogr.* **40**, 658–674 (2007).
36. Emsley, P. & Cowtan, K. Coot: model-building tools for molecular graphics. *Acta Crystallogr. D. Biol. Crystallogr.* **60**, 2126–2132 (2004).
37. Adams, P. D. *et al.* PHENIX : building new software for automated crystallographic structure determination. *Acta Crystallogr. Sect. D Biol. Crystallogr.* **58**, 1948–1954 (2002).
38. Painter, J. & Merritt, E. A. Optimal description of a protein structure in terms of multiple groups undergoing TLS motion. *Acta Crystallogr. D. Biol. Crystallogr.* **62**, 439–450 (2006).
39. Painter, J. & Merritt, E. A. web server for the generation of multi-group TLS models. *J. Appl. Crystallogr.* **39**, 109–111 (2006).
40. Massey, V. *Flavins and flavoproteins 1990*. B. Curti, S. Ronchi and G. Zanetti (eds). de Gruyter, Berlin and New York. xxiii + 945 pages, DM390 (1991). *Cell Biochem. Funct.* **10**, 55–66 (John Wiley & Sons, Ltd., 1992).
41. Waterhouse, A. M., Procter, J. B., Martin, D. M. A., Clamp, M. & Barton, G. J. Jalview Version 2- A multiple sequence alignment editor and analysis workbench. *Bioinformatics* **25**, 1189–1191 (2009).
42. Rambaut, A. FigTree v1.3.1. 2006-2009. Accessed Novemb. 29, 2012 Program package available at <http://tree.bio.ed.ac> (2009).
43. Krieger, E., Koraimann, G. & Vriend, G. Increasing the precision of comparative models with YASARA NOVA - A self-parameterizing force field. *Proteins Struct. Funct. Genet.* **47**, 393–402 (2002).

Structure of a berberine bridge enzyme-like enzyme with an active site specific to the plant family of *Brassicaceae*

Supplementary information

Bastian Daniel,¹ Silvia Wallner,¹ Barbara Steiner,¹ Gustav Oberdorfer,² Prashant Kumar,²
Christioph W. Sensen,³ Karl Gruber,² and Peter Macheroux^{1*}

¹Graz University of Technology, Institute of Biochemistry, Graz, Austria

²University of Graz, Institute of Molecular Biosciences, Graz, Austria

³Graz University of Technology, Institute of Molecular Biotechnology

To whom correspondence should be addressed:

Prof. Dr. Peter Macheroux, Graz University of Technology, Institute of Biochemistry,
Petersgasse 12/II, A-8010 Graz, Austria, Tel.: +43-316-873 6450; Fax: +43-316-873 6952;
Email: peter.macheroux@tugraz.at

Table S1: Gene names

Gene name	Abbreviation
Alyrata 946113 946113	A/BBE1
Alyrata 922142 922142	A/BBE2
Alyrata 494546 494546	A/BBE3
Alyrata 494545 494545	A/BBE4
Alyrata 472781 472781	A/BBE5
Alyrata 472779 472779	A/BBE6
Alyrata 922138 922138	A/BBE7
Alyrata 470076 470076	A/BBE8
Alyrata 472778 472778	A/BBE9
Alyrata 948675 948675	A/BBE10
Alyrata 948681 948681	A/BBE11
Alyrata 934079 934079	A/BBE12
Alyrata 934080 934080	A/BBE13
Alyrata 330958 330958	A/BBE14
Alyrata 492802 492802	A/BBE15
Alyrata 473307 473307	A/BBE16
Alyrata 492806 492806	A/BBE17
Alyrata 473304 473304	A/BBE18
Alyrata 922139 922139	A/BBE19
Alyrata 494550 494550	A/BBE20
Alyrata 948672 948672	A/BBE21
Alyrata 922140 922140	A/BBE22
Alyrata 471318 471318	A/BBE23
Alyrata 354696 354696	A/BBE24
Alyrata 492803 492803	A/BBE25
Alyrata 472780 472780	A/BBE26
Esalsugineum Thhalv10017619m.g Thhalv10017619m	<i>Es</i> BBE1
Esalsugineum Thhalv10016496m.g Thhalv10016496m	<i>Es</i> BBE2
Esalsugineum Thhalv10009705m.g Thhalv10009705m	<i>Es</i> BBE3
Esalsugineum Thhalv10007344m.g Thhalv10007344m	<i>Es</i> BBE4
Esalsugineum Thhalv10007327m.g Thhalv10007327m	<i>Es</i> BBE5
Esalsugineum Thhalv10007354m.g Thhalv10007354m	<i>Es</i> BBE6
Esalsugineum Thhalv10007308m.g Thhalv10007308m	<i>Es</i> BBE7
Esalsugineum Thhalv10007341m.g Thhalv10007341m	<i>Es</i> BBE8
Esalsugineum Thhalv10007337m.g Thhalv10007337m	<i>Es</i> BBE9
Esalsugineum Thhalv10007352m.g Thhalv10007352m	<i>Es</i> BBE10
Esalsugineum Thhalv10007313m.g Thhalv10007313m	<i>Es</i> BBE11
Esalsugineum Thhalv10007336m.g Thhalv10007336m	<i>Es</i> BBE12
Esalsugineum Thhalv10024789m.g Thhalv10024789m	<i>Es</i> BBE13
Esalsugineum Thhalv10027426m.g Thhalv10027426m	<i>Es</i> BBE14

Esalsugineum Thhalv10027126m.g Thhalv10027126m	EsBBE15
Esalsugineum Thhalv10027093m.g Thhalv10027093m	EsBBE16
Esalsugineum Thhalv10026881m.g Thhalv10026881m	EsBBE17
Esalsugineum Thhalv10024886m.g Thhalv10024886m	EsBBE18
Esalsugineum Thhalv10027353m.g Thhalv10027353m	EsBBE19
Esalsugineum Thhalv10000843m.g Thhalv10000843m	EsBBE20
Esalsugineum Thhalv10000843m.g Thhalv10000842m	EsBBE21
Esalsugineum Thhalv10000840m.g Thhalv10000840m	EsBBE22
Esalsugineum Thhalv10000851m.g Thhalv10000851m	EsBBE23
Esalsugineum Thhalv10000846m.g Thhalv10000846m	EsBBE24
Esalsugineum Thhalv10001137m.g Thhalv10001137m	EsBBE25
Esalsugineum Thhalv10000841m.g Thhalv10000841m	EsBBE26
Esalsugineum Thhalv10000845m.g Thhalv10000845m	EsBBE27
Esalsugineum Thhalv10000844m.g Thhalv10000844m	EsBBE28
Esalsugineum Thhalv10003322m.g Thhalv10003322m	EsBBE29
Esalsugineum Thhalv10016482m.g Thhalv10016482m	EsBBE30
Crubella Carubv10012287m.g Carubv10012287m	CrBBE10
Crubella Carubv10011480m.g Carubv10011480m	CrBBE11
Crubella Carubv10011178m.g Carubv10011178m	CrBBE12
Crubella Carubv10008831m.g Carubv10008831m	CrBBE13
Crubella Carubv10008739m.g Carubv10008739m	CrBBE14
Crubella Carubv10006505m.g Carubv10006505m	CrBBE15
Crubella Carubv10004576m.g Carubv10004576m	CrBBE16
Crubella Carubv10007418m.g Carubv10007418m	CrBBE17
Crubella Carubv10007797m.g Carubv10007797m	CrBBE18
Crubella Carubv10004466m.g Carubv10004466m	CrBBE19
Crubella Carubv10007331m.g Carubv10007331m	CrBBE20
Crubella Carubv10006337m.g Carubv10006337m	CrBBE21
Crubella Carubv10022971m.g Carubv10022971m	CrBBE22
Crubella Carubv10022944m.g Carubv10022944m	CrBBE23
Crubella Carubv10026133m.g Carubv10026133m	CrBBE24
Crubella Carubv10026198m.g Carubv10026198m	CrBBE25
Crubella Carubv10027532m.g Carubv10027532m	CrBBE26
Crubella Carubv10026203m.g Carubv10026203m	CrBBE27
Crubella Carubv10026190m.g Carubv10026190m	CrBBE28
Cgrandiflora Cagra.6571s0003 Cagra.6571s0003.1	CgBBE1
Cgrandiflora Cagra.1508s0130 Cagra.1508s0130.1	CgBBE2
Cgrandiflora Cagra.1508s0129 Cagra.1508s0129.1	CgBBE3
Cgrandiflora Cagra.1508s0128 Cagra.1508s0128.1	CgBBE4
Cgrandiflora Cagra.1508s0127 Cagra.1508s0127.1	CgBBE5
Cgrandiflora Cagra.1508s0126 Cagra.1508s0126.1	CgBBE6
Cgrandiflora Cagra.1508s0131 Cagra.1508s0131.1	CgBBE7

Cgrandiflora Cagra.1508s0123 Cagra.1508s0123.1	CgBBE8
Cgrandiflora Cagra.3346s0030 Cagra.3346s0030.1	CgBBE9
Cgrandiflora Cagra.3346s0031 Cagra.3346s0031.1	CgBBE10
Cgrandiflora Cagra.7100s0001 Cagra.7100s0001.1	CgBBE11
Cgrandiflora Cagra.7100s0002 Cagra.7100s0002.1	CgBBE12
Cgrandiflora Cagra.1062s0054 Cagra.1062s0054.1	CgBBE13
Cgrandiflora Cagra.1062s0058 Cagra.1062s0058.1	CgBBE14
Cgrandiflora Cagra.1062s0053 Cagra.1062s0053.1	CgBBE15
Cgrandiflora Cagra.1062s0055 Cagra.1062s0055.1	CgBBE16
Cgrandiflora Cagra.1968s0134 Cagra.1968s0134.1	CgBBE17
Cgrandiflora Cagra.0568s0086 Cagra.0568s0086.1	CgBBE18
Cgrandiflora Cagra.0629s0019 Cagra.0629s0019.1	CgBBE19
Cgrandiflora Cagra.0629s0018 Cagra.0629s0018.1	CgBBE20
Cgrandiflora Cagra.0629s0016 Cagra.0629s0016.1	CgBBE21
Cgrandiflora Cagra.0629s0021 Cagra.0629s0021.1	CgBBE22
Cgrandiflora Cagra.0629s0017 Cagra.0629s0017.1	CgBBE23
Cgrandiflora Cagra.7100s0003 Cagra.7100s0003.1	CgBBE24
>BrapaFPsc Brara.B02784 Brara.B02784.1	BrBBE1
BrapaFPsc Brara.K01808 Brara.K01808.1	BrBBE2
BrapaFPsc Brara.K01807 Brara.K01807.1	BrBBE3
BrapaFPsc Brara.K00501 Brara.K00501.1	BrBBE4
BrapaFPsc Brara.C01758 Brara.C01758.1	BrBBE5
BrapaFPsc Brara.D02108 Brara.D02108.1	BrBBE6
BrapaFPsc Brara.E00947 Brara.E00947.1	BrBBE7
BrapaFPsc Brara.E00948 Brara.E00948.1	BrBBE8
BrapaFPsc Brara.F03747 Brara.F03747.1	BrBBE9
BrapaFPsc Brara.F03748 Brara.F03748.1	BrBBE10
BrapaFPsc Brara.F03744 Brara.F03744.1	BrBBE11
BrapaFPsc Brara.F00789 Brara.F00789.1	BrBBE12
BrapaFPsc Brara.G00508 Brara.G00508.1	BrBBE13
BrapaFPsc Brara.G00588 Brara.G00588.1	BrBBE14
BrapaFPsc Brara.G00589 Brara.G00589.1	BrBBE15
BrapaFPsc Brara.G01552 Brara.G01552.1	BrBBE16
BrapaFPsc Brara.A01126 Brara.A01126.1	BrBBE17
BrapaFPsc Brara.A01123 Brara.A01123.1	BrBBE18
BrapaFPsc Brara.A01124 Brara.A01124.1	BrBBE19
BrapaFPsc Brara.A01128 Brara.A01128.1	BrBBE20
BrapaFPsc Brara.A01152 Brara.A01152.1	BrBBE21
BrapaFPsc Brara.K01265 Brara.K01265.1	BrBBE22
BrapaFPsc Brara.I02784 Brara.I02784.1	BrBBE23
BrapaFPsc Brara.I01845 Brara.I01845.1	BrBBE24
BrapaFPsc Brara.I03113 Brara.I03113.1	BrBBE25

BrapaFPsc Brara.I03114 Brara.I03114.1	<i>BrBBE26</i>
BrapaFPsc Brara.I02786 Brara.I02786.1	<i>BrBBE27</i>
BrapaFPsc Brara.I01846 Brara.I01846.1	<i>BrBBE28</i>
BrapaFPsc Brara.I02785 Brara.I02785.1	<i>BrBBE29</i>
BrapaFPsc Brara.I01844 Brara.I01844.1	<i>BrBBE30</i>
BrapaFPsc Brara.I05161 Brara.I05161.1	<i>BrBBE31</i>
BrapaFPsc Brara.I01843 Brara.I01843.1	<i>BrBBE32</i>
BrapaFPsc Brara.I02779 Brara.I02779.1	<i>BrBBE33</i>
BrapaFPsc Brara.I02783 Brara.I02783.1	<i>BrBBE34</i>
BrapaFPsc Brara.I03596 Brara.I03596.1	<i>BrBBE35</i>
BrapaFPsc Brara.H01046 Brara.H01046.1	<i>BrBBE36</i>
Bstricta Bostr.12659s0359 Bostr.12659s0359.1	<i>BsBBE1</i>
Bstricta Bostr.12659s0358 Bostr.12659s0358.1	<i>BsBBE2</i>
Bstricta Bostr.12659s0356 Bostr.12659s0356.1	<i>BsBBE3</i>
Bstricta Bostr.12659s0355 Bostr.12659s0355.1	<i>BsBBE4</i>
Bstricta Bostr.3148s0020 Bostr.3148s0020.1	<i>BsBBE5</i>
Bstricta Bostr.3148s0015 Bostr.3148s0015.1	<i>BsBBE6</i>
Bstricta Bostr.3148s0017 Bostr.3148s0017.1	<i>BsBBE7</i>
Bstricta Bostr.3148s0013 Bostr.3148s0013.1	<i>BsBBE8</i>
Bstricta Bostr.3148s0018 Bostr.3148s0018.1	<i>BsBBE9</i>
Bstricta Bostr.3148s0016 Bostr.3148s0016.1	<i>BsBBE10</i>
Bstricta Bostr.3148s0014 Bostr.3148s0014.1	<i>BsBBE11</i>
Bstricta Bostr.15697s0380 Bostr.15697s0380.1	<i>BsBBE12</i>
Bstricta Bostr.15697s0370 Bostr.15697s0370.1	<i>BsBBE13</i>
Bstricta Bostr.15697s0371 Bostr.15697s0371.1	<i>BsBBE14</i>
Bstricta Bostr.15697s0372 Bostr.15697s0372.1	<i>BsBBE15</i>
Bstricta Bostr.15697s0373 Bostr.15697s0373.1	<i>BsBBE16</i>
Bstricta Bostr.15697s0376 Bostr.15697s0376.1	<i>BsBBE17</i>
Bstricta Bostr.15697s0377 Bostr.15697s0377.1	<i>BsBBE18</i>
Bstricta Bostr.13671s0285 Bostr.13671s0285.1	<i>BsBBE19</i>
Bstricta Bostr.10689s0032 Bostr.10689s0032.1	<i>BsBBE20</i>
Bstricta Bostr.10689s0037 Bostr.10689s0037.1	<i>BsBBE21</i>
Bstricta Bostr.5325s0118 Bostr.5325s0118.1	<i>BsBBE22</i>
Bstricta Bostr.23794s0623 Bostr.23794s0623.1	<i>BsBBE23</i>

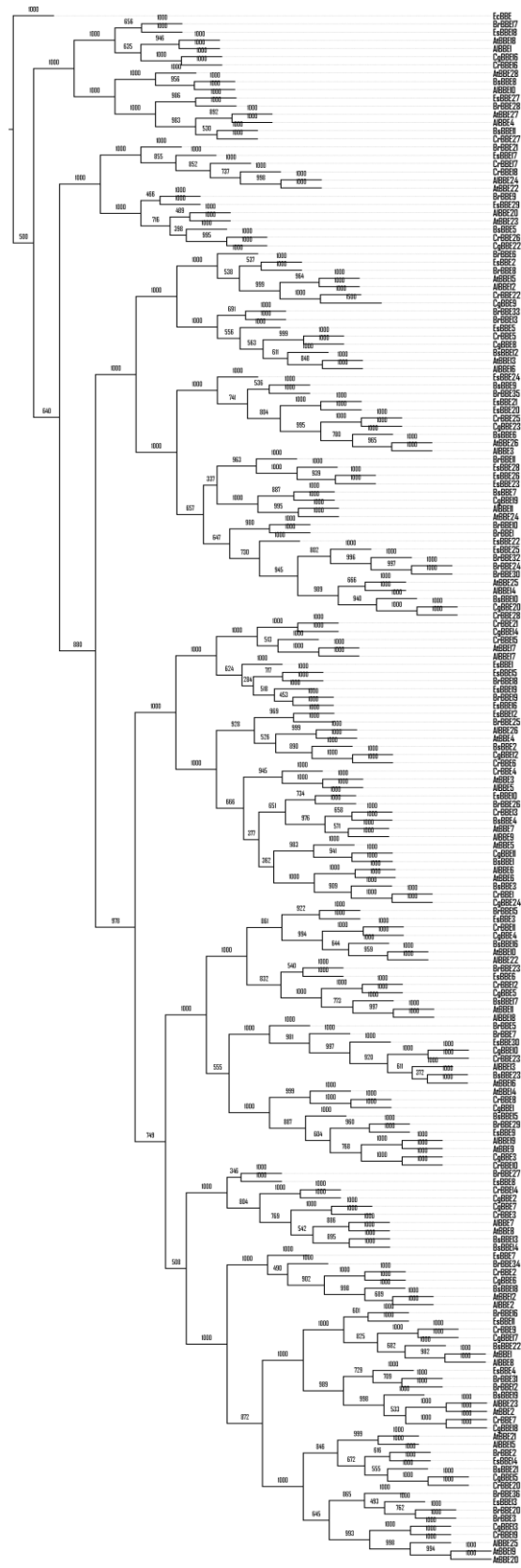


Figure S1: Phylogenetic tree with bootstrap values.

Curriculum vitae



Persönliche Angaben

Name	Daniel
Vorname	Bastian
Geburtsdatum	10.07.1983, Hemer, Deutschland
Telefon	+43 676 6612690
Email	bastian.daniel@tugraz.at
Familienstand	verheiratet, 2 Kinder

Ausbildung

10/2011-1/2016	Doktoratsstudium, TU Graz: Doctoral School: Molekulare Biowissenschaften und Biotechnologie Dissertation am Institut für Biochemie bei Prof. Dr. P. Macheroux, TU Graz: „The Family of Berberine Bridge Enzyme-like Proteins from <i>Arabidopsis thaliana</i> “
10/2004-12/2010	Studium der Chemischen Biologie, Technische Universität Dortmund Abschluss: Master of Science Note: sehr gut
12/2010	Masterarbeit am Lehrstuhl für Biomaterialien, Prof. Dr. J. Tiller, TU Dortmund: „Darstellung von Mikropartikeln aus amphiphilen Conetzwirken“
10/2008	Bachelorarbeit am Lehrstuhl für Technische Chemie A, Prof. Dr. A. Behr, TU Dortmund: „Anwendung von temperaturgesteuerten Multikomponenten-Lösungsmittelsystemen zum Recycling von Enzymen“
08/1994-06/2003	Allgemeine Hochschulreife Walburgisgymnasium, Menden

Studentische Tätigkeiten

- 10/2008-11/2009 **Entwicklung eines Verfahrens zum Recycling von Biokatalysatoren,**
Lehrstuhl Technische Chemie A, Prof. Dr. A. Behr
- 03/2007-03/2008 **Durchführung von organischen Synthesen und Mitarbeit in der Prozessanalytik**
Lehrstuhl Technische Chemie A, Prof. Dr. A. Behr

Veröffentlichungen

Daniel, B. *et al.*: Oxidation of Monolignols by Members of the Berberine Bridge Enzyme Family Suggests a Role in Plant Cell Wall Metabolism. *J Biol Chem.* 2015, 290(30), 18770-18781

Schoenfeld, I. *et al.*: Investigations on diffusion limitations of biocatalyzed reactions in amphiphilic polymer conetworks in organic solvents; *Biotechnol Bioeng.* 2013, 110(9), 2333-2342

Wallner S *et al.*: Berberine Bridge Enzyme and the Family of Bicovalent Flavoenzymes, *Handbook of Flavoproteins. Volume 2 Complex Flavoproteins, Dehydrogenase and Physical Methods* 2013, Boston: De Gruyter. ISBN: 978-3-11-029834-5

Johnen L *et al.*: A Liquid immobilisation concept for enzymes by thermomorphic solvent systems. *Green Chem.* 2011, 13 (11), 3168 - 3172

Behr A *et al.*: „Verfahren zum Recycling von Biokatalysatoren“, Patent PCT/EP2010/004 357, European Patent Office, München, Germany, 2010

Fortbildungen

09/2014	Scholarship for Fermentation Training, Eppendorf GmbH
09/2010	Summer School: Biocatalysis Using Non- Conventional Media DECHEMA/BioNoCo
06/2010	Fortbildungsseminar: Partikelmesstechnik Größen- und Formverteilung Malvern Instruments GmbH
08/2009	Summer School: Mikrotechnik IVAM Fachverband für Mikrotechnik

Sonstiges

Sprachen	Englisch fließend in Wort und Schrift Französisch Grundkenntnisse Latein
EDV	ausführliche Kenntnisse in MS-Office Strukturbiologische Software (PYMOL, COOT, Phenix)

Graz, den 21.12.2015